APPLICATION OF THE FAST FLOOD SIMULATION MODEL FOR LOCAL RISK-INFORMED DECISION-MAKING ON FLOOD RISK REDUCTION

-A CASE STUDY OF PAMBA BASIN, KERALA INDIA-

VERA GLAS

Enschede, The Netherlands, August 2023

SUPERVISORS:
Prof. Dr. C.J. van Westen
Dr. B. Van den Bout

THESIS ASSESSMENT BOARD:
Prof. Dr. N. Kerle (Chair)
Dr. T. de Haas (Utrecht University)

Summary

Flood simulation models are an important source of information in risk-informed decision making to mitigate flood risks. Conventional physically-based flood models are associated with large computational demands. Novel advancements have led to the development of the opensource Fast Flood Simulation (FFS) model, which is available on de fastflood.org website. The FFS-model is up to 1500 times faster than conventional flood models. This offers large potential for application in interactive planning tools, scenario-based flood risks assessments and real-time flood modelling.

This report reflects on the practical applicability and accuracy of the FFS-model using the case-study area of the Pamba Basin in Kerala, India. Analyses of historical timeseries led to the development of catchment-specific discharge and rainfall-related return periods. In the subsequent calibration process a Nash Sufficient Efficiency of 0.79 and a PBIAS of 2.4% was reached using six independent historic events. The main challenges in the calibration process were the quantification of base discharge and the consideration of water releases from hydropower dams. Subsequently, different methods were applied to validate the FFS-model. Comparisons with radar flood extent data, which comes with limitations due to the role of vegetation, led to Cohen's Kappa values ranging from 0.23 to 0.53, which indicates fair to moderate agreement.

Additionally, the practical applicability of the FFS-model was studied for climate change scenarios, different intervention designs and by executing a flood exposure and risks assessment for local self-governments (LSGs). During this process, a model flaw concerning the unintentional sensitivity to the grid cell size was detected. Moreover, the quantitative results of these analyses are subject to uncertainties due to simplifications in input data. Nevertheless, the different FFS-model usage scenarios showed that the FFS-model offers large potential to contribute to the understanding of scenario-based flood hazard and consequently, risk-informed decision-making.

It is recommended to carry out additional performance tests of the FFS-model by comparing its output with results from conventional flood models, in particular for the design of flood mitigation measures. Moreover, additionally research regarding the model accuracy in areas with limited variations in elevation is suggested. For the Pamba Basin area, it is advised to select pilot local self-governments (LSGs) and collaborate with stakeholders to compose flood risk assessments using the FFS-model and the RiskChanges tool. Finally, several new features for the FFS-model are suggested. These features address the potential to use the FFS-model for probabilistic flood hazard analyses, integration of dynamic rainfall input and the generation of flow velocity and duration maps.

Keywords: Fast flood Simulation, risk-informed decision-making, flood risk assessment, flood mitigation design, Kerala, Pamba Basin

Acknowledgements

Table of contents

List of acronyms

DEM   Digital Elevation Model
EAR   Element-At-Risk
FFS   Fast Flood Simulation
GEE   Google Earth Engine
IMD   Indian Meteorological Department
KSDMA   Kerala State Disaster Management Authority
LSG   Local-Self-Government

List of figures

List of tables

Chapter 1: Introduction

Of all natural hazards, floods are globally the most damaging (Hamidifar & Nones, 2021). The EM-DAT database indicates that between 2010 and 2020 floods have caused globally almost 50.000 registered casualties (EM-DAT, 2023). Besides immediate effects, such as loss of human life, property damage and agricultural yield loss, floods also have large mid- and long-term disruptive consequences. Examples of these consequences are the spread of waterborne diseases, food shortages, declined mobility and a decrease in economic activities related to tourism (Du et al., 2010).

The enormous social and economic impacts of flood events emphasize the need for flood risk reduction. To tackle flood risks, risk-informed planning strategies on different geographic and governmental levels is needed. Risk-informed planning aims to strengthen resilience by identifying and addressing the root causes and drivers of risk including vulnerabilities, lack of capacity and exposure (INEE, 2018). An important tool that can be applied in all phases of the disaster risk cycle are flood hazard assessments, which create insight in the return period and spatial extent of flood events in a certain region (Uddin & Matin, 2021). Based on this hazard information the flood exposure, loss and risk can be derived. Due to its knowledge and data driven character, flood risk assessments are commonly not applicable for local authorities. This limits the possibilities of local authorities to apply risk-informed decision-making for flood risk reduction.

To create flood hazard maps, the common practise it to apply physically-based flood modelling tools. These modelling approaches are usually based on the Saint-Venant equations and the assumption of the depth-averaged, shallow water flow (Moussa & Bocquillon, 2000; Akbari & Firoozi, 2010). This approach has shown great accuracy and applicability in many regions of the world (Uddin & Matin 2021; Tsakiris, 2014). However, physically-based flood modelling is associated with large computational demands. For this reason, it is not applicable for real-time simulations in larger areas (Nguyen & Chua, 2012; Valeriy et al., 2021). This hinders the applicability for early warning systems and interactive planning tools.

To tackle the obstacles related to the high computational demand of physically-based flood modelling, recently several new tools have been developed for efficient and rapid simulation of flood maps. Van den Bout et al., (2022) have developed a new and opensource method for fast flood simulations. This novel method applies the physically-based principles of steady state flow and generates maps representing the peak flow height with a computational demand that is reduced with a factor of 1500. This state-of-the-art method has a large potential to contribute to risk-informed planning, especially on a local authority level. However, the additional assumptions and limitations of the model might prevent the increased speed from actually benefiting end-users due to uncertainties or loss of accuracy. No trials have been executed yet to test the applicability of the fast flood simulation model in practice.

The research presented in this report explores the applicability of the Fast Food Simulation (FFS) model for scenario-based flood hazard assessments and decision-making related to flood mitigation. As case-study area, the Pamba Basin in Kerala is selected. For the calibration and validation of the FFS-model an extensive rainfall-discharge and flood extent analyses is executed.

1.1. Problem statement

The central research problem addressed in this report is the lack of information concerning the practical applicability and accuracy of the FFS-model, and the applicability of this model for risk-informed decision-making by local authorities.

Flood models are a valuable tool for flood risk assessments and mitigation design. Numerous methodologies and software packages are available that support the development of such flood models. However, an overarching challenge associated with these models is the high computational demand and related long simulation times. The large computational demands limit the possibility to evaluate a large variety of risk reduction measures. Additionally, uncertainties persist regarding the accuracy of input data, as well as calibration and validation processes. The utilization and interpretation of flood models often necessitates the involvement of experts. Consequently, flood simulation models are generally not accessible to local authorities.

State-of-the-art developments in the area of flood simulation led to the creation of the Fast Flood Simulation (FFS) model by Bout et al. (2022). The overall set-up of this model is described in section 3.1. The model offers large potential for conducting real-time flood simulations and fast feedback on risk reduction alternatives. In the development, application to flash flood and usage of discharge boundary-conditions for small river segments was tested. However, there have not been any studies yet that assess the applicability of the FFS-model in a practical setting. It is still uncertain to which extent the FFS-model can be effectively applied to investigate the effects of physical mitigation measures and climate change developments. The lack of practical experience in utilizing the FFS-model and assessing its accuracy and applicability in real-world scenarios represents a notable research gap.

The Pamba Basin, in the Indian state of Kerala, was selected as study area to analyse the applicability of the FFS-model. The Kerala government strives to implement risk-informed decision-making on a local level to reduce the flood risks in the region. An internal interview study by Glas et al., (2022) showed that local authorities in the region are often aware of flood threats. However, the size and spatial distribution of flood hazards are mostly unknown and unquantified. Available datasets for risk-informed decision-making are subject to numerous uncertainties and limitations.

Currently, local policy makers do not have access to flood simulation models in their decision-making process addressing flood risk reduction. For the application of flood modelling tools on a local level, the assistance of specialized organizations would be needed. Moreover, the modelling and calibration process is very time consuming. The lack of flood hazard and risk data complicates the design of effective flood mitigation measures and the application of risk-informed planning strategies. Overall, the limited insights of local authorities in Pamba Basin concerning their flood hazard and risk situation is considered a research problem.

1.1.1. Problem wickedness

The formulated problem statement mainly addresses a lack of knowledge and a large degree of uncertainty in the available knowledge as research problems. A wicked problem faces, besides uncertainty in knowledge, also stakeholder disagreement. Overall, it can be stated that stakeholder groups agree that flood hazard is a threat to Kerala state and the Pamba Basin (Technical Stakeholder Consultation, 2020). Several recent tragic flood events are serving as reminder of the problematic situation.

In the Kerala governmental structure, large responsibilities regarding disaster risk reduction are given to local authorities. The FFS-model's user-friendly interface, along with its reduced data requirements and lower computational demands, opens opportunities for local authorities to apply flood simulation tools. This can empower them to perform risk-informed decision-making to reduce flood risk.

An arising difficulty with respect to flood hazard and risk assessments, is the question when results are sufficient to take action. With limited data availability, hazard and risk assessments are subject to many uncertainties. Interpreting and communicating these uncertainties is complex. One can argue that in an area as Pamba Basin, where previous flood events already show the need for action, all additional insights are of value. Independent of the exact quality and validity of this data.

However, it is possible that drastic interventions, such as permanent relocation of residents, need to find place to reduce flood risks in the area. This type of interventions have a large social-economic impacts and should not be taken lightly. By enabling local decision-makers to apply flood modelling tools, modelling experts could argue that you dangerously remove the required expertise needed for accurate flood modelling and interpretation. The balance between creating insight, despite unavoidable uncertainties, and making well substantiated decisions identifies the complexity of using tools, such as the FFS-model, for risk-informed decision-making.

Local decision makers in Kerala are elected. While there seems to be communal agreement that flood risks should be reduced, the approach to reach this goal can be a serious point of disagreement. Possibly, local elected authorities are reluctant to take drastic decisions which may affect many of their voters. The FFS-model enables stakeholders to increase their understanding regarding flood hazard in their area of interest. By using the FFS-model as interactive planning tool a dialogue between local authorities and effected communities can be facilitated. Nevertheless, the wickedness related to the understanding, interpretation and communication of unavoidable uncertainties remains challenging.

1.2. Research objectives and questions

Based on the problem statement and identified research gap the following research objective is formulated.

Evaluate to what extent fast flood simulations can contribute to risk-informed decision-making for local administrative units in the Pamba Basin, Kerala.

To reach this main objective, the following division into sub-objectives and related research questions is made:

Sub-objective 1: Compose a series of return periods for rainfall and river discharge that can be used for flood hazard analyses in the Pamba Basin.

Q1.1. In which manner can rainfall and discharge variability in the Pamba Basin be characterized and used as data input for flood modelling scenarios?

Q1.2. What is the spatial variability in return period rainfall for the Pamba Basin?

Sub-objective 2: Investigate the applicability of the Fast Flood Simulation (FFS) model for the Pamba Basin.

Q2.1. Which calibration setting in the FFS-model should be applied to achieve the best approximation of the observed rainfall-discharge relationship in Pamba Basin?

Q2.2. To what extent can the calibrated FFS-model be validated using radar flood extent data of the 2018 and 2019 flood events?

Q2.3. How do the results of the FFS-model compare with other available flood hazard studies conducted in the Pamba Basin, and what are the probable causes of disparities?

Sub-objective 3: Analyse the application of the Fast Flood Simulation (FFS) model in combination with the RiskChanges tool to provide insights into the effects of flood mitigation measures on flood risk at a local self-government level (LSG) in the Pamba Basin.

Q3.1. What insights can be obtained regarding flood hazard, exposure, loss, and risk for local self-governments (LSGs) in the Pamba Basin by integrating the FFS-model and the RiskChanges tools?

Q3.2. To what extent can flood mitigation options be verified using the combination of the FFS-model and the RiskChanges platform?

1.3. Spatial-dynamic flood modelling methods

Due to the chaotic and multifaced nature of fluid dynamics, and flooding in particular, reliable flood modelling is complicated (Bulti & Abebe, 2020). A large variety of hydrological and hydraulic models have been developed to analyse flood conditions. The most commonly used models for flood hazard assessments are hydraulic models that focus on spatially variating water levels and flow velocities throughout a river network and floodplain area (Ramírez, 2000).

The research described in this report focusses on the accuracy and applicability of the Fast Flood Simulation (FFS) model as developed by Bout et al., (2022). An elaboration regarding the FFS-model methodology is given in section 3.1. To place the novel FFS-model methodology in a larger perspective, the following sections describe an overview of regularly used spatial-dynamic flood modelling methods, as presented in literature. Firstly, traditional flood modelling methods are addressed and secondly developments in the field of fast flood modelling are discussed. In table 1 the discussed methods are presented in a table with their main advantages and disadvantages.

1.3.1. Traditional physically-based flood modelling techniques

The backbone of physically-based flood models are the Saint-Venant equations. A large variety of literature can be found in which the applicability of these equations for flood models is validated (Akbari & Firoozi, 2010; Saleh et al., 2013; Bout & Jetten, 2018). The Saint-Venant equations are derived from the Navier-Stokes equation and are also known as the shallow water equations. Compared to the Navier-Stokes equations, Saint-Venant flow is simplified by assuming shallow water flow and a hydrostatic pressure distribution in vertical direction. Moreover, water incompressibility is assumed and the vertical velocity and

viscosity are ignored. Overall, the Saint-Venant equations describe the unsteady flow in open-channels using the base principles of mass and momentum conservation.

Besides the Saint-Venant equations, also the Boussinesq equations are a simplification of the full Navier-Stokes equations that are used in flood modelling tools. The Boussinesq equations are specifically applicable for modelling long wave lengths with a small amplitude. Consequently, they are commonly used for the simulation of tidal waves in coastal regions and estuaries (Ahmadian, 2016). Because of their applicability in a wider range of flow scenarios, this section focusses on the Saint-Venant equations.

Many research papers can be found who describe the application of the Saint-Venant equations for 1D and 2D flood modelling. 1D flood models focus on water flow along the longitudinal direction of a river or channel. In the lateral cross-section it assumes a uniform width, flow depth and velocity. Advantages of a 1D flood model is that there is not much input data required and the computational demands are small. Nevertheless, 1D flood models are quite simplified. Due to their inability to cope with multidirectional flow conditions, flood extent studies in areas with spatially variating landscapes cannot be captured. (Horritt & Bates, 2002; Basnayaka & Sarukkalige, 2011; Henonin et al., 2013).

2D flood models consider longitudinal, as well as lateral flow directions by using a grid-based setup. They are widely used for generating flood hazard maps that present flood extent as well as flood depth. By using a Digital Elevation Model (DEM), 2D flood models are able to include the effect of complex terrain variations, for example in urban areas, in the flood hazard estimations. However, 2D flood models have significantly more data requirements and increased computational demands then 1D models. For this reason, detailed 2D flood modelling for larger catchments leads to computational complexities (Bulti & Ababe, 2020; Fewtrell et al., 2008).

For both 1D and 2D hydraulic models, kinematic, diffusive and dynamic flow approximations are commonly used to reduce computational time (Bout & Jetten, 2018). Kinematic flow approximations only consider gravitational and friction forces and neglect inertial momentum and pressure. By using a predefined flow network, kinematic flow approximations reduce computational demands. However, there exists a continuous connectivity between spatial elements. In contrast to kinematic flow, diffusive flow does consider a momentum attribute in its flow approximation. Nevertheless, it neglects inertial terms. In dynamic flow, the pressure and inertial forces are both considered. The paper of Bout & Jetten (2018) compares the calibration performance of the different flow approximations for catchment based flood simulations. The research concludes that diffusive and dynamic flow show a significantly higher accuracy then kinematic flow.

1.3.2. Developments concerning fast flood modelling

To avoid the computational demands and data requirements for physically-based flood modelling, empirical flood modelling methods can be applied. These revolve around historical data of past flood events and the statistical relationships between input parameters and flood behaviour. In this manner insight in flood patterns can be created without detailed knowledge or computations of underlying physical processes.

Cellular Automata is an empirical flood modelling approach that is frequently discussed in literature. This method uses a network of grid cells with cell specific states as function of time (Michael et al., 2016). The status of a cell (for example flood depth or velocity) is derived by a defined set of rules and the states of the neighbouring cells. Guidolin et al., (2016) describes the development of a two-dimensional cellular automata flood model which is up to 8 times faster than a traditional physically-based model, with minimal compromise in accuracy. Major advantages related to the high computational speed of the cellular automata methods are also described by Jamali et al., (2019). With respect to accuracy, the study concluded that the cellular automata technique performed very well in areas with low-laying depressions. However, in regions with larger elevation changes and associated higher water velocities, the estimation of inundation depths was limited. An additional drawback of the cellular automata approach is the inability to represent the temporal evolution of flood extent and velocity.

Other developments concerning empirical (fast) flood modelling are based on machine learning techniques. Mosavi et al., (2018) presents an overview of machine learning techniques used for flood predictions. High quality datasets representing (observed) flood and rainfall records are required for training and validating a machine learning flood model (Petty & Dhingra, 2018). Without sufficient data, there is a risk of overfitting

the flood model or creating a data bias. Another disadvantage is that machine learning approaches can be experienced as black box. This can make it challenging for decision makers to get grip on the applied algorithms in the model. (Loyola-González, 2019).

Besides divers empirical methods, there are numerous developments that focus on reducing the computation demands of physically-based flood models. An example of such a method is the usage of Graphs Processing Units (GPU), which enable parallel processing of computational tasks (Morales-Hernández et al., 2021). Another method to reduces computational demands is the application of quad tree structures. Quad tree structures allow for adaptive spatial resolutions. In this manner the resolution for the area of interest can be increased without changing the complete catchment resolution (Liang et al., 2008).

Table 1 Overview of commonly discussed flood model approaches in literature

Flood modelling approach	Advantages	Disadvantages
Physically-based flood modelling equations		
Navier-Stokes equations	-Provide fundamental representation of fluid dynamics	-High computational demands -Requires detailed and high quality input data
Saint-Venant equations	-Suitable for open-channel flow -Widely used for flood modelling	-Not suitable for 3D flood modelling -For large catchments the computation demands remain high
Boussinesq equations	-Suitable for situations with limited vertical flow, e.g. tidal waves	-Reduced accuracy for rapidly varying flood events
Physically-based spatial dynamic flood modelling approaches		
Kinematic wave approximation	-Suitable for rapid flood wave propagation simulations -Computational efficient	-Neglects momentum and inertia forces -Creates a continuous connectivity between spatial elements
Diffusive wave approximation	-Creates balance between computational efficiency and dynamic flow representation	-Ignores inertia terms -For large catchments the computation demands remain high
Dynamic wave approximation	-Suitable for simulating (highly) dynamic flood events	-High computational demands -Requires detailed and high quality input data
Methods to increase computational efficiency		
GPU parallel processing	-Reduces computational demands	-Required hardware may not always be available -Initial setup can be time consuming
Quad Tree spatial approximation structure	-Through adaptive spatial resolutions it reduces computational demands -Can capture complex floodplain geometries	-Initial setup can be time consuming
Empirical spatial dynamic flood modelling approaches		
Cellular automata	-Computational efficient	-Simplified representation of hydraulic processes -Lacks continuous flow representation
Machine learning	-Can learn from complex patterns and relationships in data	-Requires large and high quality datasets for training and validation -Can be perceived as "black box"

1.4. Outline of the thesis

This thesis is structured in eight chapters. Chapter 2 elaborates on the case-study area: the Pamba Basin in the Indian state of Kerala. A short background is given regarding the landscape and governmental structure, including the current disaster risk management organisation. Chapter 3 describes the methodology that is applied to reach the stated research objectives. This chapter also includes an overview of used data sources.

Chapter 4, 5 and 6 present the research results of the respectively sub-objectives 1, 2 and 3. In the used research setup the results of each sub-objective are used as input for the following sub-objective. The research for this thesis is highly data reliant and many of the used data sources are subject to uncertainties and limitations. To ensure a good understanding of the involved uncertainties, an extensive discussion section is given in the end of each result chapter. In this manner, the uncertainties, limitation and assumptions, related to the presented results, are discussed before using them as input for the following sub-objective. The conclusions concerning the main research objective are presented in chapter 7. Finally, recommendations for further research and suggestions regarding the applicability and development of the FFS-model are given in chapter 8.

Chapter 2: Case-study area

2.1. Introduction to Kerala state, India

Kerala state is located in the southwest of India and has a tropical monsoon climate. The state, with a population size of around 35.8 million in 2022, has a highly decentralized government structure. Firstly, there is the state government, led by the Chief Minister. Subsequently, Kerala state is divided into 14 districts all led by their own District Collector. District administration is responsible for the implementation of government policies and focusses on activities related to law and order, revenue administration, land records and public welfare. Finally, there are 1186 Local Self-Governments (LSGs), which consist of 941 Grama Panchayats, 152 Block Panchayats, 87 Municipalities and 6 Corporations (Local Self-government department, n.d.). In Kerala, LSGs are responsible for education, primary healthcare, infrastructure, public order and many other day-to-day issues. Also, disaster management is largely organized at LSG level.

Kerala is prone to a wide diversity of natural hazards such as flooding, coastal erosion, droughts and landslides. In 2005 the Disaster Management Act was declared by the government of India. This act aims for efficient management of disasters including capacity-building, disaster preparation and mitigation strategies (ENVIS, n.d.). Consequently, the Kerala State Disaster Management Authority (KSDMA) was constituted in 2007. KSDMA focuses on identification of disaster-prone areas, the planning of disaster management and the formulation of state hazard action plans. Additionally, all 14 districts have a District Disaster Management Authority (DDMA). At each DDMA office a KSDMA employee is situated.

The monsoon rainfalls have a long record in causing floods in Kerala. On an annual basis flood damages and fatalities are recorded. Table 26 in appendix A shows a record of historic flood events in Kerala derived from the EM-DAT International Disaster Database. Important to note is that all of the presented floods are covering Kerala, however part of their affected area can also be located outside of the Kerala administrative boundaries.

The 2018 flood events and triggered landslides affected 5.4 million people in their livelihoods. More than 400 lives were lost, and the government of Kerala estimated an economic loss of 33.8 million US dollars (Kieran & Hunt, 2020; Umar 2019). Additionally, in 2019 and 2020, respectively 121 and 104 flood fatalities were registered (Mishra et al., 2018; Ali & George, 2021). These statistics stress the urgent demand for action to improve flood resilience in the area.

After the extreme floods of 2018, the Rebuild Kerala Development Plan (RKDP) was composed. This plan is supported by the World Bank and aims to make Kerala resilient to future disasters by implementing a risk-informed planning strategy. To effectively implement such a strategy, hazard and risk analyses are of high importance (GNDR, 2022).

Currently, most of the flood risk reduction measures at a local level have a strong focus towards the response phase of the disaster cycle. Large size integrated physical flood mitigation actions are limited (George, 2020; Samuel & George, 2019). However, serval local authorities are active in initiatives which focus on the permanent relocation of residents and monsoon preparation, such as channel dredging.

The currently applied flood early warning system in Kerala is based on rainfall intensity forecasts and not on real-time flood modelling (Municipal Corporation of Thiruvananthapuram, 2016; Varghese, 2020). Therefore, it is challenging to take into account complex water management aspects such as the real time storing capacity of dam reservoirs and soil infiltration capacity. The weather forecasting is dominantly executed by the Indian Meteorological Department (IMD). The IMD provides warnings to districts when precipitation exceeds the 70 mm per hour. Based on the weather forecasting, KSDMA provides a color-coded warning system with the following attributes: standby (yellow), preparation (orange) and evacuation (red) (Municipal Corporation of Thiruvananthapuram, 2016). The flood warnings in Kerala are communicated by television, radio and social media. According to the research of Varghese (2019), there is a lack of technical expertise at a local level and therefor the warnings cannot be accurately interpreted. Important to note is that there are ongoing developments concerning the creation of a Flood Early Warning system on a state level.

2.2. Introduction to the study area: the Pamba River Basin

Within the South Indian state of Kerala, the Pamba River Basin is chosen as study area. Historic flood events show that it is an highly flood prone area. For this reason, the Kerala State Disaster Management Authority (KSDMA) has specified a special interest in the area. Moreover, in the NWO-DST research proposal on "Climate Downscaling for Risk-informed Planning by local authorities in Kerala (CDRIP)", the Pamba Basin is also introduced as pilot region. The CDRIP proposal aims, among other things, to provide downscaled climate variables, create localized multi-hazard risk assessments and contribute to capacity building of local authorities through a spatial decision support system.

With a length of 176 km the Pamba River starts off in the Peermade Plateau in Idukki district at a height of 1670 meter above sea level. In Alappuzha district the Pamba River flows into the Arabian Sea. The complete Pamba Basin has an area of 2235 km^2 and spreads over four districts. Figure 1 shows the landcover of the basin. In the region 80% of the annual rainfall falls during the southwest monsoon season (June-September). The average annual rainfall is approximately 2600 mm, the daily mean minimum temperature in Pamba Basin is 22.6 °C and the maximum 32.7 °C (INDIA WRIS, n.d.). Pamba Basin has high humidity with rates between 68% and 91% (ENVIS, n.d.).

Overall, the Pamba Basin can be subdivided in three regions: the highland, the midland and lowland region. Each of these regions has their own geomorphological characteristics and associated hazards. In the higher regions and midlands, the large differences in elevation creates threats for landslides and flash floods. The lower regions are at risk of river floods, saline water intrusion and coastal erosion (KSDMA, 2022).
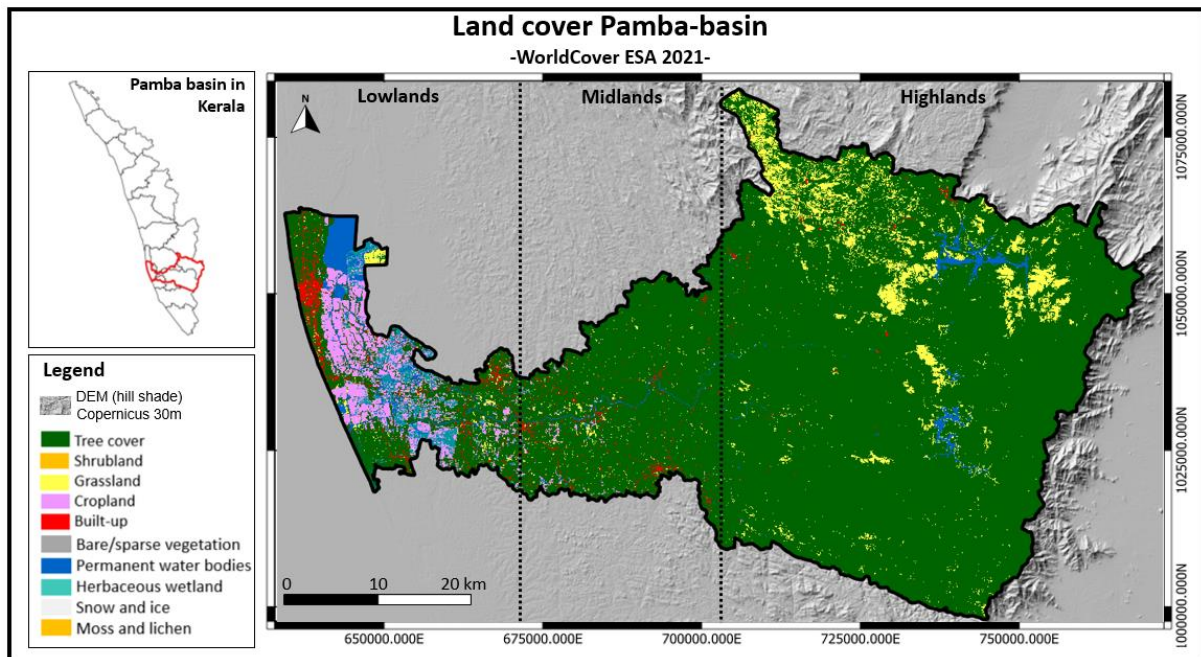
Figure 1 Landcover Pamba Basin study area (WorldCover ESA, 2021)

2.4. Historic flood events in Kerala

The historic flood records of table 26 in appendix A show the high flood prone characteristics of Kerala state. Due to its extreme nature and relative recent occurrence, most research concerning floods in Kerala focus on the August 2018 flood event. Figure 2 shows the rain- and flood affected areas in Kerala state. The dominant cause for the severe floods in 2018 was the extreme amount of rainfall. In the period between the 1st till the 19th of August, Kerala received 164% more precipitation then normal for this period of the year (Kieran & Hunt, 2020). The Central Water Commission measured an average cumulative rainfall between the 15th and 17th of August of 414 mm. According to Mishra & Shah (2018), the return period of 1, 2 and 3-day extreme rainfall during August 2018 were respectively 75, 200 and 100 years compared to the long-term record of 1901 till 2017. Moreover, the extreme rainfall in the upstream catchments of the three reservoirs (Idukki, Kakki and Periyar) had a return period of more than 500 years for 1-15 days duration.

Figure 3 shows the spatial water occurrence derived from radar imagery by the Global Surface Water opensource data initiative. It is visible that large proportions of the lower laying regions have regular water coverage. This are seasonal inundation areas caused by monsoon rainfall. The landscape and agriculture are adjusted and partly depended on these regular inundations. Additionally, figure 3 presents the drainage network, dams and available discharge measurement points in the catchment.

Due to the high precipitation volumes preceding the August 2018 rainfall, most of the reservoirs in Kerala state were already at 90% of their capacity before the extreme rainfall started. This left limited possibilities to mitigate the enormous water discharge. Sudheer et al., (2019) presents a hydrological modelling study which addresses the consequences of dam and reservoir management on the 2018 flood effects in the Periyar river basin. Overall, the paper concludes that a difference in reservoir operation would not have avoided a flood situation. The modelling study derived that 16-21% of the peak discharge could have been attenuated, if the reservoirs were emptied beforehand. Nevertheless, the study indicated a shortage of reliable extreme rainfall forecasts that is coupled with reservoir inflow predictions.

With respect to climatic influences, there is a variety of studies that analysed the relationship between the 2018 floods and climatic developments over the past decades. Mishra & Shah (2018) provide a hydro-climatological perspective using a variable infiltration capacity model (VIC). The study showed that the mean monsoon precipitation has declined over the 1951-2017 time period while the air temperature has increased. The paper does not address potential trends in rainfall intensity. Even though the precipitation during the monsoon season shows a decreasing trend over time, Krishnakumar et al., (2009) observed an increasing rainfall trend in the post-monsoon season. Nevertheless, the extreme discharge condition in

Figure 2 Rain- and flood-affected parts of Kerala during 2018 flood events (Ramasamy et al., 2019)

August 2018 exceeded the long term 95th-percentile of the 1951-2017 recordings (Mishra et al. 2018). Consequently, the article concludes that the 2018 event was likely driven by anomalous atmospheric conditions due to climate variability. This conclusion is in line with the findings of Hunt & Menon (2022).

Moreover, Hunt & Menon (2020) state that the severity of the 2018 floods would have been 18% more severe had human-induced climate change never occurred, because climate change has weakened monsoon depressions. Additionally, the research of Hunt & Menon (2022) indicates that the high impact of the 2018 flood event is partly due to the anthropogenic developments in the area such as land cover change, reservoir operation and encroachment of flood plains. These conclusions are confirmed by a study of Dixit et al., (2022).

2.5. Climate change in Kerala
Eventough the 2018 floods were likely less severe due to human-induced climate change, there is increasing evidence that climate change will increase the frequency and intensity of extreme monsoon rainfall in the future. (Hunt & Menon, 2020; Rudari et al., 2020). In an RCP 8.5 analyses for 2100, the rainfall affecting Kerala in a similar event as the 2018 floods would be 36% higher. According to Hunt & Menon (2020) this is caused by increased tropical humidity which outweighs the weakened depressions. Additionally, a study by Katzenberg et al., (2022), states that under socioeconomic pathway SSP5-8.5 extreme monsoon rainfall

events that occurred once every 5-years in the time period 1965-2015 are expected 8 times more frequently in 2050-2100.

In 2020, the CIMA research foundation composed flood hazard maps for different return periods addressing a historic and an RCP 8.5 climate scenario in Kerala. These hazard maps are currently the only available simulation-based flood hazard maps for risk-informed planning purposes in Pamba Basin. The maps in figure 38 in appendix B give insight in the large difference in flood hazard for the different scenarios. An interesting conclusion of the CIMA research is that the flood hazard map with a 500-year return period for the historic inventory, shows a smaller flood extent then a 10-year return period event in the RCP 8.5 scenario. Unfortunately, details regarding the used input data concerning river discharge or rainfall are lacking. In the internship report of Glas et al., (2022), the CIMA flood hazard maps and related uncertainties are discussed in more detail.
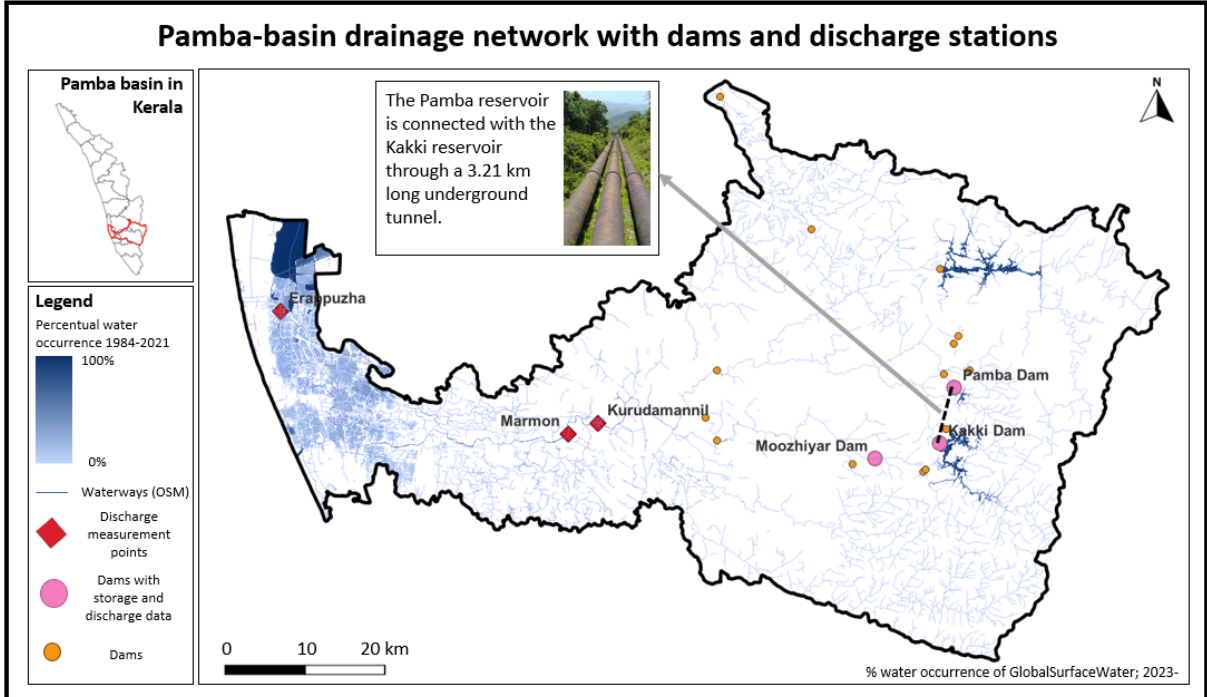
Figure 3 Pamba Basin drainage network with dams and discharge stations

2.6. Flood modelling studies Kerala

Already before the devastating events of 2018, a modelling study was done on the damaging effects of the Pamba River floods during the monsoon season (Mayaja, 2016). The study attempted to classify flood risk in 52 villages of the Pamba Basin. The main differentiation in flood risk was characterized by a variety in geospatial factors. The study revealed that areas with a high population density and recent landcover changes are more vulnerable to floods. These conclusions are substantiated by a study of Mayaja & Srinivasa (2016), who show that between 2001 and 2010 the built-up area in the Pamba Basin had a growth of 354%, especially in the downstream regions the urbanization rate was very high. In the same time period, the forest cover reduced with 14.5% and the agricultural land-use decreased by 7.73%. Anju et al., (2020) presents a research using a 1D-2D coupled model to create flood simulations of Pamba basin. It is interesting that Anju et al., (2020) makes a remark on the long computational time of the model set-up, the simulation takes more than half a day.

At the moment, only one literature source can be found that specifically addresses the simulation of potential flood mitigation measures in the Pamba Basin. This is the article of Mayaja & Srinivasa (2021), and the study elaborates on a GIS-based impact analyses concerning the revitalization of dried rivulets due to excessive human interference. In this study a HEC-RAS model is used to generate a flood plain inundation map. The scenario simulation that revitalized the two dried up rivulets showed a 20% reduction of flood inundation area. This study is an important indicator that flood mitigation measures can have a large impact on the flood risk in the area.

Chapter 3: Methodology

This chapter elaborates on the applied methodologies to reach the presented research objectives. In figure 4 a conceptual research framework of the methodology setup is presented. In the following sections the different aspects of the methodology are discussed in more detail. This chapter finalizes with a table presenting all used data sources.
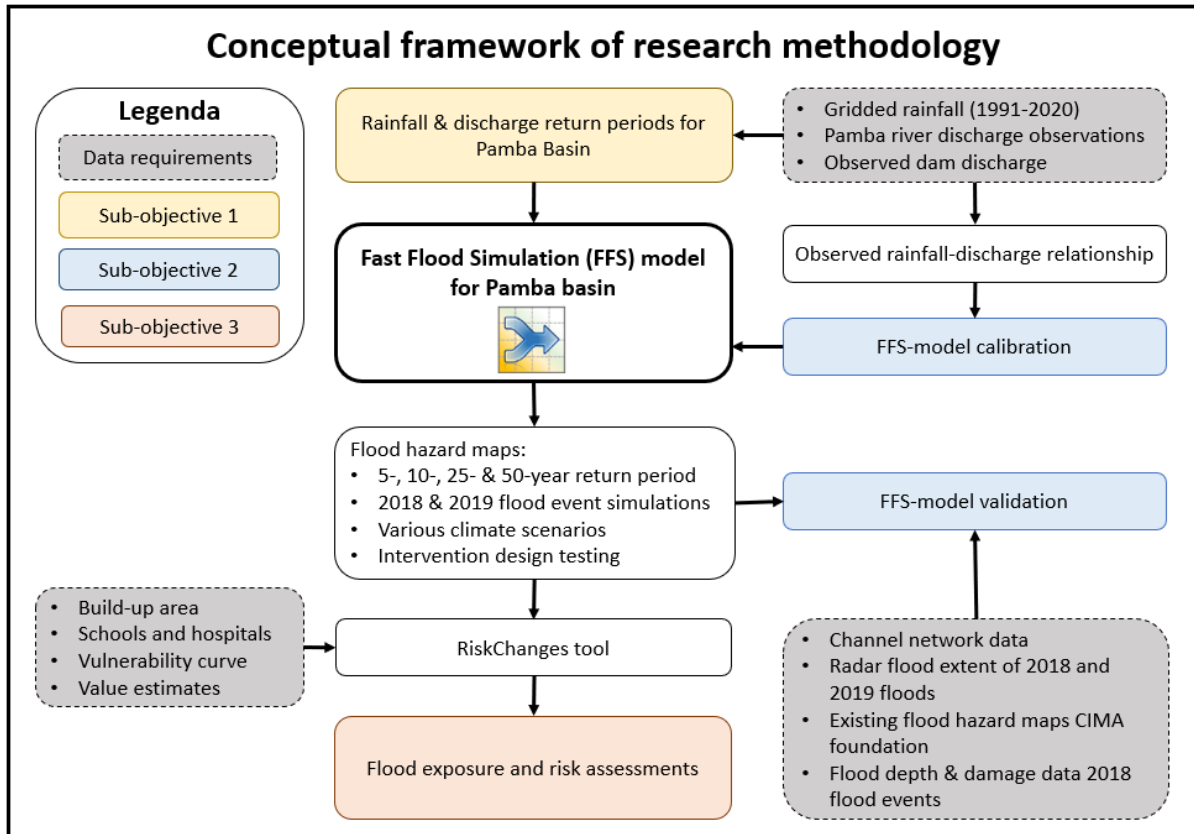
Figure 4 Conceptual framework of research methodology

3.1. Fast Flood Simulation (FFS) model

The FFS-model as presented by Bout et al. (2022) is a state-of-the-art development in the research area of rapid flood modelling. The method is based on the steady-state assumption, which concerns stabilized flow states without further change. Steady state flow heights can be solved significantly more efficiently but must be corrected later as steady-states do not occur on large scales in nature. By applying a series of algorithms, the need for dynamic simulation is avoided while maintaining a high accuracy. As data-input the model requires data representing event duration, rainfall intensity, terrain roughness end elevation. The FFS-model generates peak flow height, peak discharge and flood arrival time as output.

The applied methodology in the FFS-model can be split in four main steps, in figure 5 these steps are illustrated. The first step is the application of a steady-state flow accumulation solver. This solver creates a constant velocity field in which mass conservation is enforced. The sources of surface flow are then accumulated over this network to estimate a steady-state discharge. Using a fast-sweeping method on the velocity field, the number of required iterations is significantly reduced. The sweeping algorithm is applied to generate a monotonically increasing elevation model. The directional derivatives of this corrected elevation model directly generate a flow network. These x- and y-gradients are applied as velocity fields to accumulate precipitation and derive a spatial steady state discharge. In this first methodology step, only gravitational forces are considered for the direction of movement. In later steps of the method there is compensated for the frictional and pressure forces.

The next step in the FFS methodology is the compensation for the partial steady state. This is done by using the spatial properties of flow networks and applying a power-law distribution, catchment length and shape

parameter. By using the relative frequencies of the probability density functions of upstream pixels, the peak flow of each location can be derived. Finally, combining the peak flow with flow velocities, the effective partial steady-state confirming fraction of this catchment is determined for each location in the model.

The third step in the FFS-model is the inversed flow accumulation. The model uses an extension of Manning's law including frictional and pressure forces to estimate flow heights from the compensated steady-state discharge.

The final step is the adaptive solver to refine pressure-driven inundation based on adapted discharge-conserving diffusive wave equations. A momentum balance which is based on the Darcy-Weisbach friction law and a linearized gravity term is described. The diffusive wave solver includes gravity, friction, pressure and advection influences and ignores inertial terms.
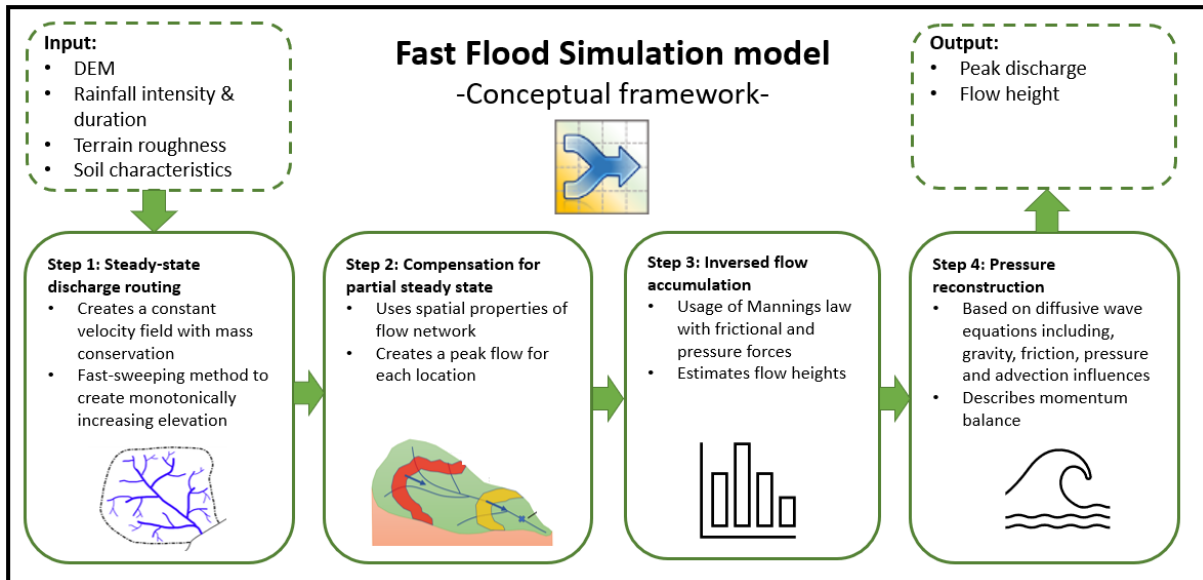
Figure 5 Conceptual framework FFS-model

3.2. Rainfall and discharge analyses

KSDMA has provided daily gridded rainfall data (IMD4) for the whole of India over a timeseries of 1991-2020 with a resolution of approximately 28 km. The paper of Pai et al., (2013) describes the applied methodology used in the development of this dataset. For the India scale dataset information 6995 gauge stations were used. The dataset was subsequently compared with other existing rainfall data sets and this showed similar climatological rainfall features. Moreover, heavy rainfall events were presented more realistically due to the increased spatial resolution and higher density of used rainfall stations.

In figure 6 the rainfall grid set-up for the Pamba Basin is presented. Within this figure also an area distribution of the catchment is indicated. Additionally, KSDMA has provided discharge data for three measurement points along the Pamba river (figure 3). The discharge data of Marmon contains a timeseries of 2016 till 2020, and for Erappuzha and Kurudamannil from 1978 till 2020, although the discharge observation records have quite some missing data. The Erappuzha time series misses 37.3% of its values, Marmon and Kurudamannil respectively 8.5% and 4.2%.

The Gumbel analyses method was applied to derive rainfall and discharge return periods per grid cell. First the maximum rainfall and discharge values per year were identified and sorted in size from low to high. Every value is linked to a rank, with 1 representing the highest value. Subsequently, the Gumbel equations as presented in equation 1 and 2 were applied.

$$\text{Eq 1: } P_{\text{Theoretical}}(x) = \exp\left(-\exp\left(-\frac{x-u}{\alpha}\right)\right)$$

$$\text{Eq 2: } T_p(x) = \left(\frac{1}{1-P(x)}\right)$$

Where:
x = observed annual maxima data point
$\bar{x}$ = average of observed annual maxima
N = Number of annual maxima observations
$i = Rank\ of\ specific\ obsrevation\ (i = 1\ being\ the\ largest\ and\ i = N\ the\ smallest)$
$u = \bar{x} - 0.5772\alpha$

$$\alpha = \frac{\sqrt{6}s_x}{\pi}$$

$$s_x^2 = \frac{1}{(n-1)}\sum_{i=1}^{n}(x_i - \bar{x})^2$$

With the derived return periods per annual maxima a graph was fitted, and the expected return period rainfall and discharges were derived. An area weighted average was used to derive return period rainfall events for the complete Pamba Basin.

Gridcell	Percentage of Pamba basin surface within grid cell
A	0.03%
B	3.30%
C	0.23%
D	3.29%
E	4.17%
F	7.15%
G	17.79%
H	15.12%
I	0.51%
J	0.12%
K	7.76%
L	10.46%
M	16.74%
N	11.66%
O	0.42%
P	1.27%
Total	100.0%
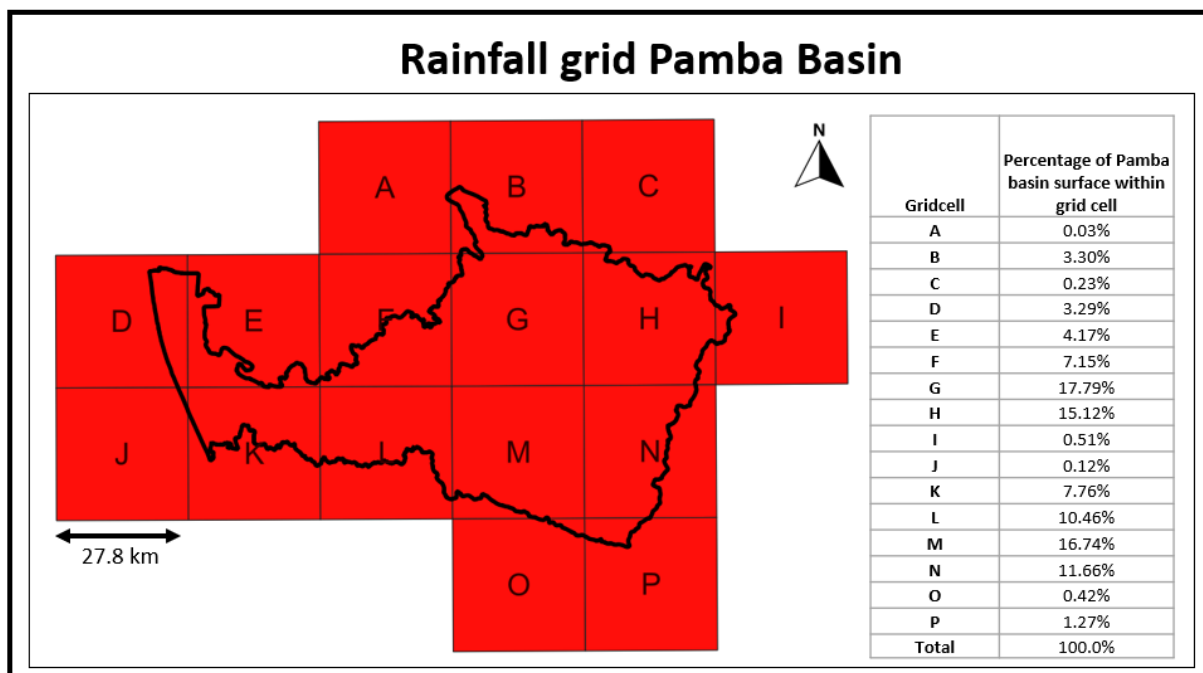
Figure 6 Rainfall grid Pamba Basin

3.2.1. Climatic analyses

For risk-informed planning purposes it is of value to incorporate the effects of climate change on flood hazard. Originally, the idea was to use downscaled climate scenarios of the Pamba Basin generated by the Dutch meteorological institute (KNMI). Unfortunately, this research got delayed and detailed climatic data is not (yet) available. Conducting a detailed climate change assessment for Pamba Basin is beyond the scope of this research. Nevertheless, it is considered of additional value to analyse to what extent the FFS-model is an applicable tool to reflect on the effects of climate change on flood hazard and risks.

As method to evaluate on the effects of climate change, rainfall multipliers were selected. These rainfall multipliers were generated by dr. B van den Bout for a project titled "Flood Modelling and Flood Hazard Assessment for districts in selected River Basins in Bangladesh, Nepal and Pakistan", carried out in collaboration with ADPC for the World Bank.

During this project rainfall multipliers were composed on a global scale. Table 2 shows the rainfall multipliers for Pamba Basin for a return period event of 10 years. To produce the rainfall multipliers the method as described by Li et al., (2021) has been used. The five daily global rainfall CMIP5 data layers available from Copernicus were downloaded for the RCP 4.5 and RCP 8.5 climate scenarios. Subsequently, time intervals of 20 years were constructed representing the time thresholds of 2025, 2050 and 2075. For

these time intervals the average rainfall multiplier from the five CMIP5 models was derived and used as 10-year return period rainfall multiplier.

To analyse the effects of climate change of flood hazard, the resulting flood hazard maps were analysed on difference in flood depth. Moreover, a water volume comparison was executed in which the sum of all raster depth values was multiplied with the raster cell size. Using this approach, it is possible to analyse what effects a percentual change in rainfall has on the total hazardous water volume. Finally, the composed hazard maps using the FFS-model were compared with the CIMA climate scenarios.

Table 2 Rainfall multipliers Pamba Basin for 10-year return period derived from CMIP5 data

Climate scenario	Rainfall multiplier
2025 RCP 4.5	0.97
2050 RCP 4.5	1.11
2075 RCP 4.5	1.01
2025 RCP 8.5	1.05
2050 RCP 8.5	1.06
2075 RCP 8.5	1.39

3.3. Calibration

The FFS-model used in this research is opensource available on the fastflood.org website. In section 3.1 an elaboration is given on the technical model structure. The philosophy of the FFS-model is that all required input layers can be downloaded from opensource data platforms with a global coverage. For higher resolution analyses on a local level, more detailed input layers can be imported. In table 3 the data layers included in the FFS-model are stated.

Table 3 Data input for FFS-model

Required data input for FFS-model	Description
Elevation	Digital Elevation Model (DEM), downloaded from Copernicus GLO-30 with a resolution of 30 meter. For the analyses of the complete Pamba Basin the DEM is rescaled to 150 meters to reduce computational demands.
Land Cover	Sentinel-2 based WorldCover on 10-meter resolution is applied for which fastflood.org automatically derives Manning Coefficients per land-use class.
Infiltration	Fastflood.org uses data from Soilgrids.org for a depth of 5-15 cm and estimates the infiltration rates using the Saxton et al., pedotransfer functions which are automatically processed in the FFS-model set-up.
Rainfall	Rainfall data can be included as raster rainfall intensity map or as single rainfall intensity thresholds.

Calibration of the FFS-model was done by modifying a number of parameters. In total the FFS-model includes five calibration parameters; a multiplier for the Manning coefficient as well as the infiltration rate, the baseflow condition, discharge diffusivity and concentration speed multiplier. Important to note is that for a large catchment area with variating landscape characteristics, such as Pamba Basin, the solver accuracy in the FFS-model needs to be set on "Very High". A high solver accuracy increases the amount of iterations of the fast sweeping algorithm in the FFS-model setup.

In sub-objective 1 of this research, a rainfall-discharge relationship was derived for Pamba Basin. The goal was to modify the calibration parameters in such a manner that the observed rainfall-discharge relationship was represented by the FFS-model. For the calibration six historic peak events were selected, see table 4. All six events are relatively recent to ensure similar land-use conditions as in the current situation. Moreover, the six scenarios were selected based on the criteria that the observed rainfall and discharge data is practically complete. The discharge measurement point at Kurudamannil was chosen as focus point for the calibration efforts because it has the most complete data string and a position in the main river channel.

Table 4 Calibration scenarios for fast flood model

Peak events	Area weighted average cumulative rainfall in Pamba Basin				Peak discharge		
Date	1-day (mm)	3-day (mm)	5-day (mm)	7-day (mm)	Discharge Erappuzha (m3/s)	Discharge Marmon (m3/s)	Discharge Kurudamannil (m3/s)
27-6-2017	56.1	108.1	130.3	135.5	312.9	527.0	627.7
18-9-2017	52.0	107.1	171.0	186.1	372.9	633.9	846.6
11-8-2018	4.4	132.5	181.5	183.6	314.8	1080.8	866.2
9-8-2019	93.5	192.0	225.1	233.3	379.5	Missing value	1360.3
8-8-2020	63.7	156.7	222.6	257.2	815.4	1041.5	1028.3
22-9-2020	33.5	93.1	115.9	130.2	427.7	658.6	610.0

To analyse the model performance the Nash-Sutcliffe Efficiency coefficient (NSE) and the percent bias (PBIAS) was used. The NSE can be derived using equation 3 and the PBIAS with equation 4. With these performance indicators a wide variety of calibration combinations were compared. The final chosen calibration setting is the combination with the highest NSE performance and a PBIAS approximating 0. Subsequently, the performance of the selected calibration setting was tested by analysing whether the derived return period rainfall threshold led to simulated discharges that closely match the derived return period discharges obtained from observed data.

$$\text{Equation 3:} \quad NSE = 1 - \frac{\sum_{t=1}^{T}(Q_o^t - Q_m^t)^2}{\sum_{t=1}^{T}(Q_o^t - \overline{Q_o})^2}$$

$$\text{Equation 4:} \quad PBIAS = 100 \frac{\sum_{t=1}^{T}(Q_m^t - Q_o^t)}{\sum_{t=1}^{T} Q_o^t}$$

Where:
Q_o^t = observed discharge at time t
Q_m^t = modelled discharge at time t
$\overline{Q_o}$ = mean of the observed discharges
T = Total amount of selected calibration scenarios

3.4. Validation

The calibration of the FFS-model focussed on approximating the observed rainfall-discharge relationships in Pamba Basin. To validate the selected calibration settings, a variation of methods was used. Figure 7 shows a conceptual framework of the validation research methodology.

Firstly, the flow network, as automatically derived by the FFS-model, was compared with aerial photographs to ensure that network follows the actual river pattern. Subsequently, the rainfall events that led to the Kerala floods in August 2018 and 2019 were simulated using the FFS-model. The simulated flood extents were compared with observed flood extents, derived from Sentinel-1 radar imagery. Additionally, the flood hazard data of the 2018 floods was compared with crowdsourced flood depth and damage data. Finally, the flood hazard maps of the FFS-model were compared with the return period hazard maps as generated by the CIMA research foundation.

To reconstruct the flood extents of the 2018 and 2019 events, the opensource Google Earth Engine (GEE) software was used. The UN Office for Outer Space Affairs provides via their UN-SPIDER knowledge Portal a script that enables flood extent mapping using Sentinel-1 data. By modifying this script for the Pamba Basin, flood extent data was obtained.

Figure 3 shows that large areas in the downstream region of Pamba Basin are subject to seasonal inundation. These areas are not considered as flood extent, however they are included in the water extent. For this reason, the GGE flood extent data has been merged with all areas that have a percentual water occurrence of more than 5%. The resulting binary water extent raster layer is uploaded into the FFS-model and the interface calibration tool is used to derive the Cohens kappa and percentual accuracy as performance indicators.

Conceptual framework of validation research methodology

Observed 72h peak rainfall intensities 2018 & 2019 floods

72h rainfall intensities for various return periods

Calibrated FFS-model for Pamba basin

Simulated flood hazard maps of 2018 & 2019 flood event

Flood hazard maps for different return periods

Validation approaches

Flow pattern validation
Compare the automatic generated flow network of FFS-model with arial photographs

Flood extent validation
Compare simulated flood extent with radar-based flood extent data of 2018 and 2019 flood events

Validation through flood attributes
Correlate the 2018 simulation results with observed flood depth and damage data

CIMA comparison
Compare the hazard maps of the FFS-model with the hazard maps of the CIMA foundation

Figure 7 Conceptual framework of validation research methodology

Water extent validation regions for Pamba basin

Pamba basin in Kerala

N

5.

4.

2.

1.

3.

Legend

Digital elevation model

0   10   20 km
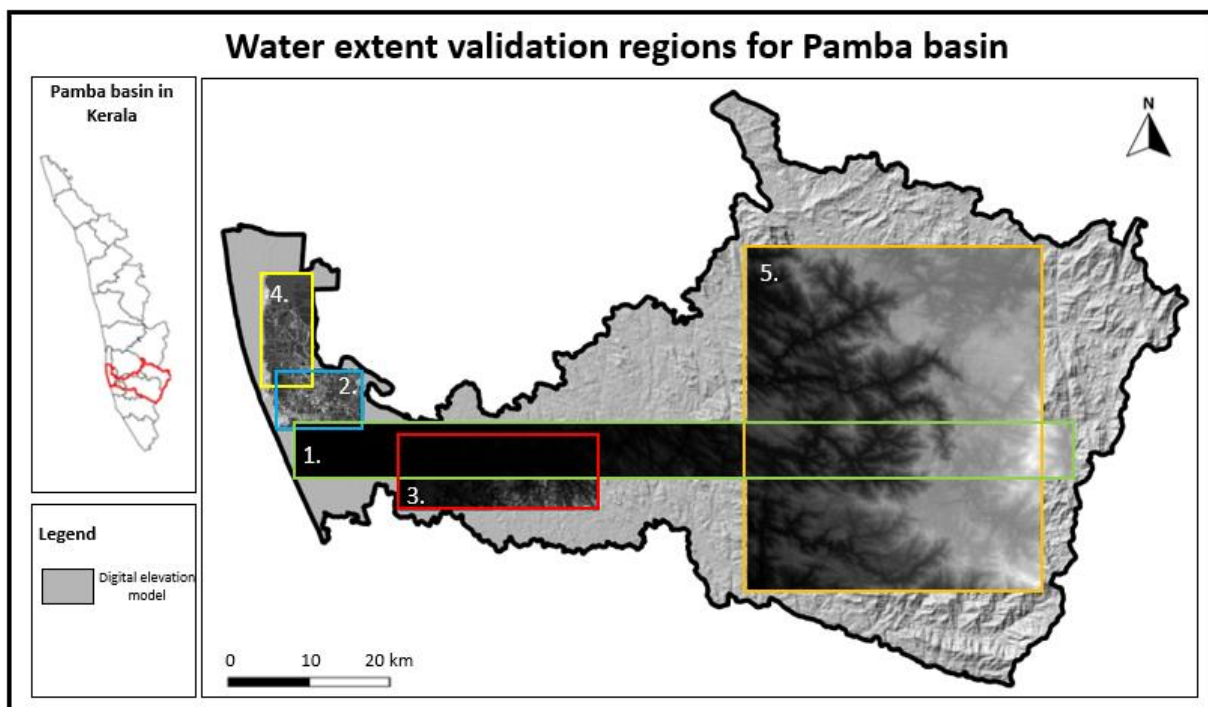
Figure 8 Water extent validation regions for Pamba Basin

To compare the radar-derived water extent of the 2018 and 2019 floods with the simulation data, the event conditions were represented in the model input parameters. Figure 39 in Appendix C shows the used the rainfall intensity maps of the 2018 and 2019 flood events. For these simulations the 72-hour cumulative peak rainfall was derived and subsequently used as uniformly distributed rainfall intensity. Moreover, the baseflow condition was determined by averaging the three preceding days of discharge before the peak event. In August 2018 the discharge measurement equipment broke down, therefore an extreme base discharge threshold of 640 m^3/s was used. See section 3.3 for an elaboration regarding the quantification of this base flow setting. Dam discharges and storages were not included in the simulation attempts of the

2018 and 2019 floods. This decision was made based on the observation that dam discharges are not correlating with rainfall intensities. Consequently, the choice was made to not include dam discharges in the return period flood maps. The 2018 and 2019 flood simulations were used as validation attempts for these flood maps, therefor dam discharge and storage was not incorporated in these event flood simulations. For a more extensive elaboration regarding the role of dams in the Pamba basin see section 4.3.

The complete flood simulation was executed with a resolution of 150 meter. However, for the flood extent performance analyses the upscaling ability of the FFS-model was used to compile a resolution of 30 meters. Figure 8 shows the used validation regions. Additionally, the flood extent analyses was executed for three case-study local self-governments (LSGs) namely, Aranmula, Edathua and Pandanad, see figure 9. These case-study areas were selected in collaboration with KSDMA and represent different types of landscapes in the mid- and lowlands of the Pamba Basin. The three case-study areas were also used for the flood risk assessment as discussed in section 3.5.
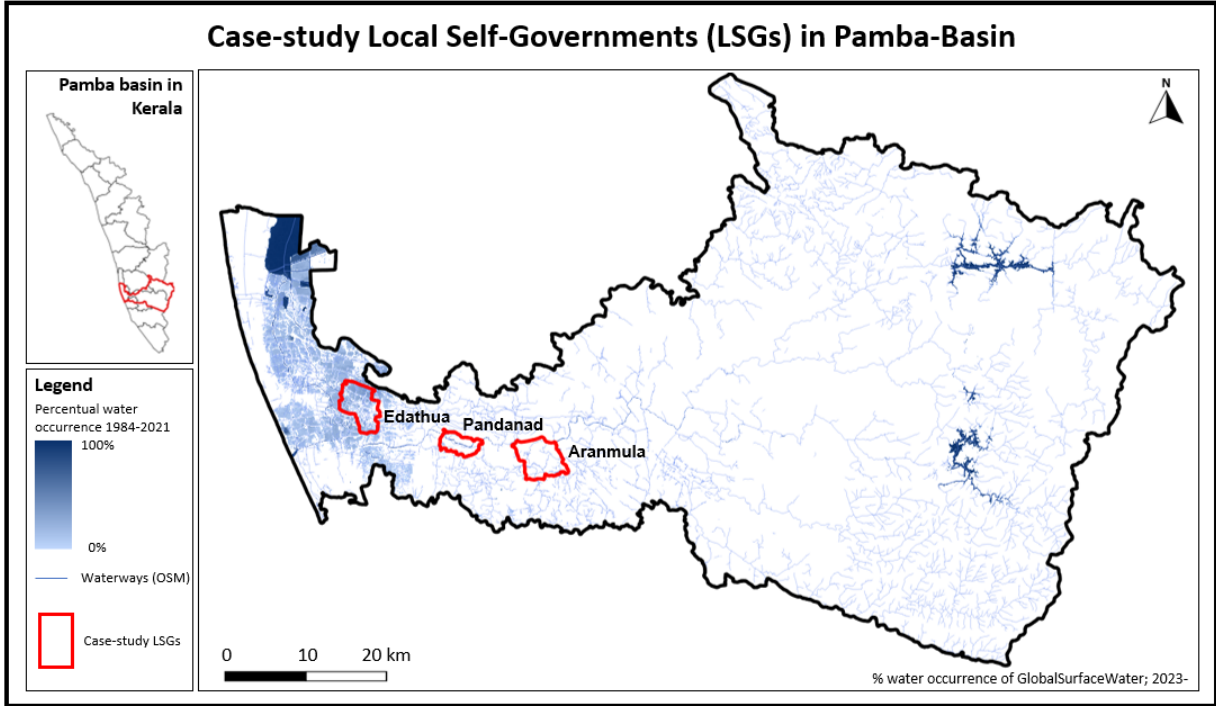
Figure 9 Case-study Local Self-Governments (LSGs) in Pamba Basin

3.5. Flood risk assessment using the RiskChanges tool

Flood risk was derived by integrating flood hazard for different return periods with element-at-risk and vulnerability data. By multiplying element-at-risk exposure with vulnerability, loss can be defined. The combination of loss with the temporal probability of a hazard, defines the final flood risk. For this research the choice was made to analyse the flood exposure of schools and hospitals for the complete Pamba Basin. Furthermore, for Edathua, Pandanad and Aranmula LSGs, see figure 9, a complete flood risk assessment for built-up area is composed.

The FFS-model was used to generate LSG specific flood hazard maps. These maps with return periods of 5, 10, 25 and 50 years have a resolution of 30 meters and were created using the FFS-model upscaling tool. To create these hazard maps, modified rainfall intensity maps were used. In these rainfall intensity maps, all grid cells retain their area weighted return period rainfall, as derived in the first research objective. However, the rainfall in the grid cell(s) covering the case-study LSG was adjusted to the return period rainfall linked to that specific location.

For the flood exposure and risk study, the water depth was taken as flood intensity attribute. The flood hazard maps were subsequently uploaded in the RiskChanges software. RiskChanges is an opensource spatial decision support tool for the analyses of (multi)hazard risks and can be found on the riskchanges.org website. Within the RiskChanges tool it is possible to upload hazard maps, element-at-risk data and

vulnerability curves. The calculation tool derives the associated exposure, loss and risks. Furthermore, the website has multiuser functionalities in which it is possible to collaboratively work on the same project. When composing a variation of exposure and risk scenarios, the tool includes features to compare hazard exposure and risks. This is of value when analysing different planning alternatives and future scenarios.

Element-at-risk data for the Pamba Basin are limited. Available data sets of KSDMA were used for schools and hospitals. For the building exposure the World Settlement Footprint of 2019 and the built-up area classicisation of the 2021 ESA WorldCover data were considered. When comparing these data sets with arial photographs, it was visible that both have a good accuracy, but are quite incomplete. To optimize the completeness of the building data, the choice was made to merge the data layers and use that output as a built-up area map. To do this the World Settlement Footprint data is first converted from raster to vector. Subsequently, this layer is merged with the ESA vector layer of built-up area. The resulting vector layer was uploaded in the RiskChanges software for the exposure analyses.

To analyse the population exposure, first the available 2011 population statistics per LSG were compared with the opensource WorldPop counts of 2020. As quantified in section 6.4, the WorldPop data led to lower population statistics then the KSDMA population data. This is questionable because local experts did not observe a drop in population over the past years. Therefore, the choice was made to use the KSDMA population data in the exposure analyses. To derive the population exposure the population per LSG was divided equally over all built-up area cells of that administrative unit.

An additional input requirement for a flood risk assessment are vulnerability curves. There are currently no area specific vulnerability curves available which are validated for the Pamba Basin or Kerala. In the internship report of Glas et al., (2022) research attempts to create a vulnerability curve based on the 2018 and 2019 building damage data in Pamba Basin are described. This research concluded that no validated vulnerability curve could be constructed due to the large range of uncertainties related to the available damage data. For the research described in this report, a vulnerability curve based on literature seemed the most logical choice.

JRC (2017) created vulnerability curves for different continents. When discussing the construction of a vulnerability curve of residential buildings in Asia with local experts, their opinion was that the vulnerability values were estimated too high for the Pamba Basin. Therefor an adjusted vulnerability curve was composed which integrates local expert insights. Also, the loss estimation for this research was based on local expert insights. To put the final composed flood loss and risk results in perspective, they were compared with the financial aid distributed by the Kerala government to households after the 2018 floods.

3.6. Intervention simulation

The FFS-model includes options to analyse the effects of flood mitigation measures on flood hazards. The core of this functionally is the possibility to draw different shapes on the map and change the elevation height of the designed features, by adjusting the DEM, water flow patterns change and consequently the flood hazard maps. Important to note is that the intervention adjustments need to be made in the main FFS-model structure and not in the scaled-up area function. In the scale-up function, water is only redistributed over a higher resolution DEM. Mitigation design in a scale-up map will therefore not adjust the actual water flow patterns. Consequently, there were challenges related to the resolution of the flood hazard simulations. Intervention designs have minimally the size of one grid cell in the applied DEM.

For mitigation testing it is important to run the flood model with the highest resolution possible. Consequently, the choice was made to do mitigation testing on LSG level with a resolution of 30 meter. To incorporate water discharge originating from surrounding areas, a river boundary condition was applied in the most upstream river location of the specified LSG. The quantification of this river discharge condition was determined by running the 150-meter flood hazard simulation for the complete Pamba Basin and determining the associated river discharge at the same location. To ensure that all water, from the discharge boundary condition, flows in the downstream direction a manual elevation increase of 10 meters was created upstream of the discharge boundary condition.

In the scope of this research, the main goal of intervention testing was to evaluate on the functionality of the FFS-model to analyse the effects of measures on flood hazard and risks. For this proof of concept, a river area in Pandanad LSG was used as case study area. This area was selected based on the criteria that it

shows a high exposure of buildings to flood hazard. Additionally, the landscape of this area is quite similar to many other areas around the Pamba river. The flood exposure analyses were executed for a 50-year return period.

For the intervention design testing three different engineering options were compared with a relocation option. As engineering interventions, a dike construction, a floodplain construction and river dredging were considered. The RiskChanges software was used to compare the flood exposure results across various intervention designs.

3.7. Data usage

In table 5 the used datasets for the different methodology steps are presented. Per dataset a short description is given regarding the application and the data source.

Table 5 Datasets used in research methodology

Used data	Application	Source
Historical record of rainfall data for Pamba Basin	Used in Gumbel analyses for return period rainfall thresholds	KSDMA, generated using the method as described by (Pai et al., 2014)
Discharge data Pamba river	Calibration of the flood model	KSDMA
Climate scenario rainfall multipliers	To analyse flood hazard under a changing climate	Previous research managed by Dr. B van den Bout using CMIP5 data and the method described by Li et al., (2021)
Historical records of dam outflow data in Pamba Basin	Analyse the effects of dam discharge on base flow conditions	Subtracted from the HEC-hms model that was shared by the local flood modelling team in Kerala.
Flood extent data of the 2018 and 2019 flood events in Kerala	Validation of FFS-model	Opensource Google Earth Engine sentinel-1 radar imagery derived using the advised methodology of the Office of Outer Space Affairs of the UN
House damage data of 2018 floods	Validation of FFS-model	KSDMA
Crowd sources flood depth data of the 2018 floods	Validation of FFS-model	KSMDA
Return period flood hazard maps derived by a conventional flood model.	Comparative analyses with FFS-model output	CIMA research foundation (2020)
Spatial percentual water occurrence	Used to merge with flood extent data to analyse validity of FFS-model results	Opensource data provided by the European commission in the Global Surface Water Explorer platform.
Schools and hospitals	Exposure analyses	KSDMA (2019)
Landcover data	Used to detect built-up areas as element-at-risk data	Opensource ESA WorldCover on 10-meter resolution (2021)
Settlement Footprint	Used to detect built-up areas as element-at-risk data	Opensource World Settlement Footprint composed by the ESA and German Aerospace Centre (DLR), (2019)
Population counts per LSG	Population exposure analyses	KSDMA (2011)
Gridded population data	Population exposure analyses	Opensource WorldPop hub (2020)

Chapter 4: Results: rainfall and discharge analyses

The first sub-objective aims to create rainfall and discharge-related return periods for the Pamba Basin (See section 3.2). This chapter presents the results, and discusses the uncertainties and limitations. The results of this first research objective are used as input for the next research phase in which observed rainfall and discharge data is used to calibrate the FFS-model.

4.1. Rainfall analyses

This section presents the results of the rainfall Gumbel analyses. The Gumbel analyses is applied for daily rainfall as well as 3-day and 7-day cumulative rainfall, because floods are often associated with a high cumulative rainfall occurrence rather than an independent rainfall peak. In figure 10 the Gumbel analyses for the three-day cumulative rainfall return period relationship is presented per rainfall grid cell. In figure 40 and 41 in appendix D the graphs for daily and weekly rainfall are shown.
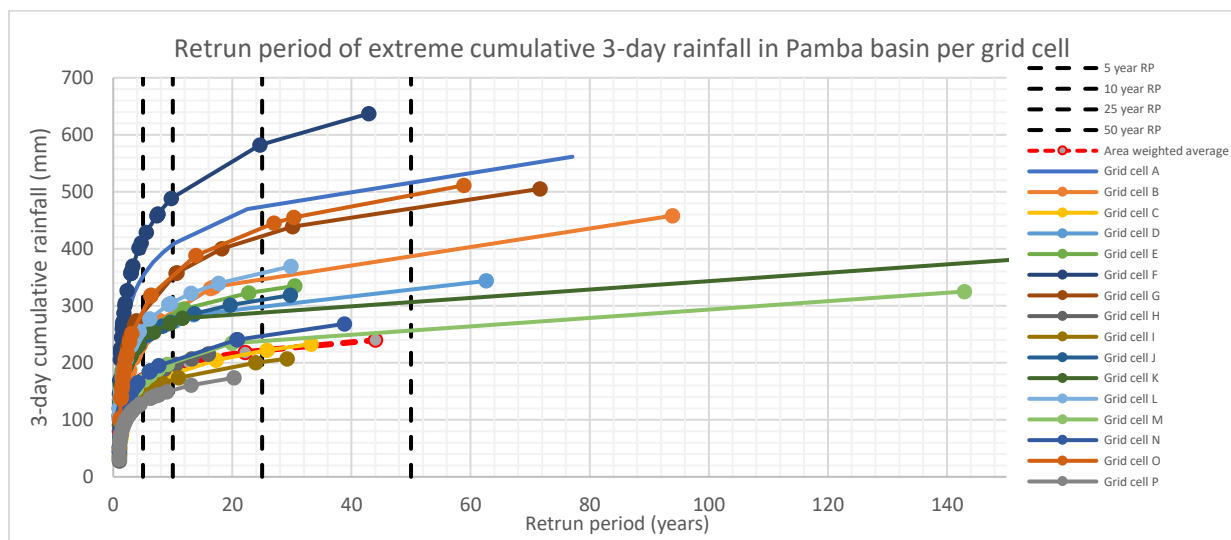
Figure 10 Return period of extreme cumulative 3-day rainfall in Pamba Basin per grid cell.

The presented graphs show some interesting characteristics concerning rainfall behaviour in the Pamba Basin. Firstly, there is an enormous variability of extreme rainfall return periods in between grid cells, sometimes up to 300%. The northern midland region of the study area shows the largest rainfall volumes, and the southern more upstream area the smallest amounts.

Moreover, it is visible that the graph length, representing return period, highly differs per grid cell. This is a consequence of the variability and occurrence of extreme annual rainfall statistics in the available data set. The rule of thumb is that return periods up to a length of twice the timeseries length can be derived using a Gumbel analyses (El Adlouni & Ouarda, 2010). For this reason, the choice is made to derive return periods up to 50 years. For the scenarios in which the area weighted average return period graph does not reach the 50 years intersection point, a logical interpretation of graph prolongation is made.

An additional observation is that the area weighted average rainfall over the study area is relatively low compared to the individual grid cell characteristics. This can be explained by the fact that the chance that extreme rainfall occurs in one specified region is larger than the chance that the whole catchment experiences extreme rainfall simultaneously.

Based in the presented Gumbel analyses over the historic timeseries of 1991 till 2020, area weighted rainfall return periods are derived for Pamba Basin, see table 6. Additionally, table 7 present the 72h return period rainfall for the grid cells covering the three case-study LSGs.

Table 6 Area weighted extreme rainfall in Pamba Basin

Return period (year)	daily rainfall (mm)	mm/h	3-day rainfall (mm)	mm/h	7-day rainfall (mm)	mm/h
5	90	3.75	170	2.36	255	1.52
10	105	4.38	193	2.68	290	1.73

25	120	5.00	221	3.07	322	1.92
50	130	5.42	245	3.40	365	2.17

Table 7 Extreme rainfall statistics for grid cells associated to the case-study LSGs

Return period (year)	Grid cell L (Aranmula) return period rainfall (mm/h) 72h	Grid cell K (Pandanad & Edathua) return period rainfall (mm/h) 72h	Grid cell E (Edathua) return period rainfall (mm/h) 72h
5	3.68	3.31	3.58
10	4.24	3.75	3.96
25	4.96	3.94	4.51
50	5.21	4.22	4.86

4.1.1. Rainfall for different climate scenarios

The rainfall multipliers, as discussed in section 3.2.1, are used to determine return period rainfall for different climate scenarios. The rainfall multipliers are composed for 10-year return period events. Consequently, only the effects of 10-year return period rainfall are presented in table 8. It is important to consider that the rainfall multipliers are an average of different climate models, which show a large variability.

It can be observed that, under the RCP 4.5 scenario, there is an initial minor decline in extreme rainfall quantifications by 2025. Subsequently, the climate scenarios indicate a gradual increase leading up to 2050, eventually resulting in a distribution of rainfall similar to the present situation around 2075. The RCP 8.5 analyses shows a gradual increase in extreme rainfall over the first decades. For 2050 the RCP 8.5 prospect is less high than the RCP 4.5 threshold. Towards 2075 the extreme rainfall statistics significantly increases with almost 40% compared to the historic derived return period rain. For the 2075 the difference between the RCP 4.5 and RCP 8.5 scenarios is very significant.

Table 8 Rainfall intensities with a return period of 10 years for different climate scenarios

	Rainfall multiplier	daily rainfall (mm)	mm/h	3-day rainfall (mm)	mm/h	7-day rainfall (mm)	mm/h
Historic		105.0	4.38	193	2.68	290	1.73
2025 RCP 4.5	0.97	101.9	4.24	187	2.60	281	1.67
2050 RCP 4.5	1.11	116.6	4.86	214	2.98	322	1.92
2075 RCP 4.5	1.01	106.1	4.42	195	2.71	293	1.74
2025 RCP 8.5	1.05	110.3	4.59	203	2.81	305	1.81
2050 RCP 8.5	1.06	111.3	4.64	205	2.84	307	1.83
2075 RCP 8.5	1.39	146.0	6.08	268	3.73	403	2.40

4.2. River discharge analyses

Similar as for the rainfall analyses, discharge return periods are derived for the three measurement points in the Pamba river, see figure 3. In figure 11 the discharge return period graphs are presented and table 9 displays the associated return periods. For Marmon it was not possible to derive return period discharges for more than 5 years because the available timeseries only includes data from 2016 till 2020.

As stated in section 3.2, the discharge observations are subject to many missing data values. For example, during the floods in August 2018, the discharge measurement equipment likely broke down. Consequently, no discharge data is available for the largest peaks. The reason for numerous missing values at other time instances remain unknown. Nevertheless, when missing values are associated with large river discharges it is possible that the discharge return periods are underestimated.

Moreover, an interesting observation is the significant smaller discharges at the downstream located Erappuzha compared to the other two measurement points. An explanation is that in the lower laying delta of Pamba river, the main river splits-up in various side branches. The Erappuzha discharge measurement point is positioned in one of these side branches.
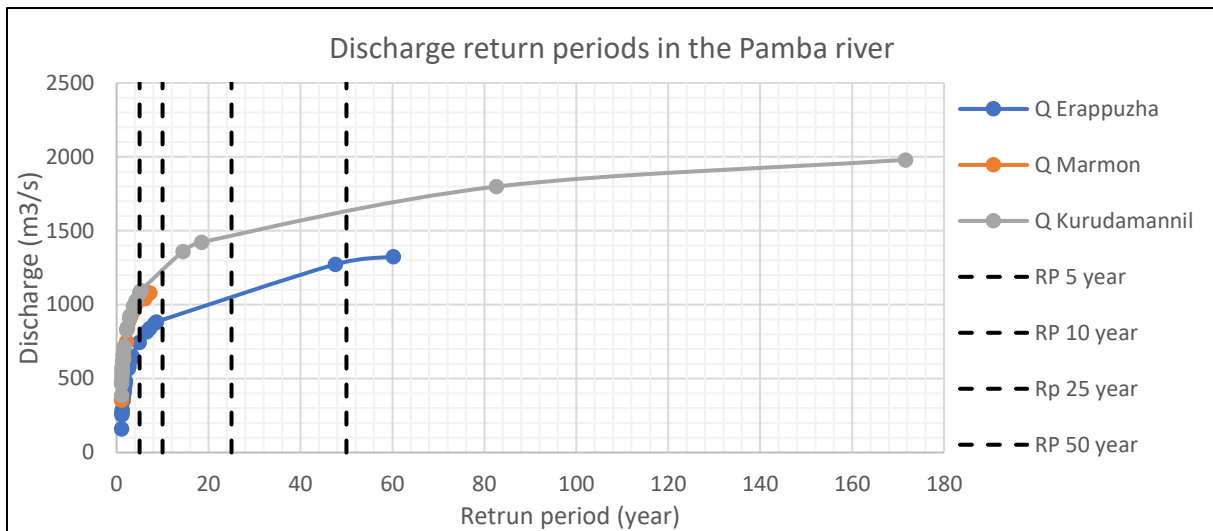
Figure 11 Discharge return periods in the Pamba River

Table 9 Discharge for different return periods in the Pamba river

Return period (years)	Discharge Erappuzha (m³/s)	Discharge Marmon (m³/s)	Discharge Kurudamannil (m³/s)
5	740	970	1090
10	900		1240
25	1050		1470
50	1300		1630

4.3. Dam discharge analyses

Within in the Pamba Basin several dams are located, see figure 3. For the Moozhiyar dam, the Pamba dam and the Kakki dam, discharge data is available. Interesting is that the Pamba and Kakki reservoirs are connected through an underground tunnel of 3.21 km. Water from the Pamba reservoir flows towards the Kakki reservoir where a large powerplant is situated. The available dam data is analysed to research in which manner reservoir management can be included in the FFS-model set-up.

Starting with the Kakki dam, figure 12 shows the available observed discharges and reservoir water level data. Most of the time, all discharge flows through the power tunnel. This discharge is on average 26.5 m³/s with minimum and maximum values of 4.4 m³/s and 47.8 m³/s. The water level in the Kakki reservoir variates between approximate 920 and 980 meter. The record shows four periods in time with discharge through the spill. By far the largest spill discharge was on the 16th of august 2018, during the large Kerala floods. At that time more than 800 m³/s was discharged through the spillway.

An analysis is made regarding the correlation of total dam discharge (power tunnel + spillway) and cumulative rainfall. This is done for the area averaged cumulative rainfall and the cumulative rainfall for grid cell N (see figure 6) which is the region upstream of the Kakki dam.

The two upper scatter plots of figure 13 do not show a correlation between cumulative rainfall and dam discharge. Also, the bottom scatterplots in figure 13, that represent the relationship between cumulative rainfall and water level in the Kakki reservoir, do not result in a clear correlating pattern. It is visible that the largest cumulative rainfall measurements are associated with higher water stages. However, this is likely caused by seasonally and not directly linked to the cumulative rainfall.

Overall, it is quite remarkable that no clear relationship can be established between dam discharge, water levels and rainfall observations. A local modelling expert from Kerala explained that the dam discharges of Kakki dam is dominantly based on electricity demand, not rainfall or discharge patterns. This explains the lack of correlation but leads to challenges in integrating reservoir management in flood modelling studies. Without insight in dam discharge strategies, it is not possible to determine a substantiated probability density function that presents dam discharges related to extreme rainfall events. For this reason, the choice is made not to include dam storage capacities or discharges in the FFS-model set-up. Without the inclusions of dams, all rainfall upstream from the dam locations is naturally flowing into the flow network of the catchment.
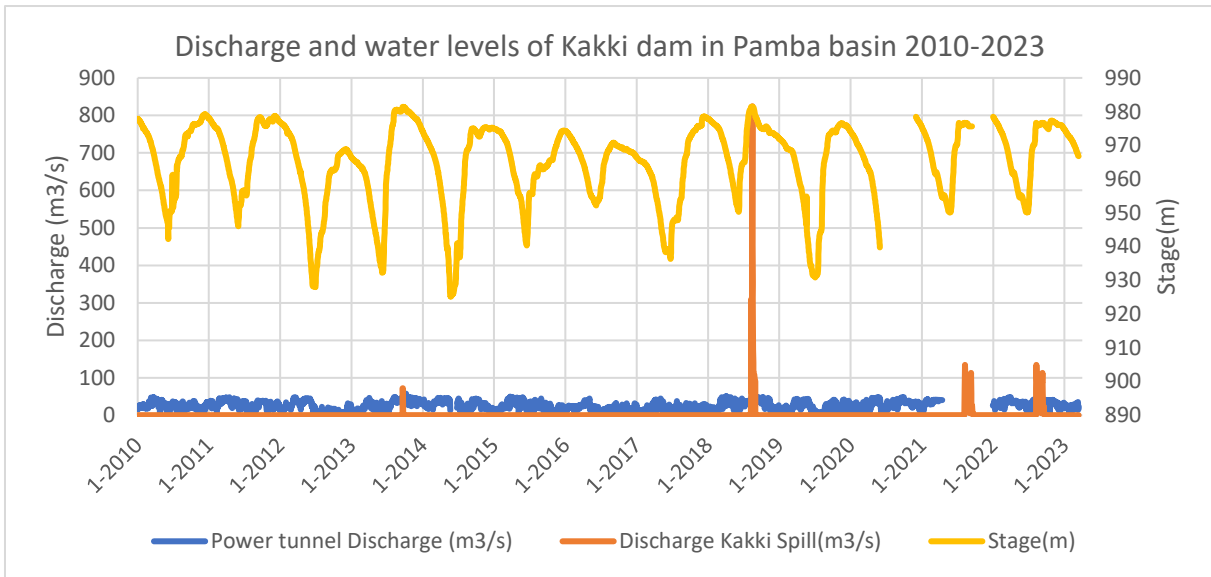
Figure 12 Discharge and water levels of Kakki dam in Pamba Basin 2010-2023

In consultation with the local flood modelling expert, also the role of the Pamba and the Moozhiyar dam in the river system is evaluated. The data of the Pamba dam only includes spillway discharges. Regularly, the Pamba reservoir water is transported to the Kakki dam through the underground tunnel. Consequently, the spillway discharge at the Pamba river is most of the time 0 m^3/s. Within the historical timeseries (2010-2023) the spill way is used 3 times, in 2013 for 50 m^3/s, in 2018 for 230 m^3/s and in 2021 for 20 m^3/s. For the Moozhiyar dam the available discharge data is limited to January-August 2022. Within this time the discharge variated between 11.42 and 67.18 m^3/s with an average of 27.6 m^3/s. The local expert explained that the storage capacity of the Moozhiyar dam is limited and could be ignored in flood modelling efforts.
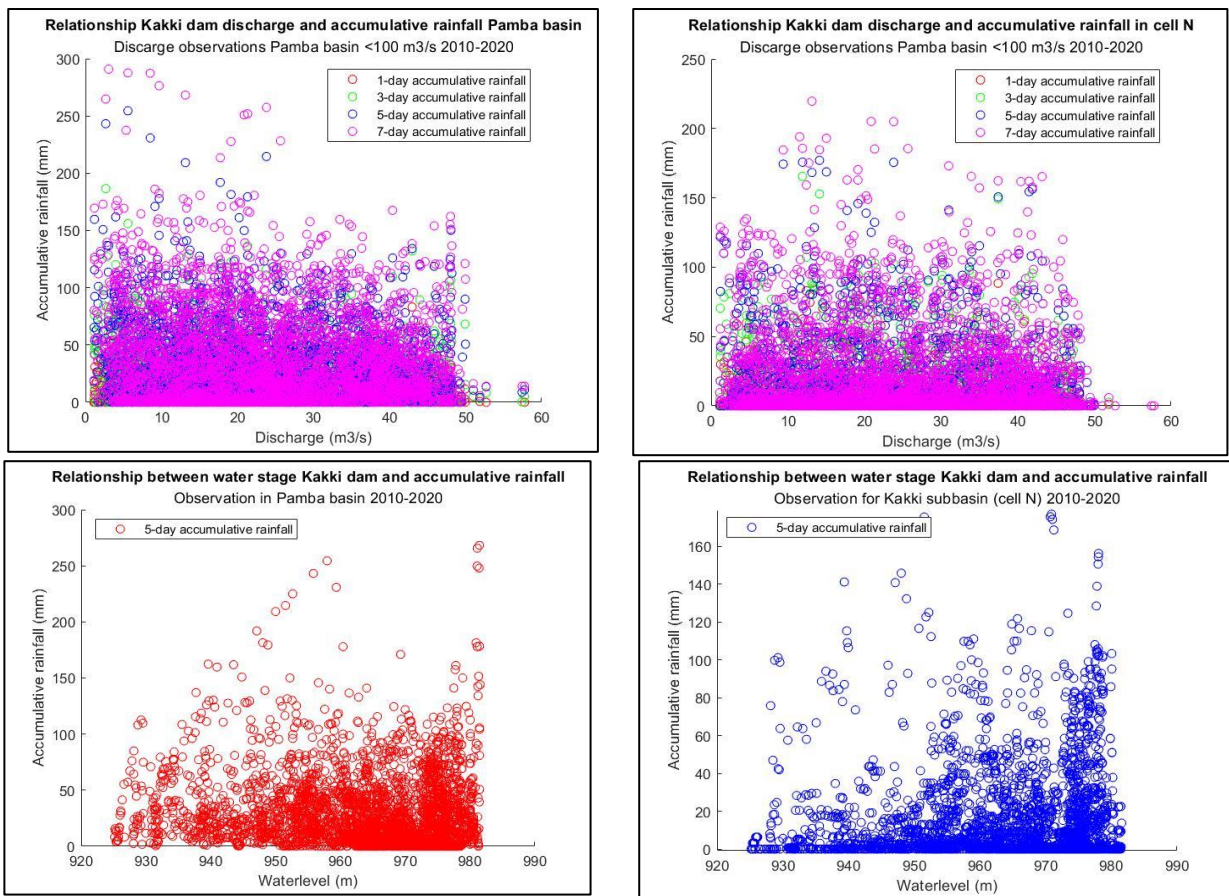
Figure 13 Scatterplots of correlation between cumulative rainfall and Kakki dam discharge and water level

4.4. Rainfall-discharge analyses

The calibration of a (hydrological) model focusses on adjusting input parameters settings to improve the models performance in representing the real world. For this process, observed real world hydrological data is needed. Consequently, it is important to study the observed rainfall-discharge relationship in the Pamba Basin area. For the complete analyses the area weighted return period rainfall is used. Moreover, Kurudamannil discharge point is used as focus point. This choice is made because it covers a long time series with the smallest % of missing data values and it provides data of the main river and not a side branch in the lower laying delta. Figure 14 shows scatter plots with the relationship between cumulative rainfall over several time periods, and the peak discharges as measured at Kurudamannil.
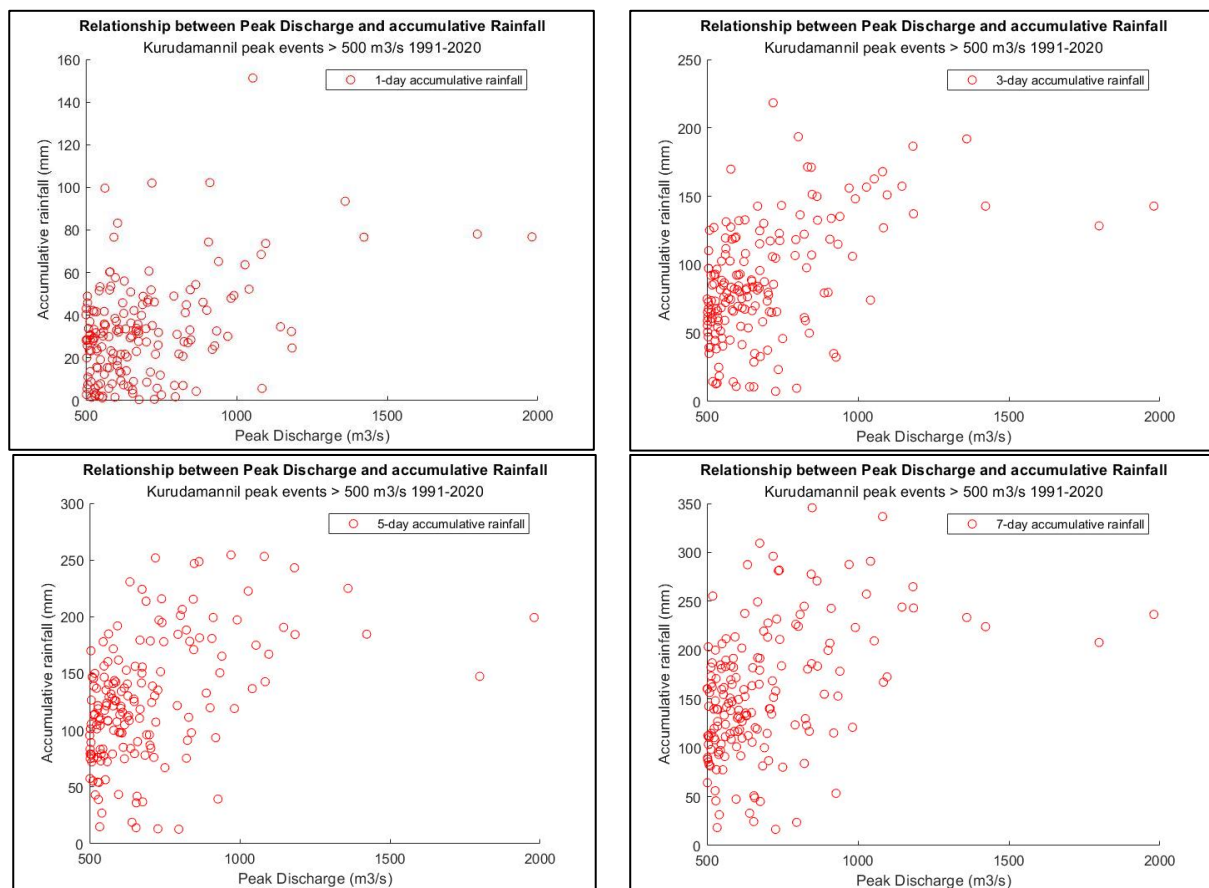
Figure 14 Scatterplots representing cumulative rainfall and peak discharges at Kurudamannil

The scatter plots in figure 14 show an approximate correlation, however it is by eye hard to determine how many days of cumulative rainfall have the highest correlation with river discharge measurements. To determine the optimal duration for input rainfall events, discharge values above 500 m^3/s are considered. Over the timeseries 1991-2020 this are 171 peaks. The derived correlation between (cumulative) rainfall and discharges is presented in table 10, with 1 representing a perfect positive correlation and 0 a non-existing one.

Table 10 Correlation matrix of cumulative rainfall and observed river discharge

	1-day cumulative rainfall	3-day cumulative rainfall	5-day cumulative rainfall	7-day cumulative rainfall	Discharge Erappuzha	Discharge Marmon	Discharge Kurudamannil
Discharge Erappuzha	0.01	0.26	0.32	0.32	1.00		
Discharge Marmon	-0.16	0.24	0.30	0.32	0.54	1.00	
Discharge Kurudamannil	0.42	0.48	0.44	0.42	0.54	0.77	1.00

The results of the correlation analyses show that peak discharges at Kurudamannil have the largest correlation with the three-day (72h) cumulative rainfall. The discharge measurements at the lower laying measurement points of Erappuzha and Marmon show a correlation with longer cumulative rainfall periods. This is logical because rainwater needs to move over a large distance to reach these points.

To analyse the rainfall discharge relationship on a more detailed level, figure 42 till 44 in Appendix E show graphs with 3-day cumulative rainfall and discharge data for example time periods. Based on the presented examples a couple of factors stand out. Firstly, it is visible that rainfall peaks earlier in the season, around June, result in lower discharge peaks than similar rainfall events later in the year, around August. This can be explained by the fact that in June the monsoon season is just starting. Consequently, much of the soil will not be saturated. Around August, the Pamba Basin has usually already experienced a lot of monsoon rain. The local reservoirs and the soil are likely more saturated, so rainfall leads to more direct discharge peaks in the river. An example is the rainfall peak in December 2017, see figure 42 in appendix E. This rainfall peak barely showed any influence on the measured discharge levels. This is quite remarkable. However, December is usually a dry month in Kerala, likely much of the available rainwater is infiltrated or stored in local reservoirs.

4.5. Discussion on sub-objective 1

4.5.1. Rainfall analyses

The first research objective aimed to create applicable rainfall and discharge related return periods that can be used for flood hazard analyses in Pamba Basin. It is important to consider that this analyses highly depends on the quality of the gridded rainfall dataset. It is unknown how many of the 6995 gauge stations, that were used for the composition of this dataset, were actually positioned in the Pamba Basin. Moreover, the paper of Pai et al., (2013), which elaborates on the methodology used to compose the gridded rainfall dataset, does not described how elevation differences were considered. In the rainfall intensity maps used for the simulation of the 2018 and 2019 flood events, it is visible that the grid cell upstream from the Kakki reservoir does not show very extreme rainfall volumes. This contradicts the finding of Mishra & Shah (2018), who state that the return period of the rainfall upstream form reservoirs preceding the 2018 events is more than 500-years.

An additional point of discussion is the large variation in return period rainfall for different grid cells in the Pamba Basin. This makes it challenging to create uniform rainfall return period intensities for the complete catchment. An area weighted average is applied to compose catchment return period rainfall for different cumulative periods of time. Important to consider is that the available rainfall data only consist of daily rainfall intensities. Monsoon rainfall events can be characterised by longer cumulative rainfall periods. However, extreme and shorter peak intensities can have a big impact on localised flash floods. By using area averaged daily rainfall statistics it is likely that local effects of extreme short term precipitation intensities are not well represented in flood hazard simulations.

Additionally, in the presented Gumbel graphs, it is visible that not all graphs reach the 50-year return period. To still derive a rainfall threshold for 50-years a logical prolongation of the Gumbel graph is interpreted, which entails increased uncertainty.

4.5.2. Climatic developments

For this research rain multipliers are used to integrate climatic developments in flood hazard assessment. This approach comes with several sidenotes. Firstly, rainfall multipliers are derived using an average of five climate models. The variation in climate models is extensive and it is difficult to get grip on the causes output variations. Using the median is common practise in the climate research field, however for this study the average value is used. Moreover, for the complete Pamba Basin the same rainfall multiplier is used. In the Gumbel analyses a large variation in rainfall return period per grid cell is observed. Differences in landscape are highly influential on local climate variations. This is currently not captured in a uniform catchment rainfall multiplier.

Additionally, climate change has more effects on the hydrological cycle then can be captured in rainfall multipliers. For example, longer consecutive periods of droughts could lead to lower groundwater tables and a change in base discharge conditions. Additionally, long term climatic changes can affect vegetation growth and consequently terrain roughness. Moreover, changes in temperature effect evaporation and

humidity conditions in the area. These examples show a first insight in the complexity related to hazard assessments in the face of climate change. Using simplified approaches, such as rainfall multipliers, is of value to get a first insight in potential consequences of climate change. However, it is important to keep in mind the associated uncertainties.

4.5.3. River discharge

Observation data used for calibration is critical in obtaining high-accuracy modelling results and verification Paul et al., (2014). For the calibration and validation of hydrological models long timeseries of rainfall-runoff data are preferred (Walsiki, 2017). The available river discharge timeseries are associated with many limitations. The Erappuzha gauging station is located in a side channel of the Pamba River. To effectively use this station for the calibration of a flood model, the bifurcation of discharge over branches needs to be represented very well in the flood model. At this moment in time, too little research is conducted using the FFS-model to ensure this condition. This reason, in combination with 37.3% of missing values, led to the conclusion that the Erappuzha station is unfit for the calibration process. The Marmon timeseries only includes five years of measurement data. This is too limited to compose return period discharge thresholds. Therefore, the Kurudamannil discharge gauging station is chosen as calibration focus data. Nevertheless, it is important to consider that this timeseries is subject to missing data values and that these missing data points are partly linked to extreme discharge events. For this reason, it is possible that the Kurudamannil return period discharge is underestimating the actual situation.

Additionally, it is unknown how the available discharge observations were measured. Paul et al., (2014) reports that water flow within a river or channel can be measured to within 5% accuracy by a skilled operator. However, determining the discharge in wide and vegetated floodplains is much more challenging due to the variation in water depth and velocity. This can lead to runoff errors up to 15% (Paul et al., 2014).

4.5.4. Dam discharges

The discharge of the Pamba River is regulated by the presence of several dams. The analyses of dam discharge data revealed an absence of correlation between rainfall quantification and dam discharges. Local experts confirmed that dam discharge is fully depending on electricity demand. This complicates the integration of dam discharge in a flood hazard assessments for specified return periods. Average dam discharges form the Kakki dam are relatively small in discharge compared to return period discharge quantifications.

Nevertheless, several spillway discharge events have been detected over time. The largest spillway discharge was during the 2018 floods and had a size of approximately 800 m^3/s. As described in section 2.4, different researchers have analysed the effects of this extreme discharge peak on the flood hazard downstream. Overall, the effects seem to be limited, compared to the destructive effects of the extreme rainfall intensities. A local expert mentioned that the vision concerning reservoir management strategies in Kerala is changed since the 2018 flood event. During the monsoon season an increased storage capacity should be maintained in the reservoir. Unfortunately, there is no access to information or guidelines indicating quantitatively how reservoir management is currently approached in relation to extreme weather conditions.

Considering the limited information regarding dam discharge management in relation to extreme weather conditions, the choice is made to not consider any dam function in the FFS-model set-up. This means that no water from the upstream dam regions is stored, and water naturally flows through the catchment. Additionally, no additional discharge is considered that originates from the relative constant dam electricity demands. This modelling choice could be perceived as questionable. Nevertheless, the goal of the model it to give on an easily interpretable manner insight in flood hazard for local governments. Current available data is insufficient to derive logical and relevant return period dam discharge statistics that have a significant influence on return period flood hazards in the downstream region. In real-time flood simulations, measured dam discharges can be added in the FFS-model set-up.

4.5.5. Rainfall-discharge relationship

For the calibration of the FFS-model the rainfall-discharge relationship is of particular interest. Water originated from rainfall does not immediately lead to a discharge peak. Depending on elevation, friction and infiltration conditions rainfall water needs a certain amount of time to reach the river. The analyses of historic rainfall-discharge behaviour showed the largest correlation between 3-day (72 hour) cumulative

rainfall and a peak in river discharge, see section 4.4. For this reason, the 72h cumulative rainfall threshold is used throughout the complete calibration, validation and application processes of the FFS-model in this thesis. The choice to focus on 72-hour cumulative rainfall is catchment- and discharge station-specific. A limitation of flood analyses based on rainfall-discharge relationships in the large focus on fluvial flooding. Pluvial flooding due to local rainfall extremes is not well represented in rainfall-discharge data. Additionally, the rainfall-discharge relationship is likely subject to seasonal influences. These influences are currently not captured in the presented research results.

Chapter 5: Results: Calibration and validation of FFS-model

The second research objective aims to investigate the applicability of the FFS-model for flood hazard assessments in Pamba Basin. This chapter starts with an elaboration on the model calibration results using the derived rainfall-discharge relationship as discussed in chapter 4. Subsequently, an elaboration is given regarding the different validation attempts. In the final section, a discussion is presented which reflects on the uncertainties and limitations associated with the calibration and validation results.

5.1. FFS-model calibration

As explained in section 3.3, the FFS-model calibration is focussed on finding a combination of calibration settings to achieve the best approximation of the observed rainfall-discharge relationship. For the calibration process six peak events are selected and the discharge point at Kurudamannil is chosen as focus point. The calibration parameters, which are available in the FFS-model set-up, are the baseflow condition, landcover multiplier, infiltration multiplier, discharge diffusivity and the concentration speed multiplier.

Firstly, the definition of a baseflow condition, the FFS-model interface allows for a single baseflow condition at the outlet. Each river segment is provided with an amount of baseflow proportional to its total drainage area. The Kurudamannil station receives water from 58.9% of the total drainage area at the outlet of the model. In section 4.4 the observed relationship between cumulative rainfall and peak discharges was discussed. Similarly, the relationship between peak discharges and the average river discharge in the days preceding a peak discharge event is analysed. This analyses is used to determine a base discharge calibration setting for the various return periods.

Figure 15 shows scatter plots presenting the relationship between peak discharges and the average river discharge 3- and 7-days before a peak event. It is visible that there is a certain degree of correlation, however the variation is quite significant. Table 11 presents the quantified correlation, between the peak discharge and the average base discharge of varying preceding days. It is visible that the 3-day preceding average base discharge has the highest correlation.
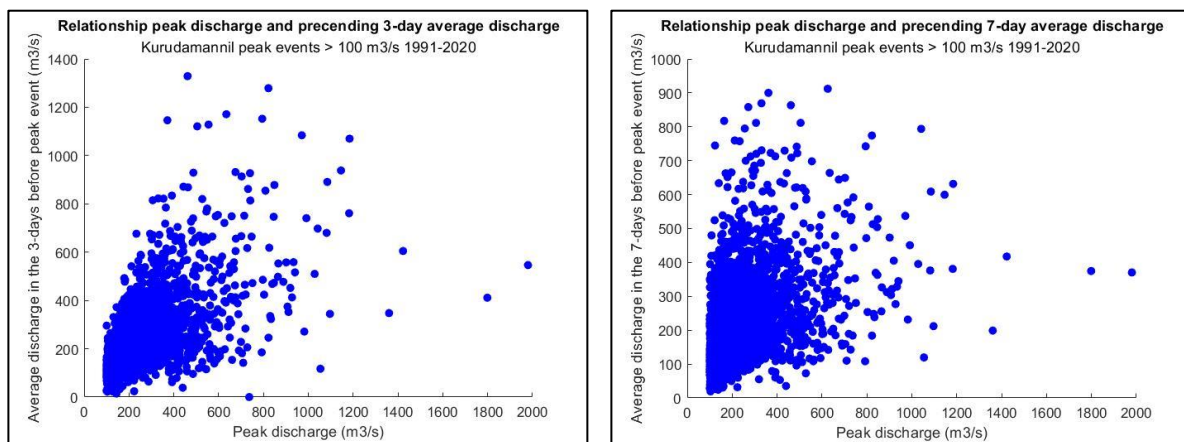
Figure 15 Scatterplots showing the correlation between peak discharges and preceding base discharge

Table 11 Correlation matrix peak discharge and preceding average base discharge at Kurudamannil

Correlation table	Peak Discharge Erappuzha	Peak Discharge Marmon	Peak discharge Kurudamannil
Preceding 3-day average base discharge	0.66	0.18	0.67
Preceding 5-day average base discharge	0.59	0.16	0.55
Preceding 7-day average base discharge	0.52	0.14	0.46

Consequently, the choice is made to derive the 3-day average base discharge at Kurudamannil together with the associated discharge at the catchment outlet, for each of the six calibration events, see table 12. This outlet base discharge condition is used as input parameter in the FFS-model.

Table 12 Details of the selected calibration events

Calibration scenarios	6-2017	9-2017	8-2018	8-2019	8-2020	9-2020
Average rainfall in (mm/h) for 72h	1.50	1.49	1.84	2.67	2.18	1.29
Average discharge 3-days before peak (m^3/s)	197.8	472.6	553.2	347.7	510.1	352.6
Base discharge setting in FFS-model (m^3/s)	325	800	925	575	850	600
Observed peak discharge at Kurudamannil (m3/s)	627.7	846.6	866.2	1360.33	1028.3	610

With the determined setting of the base discharge condition, four calibration settings remain open in the calibration process. By iterating the different calibration parameters, it became clear that the model sensitivity, on a resolution of 150 meter, is highest for the infiltration multiplier and very minimal for the landcover multiplier. Consequently, the choice is made to keep the landcover multiplier at one in the calibration test set-up. Based on the first observations a calibration testing regime is created. Table 13 shows a selection of the performed calibration tests.

Table 13 Examples of calibration test settings for FFS-model

Calibration test setting	test 1	test 2	test 3	test 4	test 5	test 6	test 7	test 8	test 9
Landcover multiplier	1	1	1	1	1	1	1	1	1
Infiltration multiplier	1	0.2	0.2	0.1	0.1	0.1	0.1	0.2	0.2
Discharge diffusivity	0.2	0.2	0.2	0.2	0.2	0.2	0.1	0.4	0.3
Concentration speed multiplier	1	1	0.5	1	0.8	0.6	0.6	0.5	0.8

The different calibration setups are tested on all six calibration scenarios. Table 27 in appendix F shows simulated discharges and the associated percentual difference, NSE value and percent bias (PBIAS). The NSE is used as leading performance parameter. Consequently, it can be concluded that calibration setting 2 has the best overall model performance with a NSE of 0.79, an average absolute percentual difference of 10.4% and a PBIAS of 2.4%. According to the papers of Cardoso de Salias et al., (2019) and Luo & Shao (2022) a hydrological model is performing well to very good with NSE values above 0.75 and a PBIAS below 10%. Consequently, the final calibration fit of the FFS-model is performing well.

With the derived calibration setting, the next test is to check if the rainfall return periods, as presented in section 4.1, correspond with the discharge return periods, as presented in section 4.2. A challenge arises from the uncertainty concerning the preceding base-discharge condition for the return period events. To analyse an historic trend in base discharges before peak events, the scatter plots as shown in figure 16 are analysed. These plots only show the average preceding base discharges of peak events above the 1000 m^3/s at Kurudamannil. The results do unfortunately not show any form of correlation.

Alternatively, the observed discharge values exceeding 1000 m^3/s are averaged, see table 14. The resulting base discharge value is tested for the return period rainfall and discharge thresholds. The results of this analyses are presented in table 15. In conclusion, the analysis reveals that using the average base discharge of the five preceding days resulted in the highest similarity between the simulated and observed return period discharge for Kurudamannil. The overall percentual difference is 2.87%. Consequently, a uniform base discharge setting of 640 m^3/s is used when simulating return periods of 5 years and higher for the Pamba Basin.
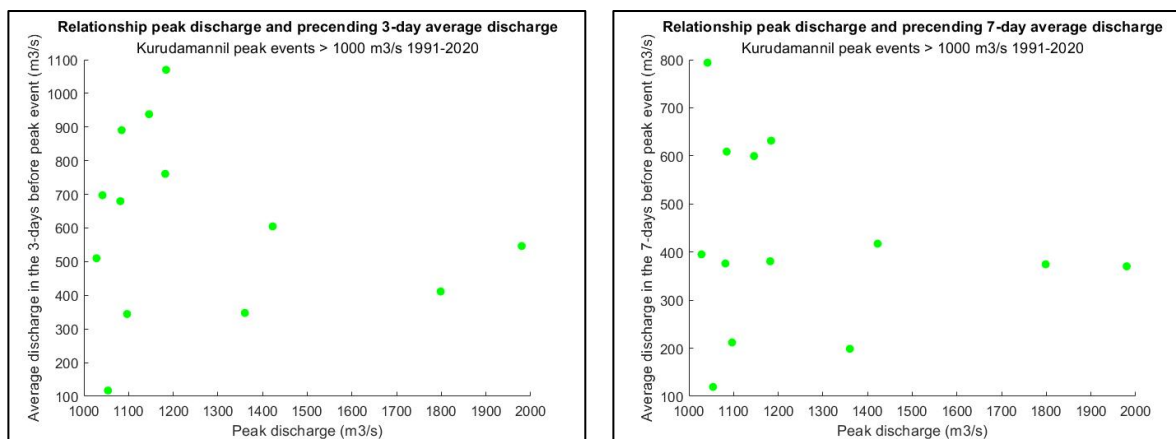
Figure 16 Scatterplots representing peak discharges and preceding base discharges >1000 m³/s

Table 14 Measured base discharge in days preceding peak events

Return period	RP discharge at Kurudamannil (m³/s)	Amount of observed independent events exceeding return period discharge (1991-2020)	Average base discharge at Kurudamannil in 3-days preceding peak event (m³/s)	Average base discharge at Kurudamannil in 5-days preceding peak event (m³/s)
5	1090	5	451	374.9
10	1240	4	477.6	405.5
25	1470	2	478.9	426.2
50	1630	2	478.9	426.2

Table 15 Comparison of observed and simulated discharges for variating baseflow conditions

	Average 3-day preceding base discharge of peaks above the 5-year RP threshold (1090 m³/s)	Average 5-day preceding base discharge of peaks above the 5-year RP threshold (1090 m³/s)
Base discharge Kurudamannil	451	374.9
Base-flow condition Fast-flood model	770	640
Simulated discharge at Kurudamannil (m3/s) using 72h return period rainfall intensities		
5-year return period	1198	1121.7
10-year return period	1334.4	1258.1
25-year return period	1500.6	1424.3
50-year return period	1641.3	1565
Percentual difference return period discharge and simulated discharge		
5-year return period	9.91%	2.91%
10-year return period	7.61%	1.46%
25-year return period	2.08%	-3.11%
50-year return period	0.69%	-3.99%
Absolute average % difference	**5.07%**	**2.87%**

Using the described calibration settings and the rainfall return period thresholds, as presented in section 5.1, flood hazard maps are generated, see figure 17. The validity of these maps is discussed in section 5.2. Additionally, an elaboration addressing the limited visual differences between flood hazard maps of different return periods is described in chapter 6.
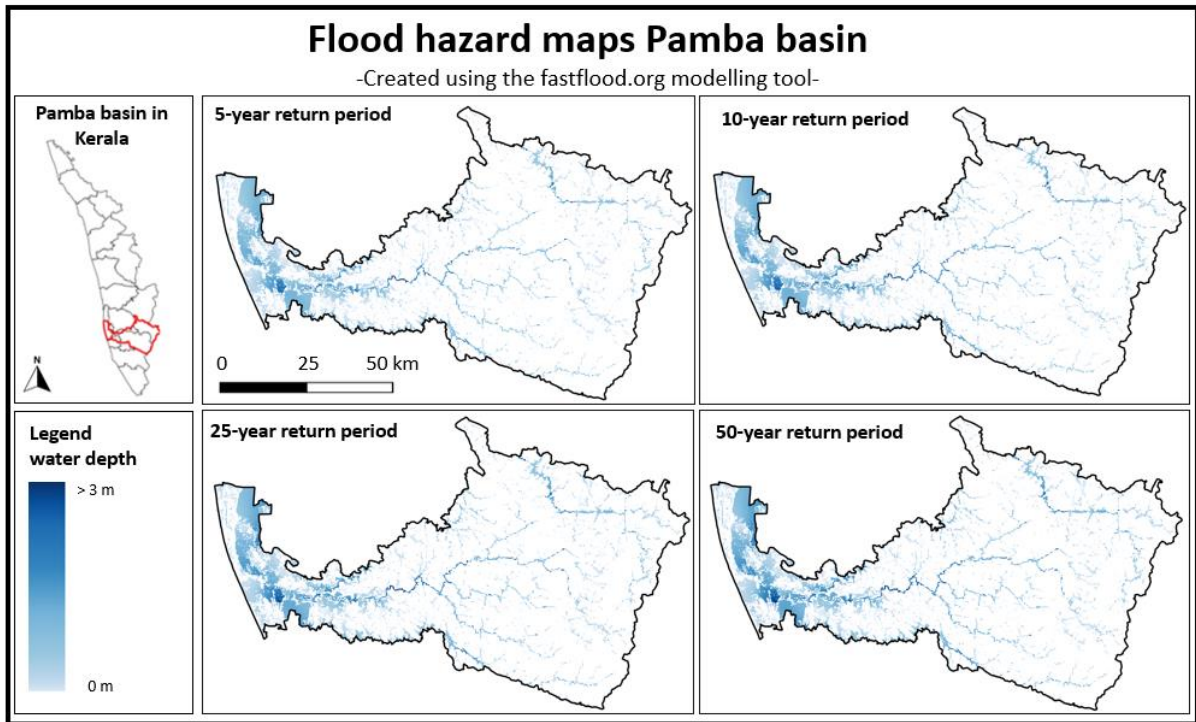
Figure 17 Flood hazard maps Pamba Basin

5.2. Sensitivity analysis

This section presents the sensitivity of the FFS-model to base discharge condition, infiltration rate and Mannings N. For this analysis, the study area of Aranmula LSG is selected due to its geographic location closest to the discharge measurement point of Kurudamannil. The calibration set-up as presented in the previous section is used as base scenario. Subsequently, the base scenario thresholds are variated up to ±50% from their original value and the resulting flood depths and river discharge is analysed. The results of this analyses are presented in figure 18.

A remarkable observation is that the Manning's N multiplier does not influence the simulated discharges. The base flow condition and the infiltration rate multiplier show a linear sensitivity in relation to the simulated peak discharges. The percentual difference are presented in table 16. Both sensitivities are substantial, and the base discharge condition shows the largest influence on simulated peak discharges. In figure 19, the sensitivity with respect to simulated water depths is presented. It is visible that the infiltration rate multiplier has more influence on water depths then the base discharge setting.

Table 16 Sensitivity of simulated peak discharges to base discharge and infiltration rate multiplier

% difference to threshold calibration setting	Base flow condition			Infiltration rate multiplier		
	input parameter	simulated peak discharge (m³/s)	% difference	input parameter	simulated peak discharge (m³/s)	% difference
-50%	320	1099.4	-17.72%	0.1	1473.4	10.27%
-25%	480	1217.8	-8.86%	0.15	1404.8	5.13%
-5%	608	1312.5	-1.77%	0.19	1349.9	1.03%
0%	640	1336.2	0.00%	0.2	1336.2	0.00%
5%	672	1359.8	1.77%	0.21	1322.4	-1.03%
25%	800	1454.5	8.85%	0.25	1267.6	-5.13%
50%	960	1572.9	17.71%	0.3	1199	-10.27%
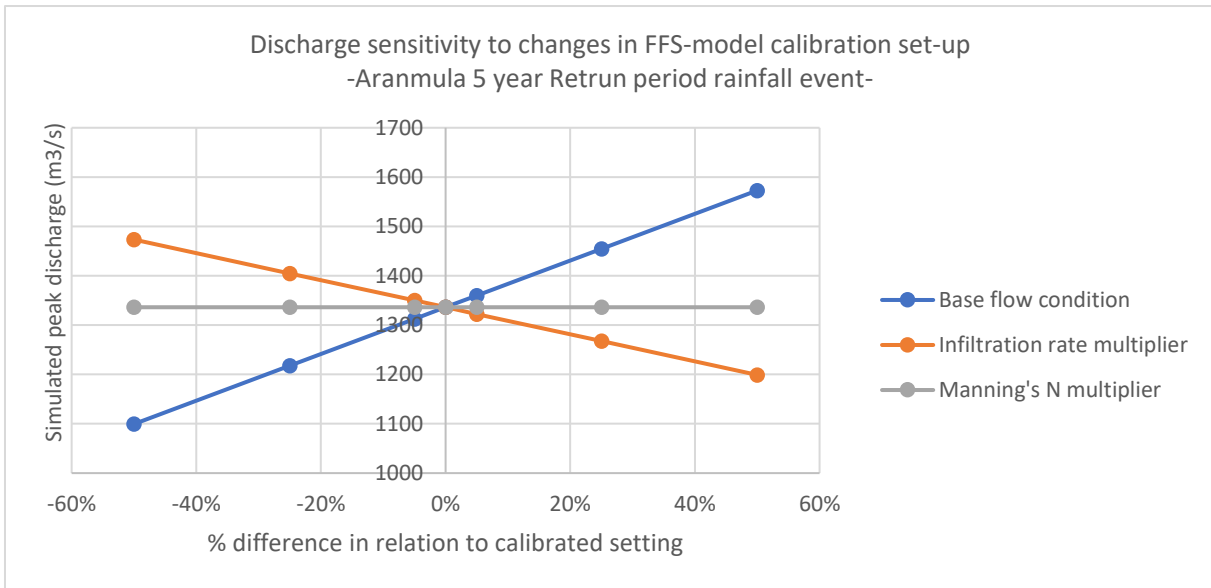
Figure 18 FFS-model sensitivity to variation calibration parameters
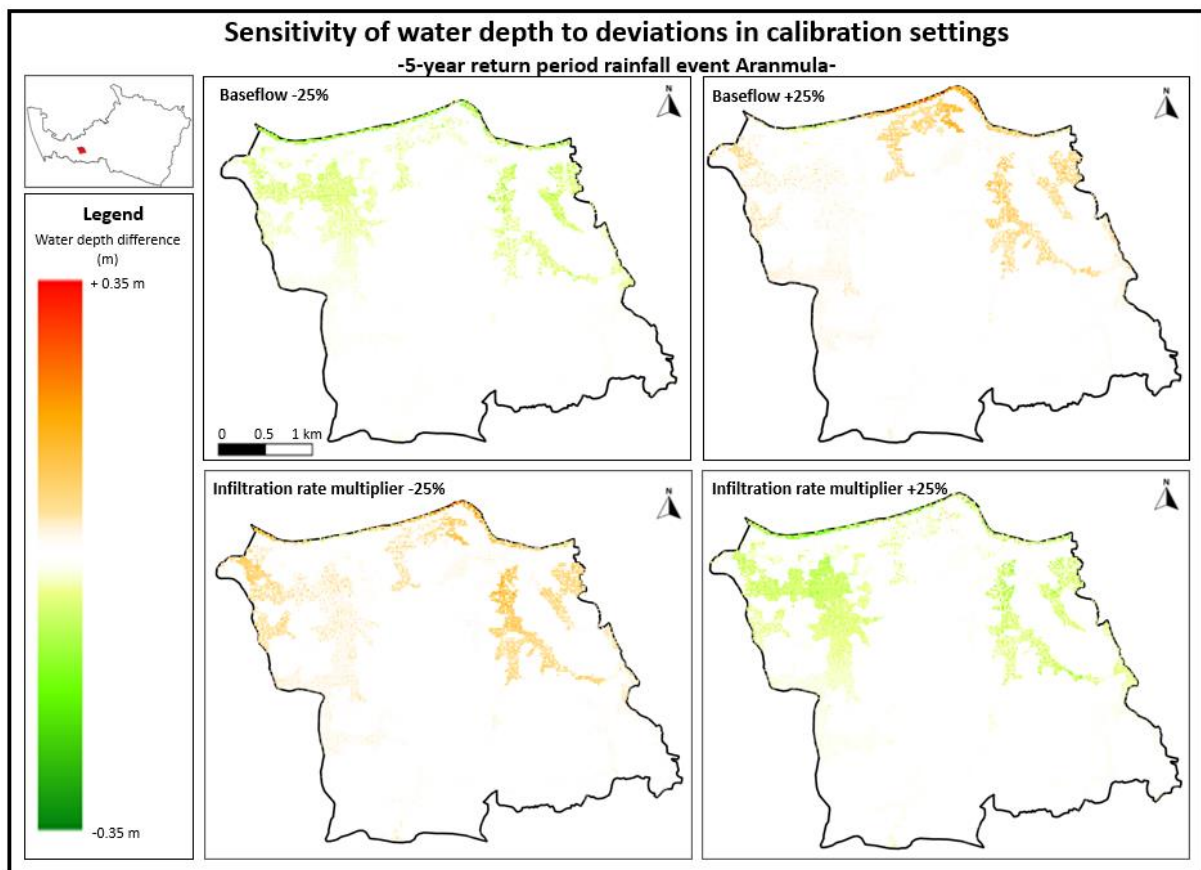
Figure 19 Sensitivity of water depth to deviations in calibration settings

5.3. FFS-model validation

This section presents the results of various validation attempts of the calibrated FFS-model. Firstly, the FFS-model channel pattern is compared with arial photographs to analyse if the flow network is correctly represented. Subsequently, a flood extent analyses is performed using radar imagery of the 2018 and 2019 flood events in Kerala. Moreover, crowdsourced flood depth and damage data of 2018 floods is used to analyse their correlations with the FFS-model results. Finally, the FFS-model results are compared with flood hazard maps as generated by the CIMA research foundation.

5.3.1. Flow network validation

During the model calibration process, the automatic channel generation function of the FFS-model is applied. This function uses the DEM to generate a flow network. The upper map in figure 20 shows the channel network as created by the FFS-model. When comparing the channel network with aerial photographs and geographic data of permanent water bodies, several observation can be made. Firstly, it is visible that in the high- and midland regions the FFS-model correctly positions the channel network. However, in the lower laying regions the FFS channel network highly deviates from the actual flow network.

To tackle this challenge dr. B van den Bout added a feature to the FFS-model. This feature enables the possibility to import a channel map in the model setup. The used channel map, as shown in lower map of figure 20, is obtained from the HEC-HMS model data that is available through the local flood modelling team in Kerala. The channel network correctly follows the main river pattern, however lacks in completeness concerning side branches in the lower laying regions. Nevertheless, by including the presented channel map as input in the FFS-model, the simulated discharge patterns approximate the observed river network much better. To ensure that water routing finds place over 1-pixel wide channel routes, the monodirectional channel option is implemented.
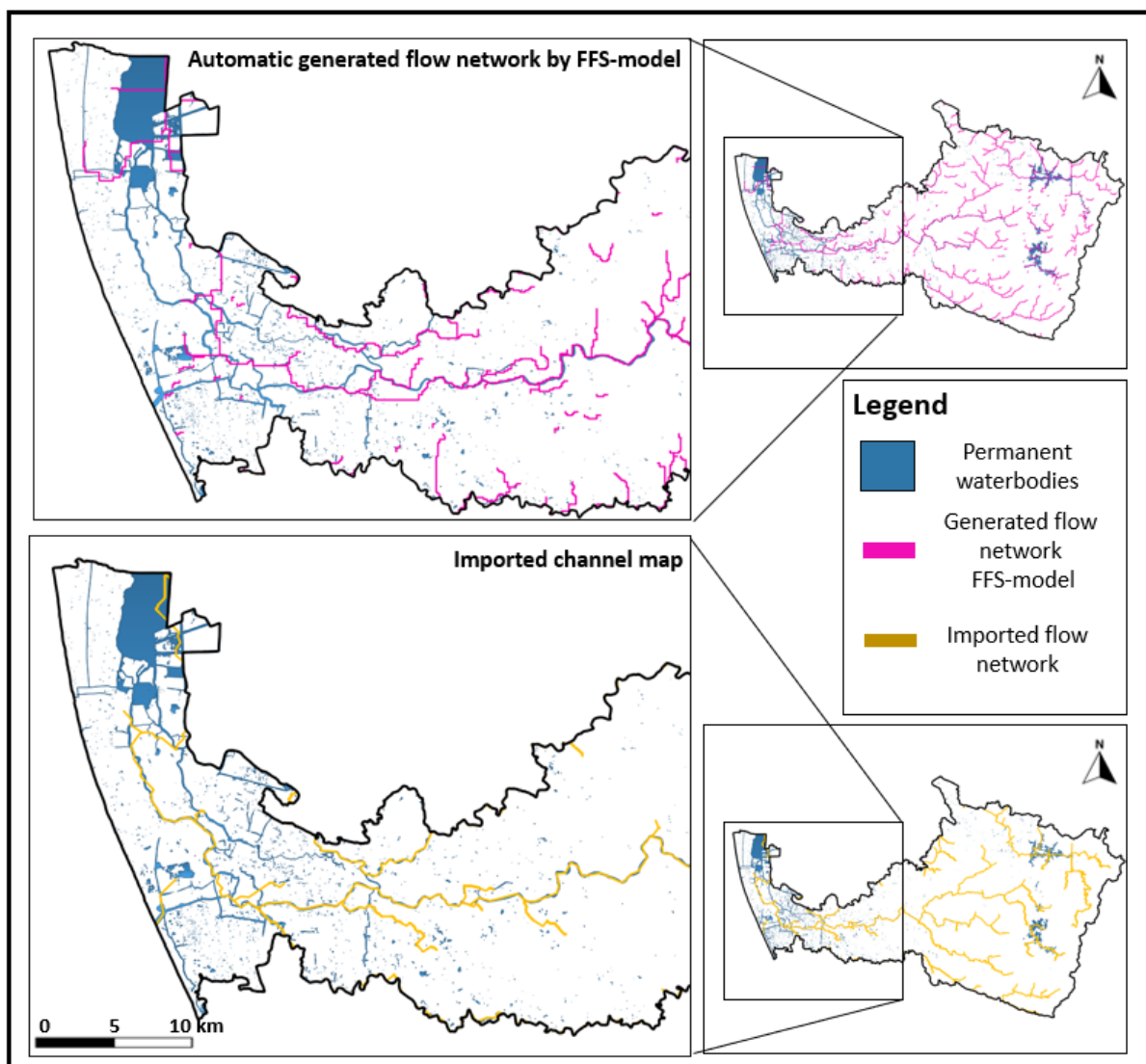
Figure 20 Channel network comparison

5.3.2. Flood extent validation

The flood extent of the 2018 and 2019 flood events are derived using processed Sentinel-1 data through Google Earth Engine (GEE). The results of this analyses are presented in figure 21 for 2018 and in figure 44

in appendix G for 2019. During the 2018 flood events, the peak rainfall intensity in is measured on the 16th of August. For the simulation of the 2018 floods, the rainfall of the 14th till 16th of August is considered. The available radar imagery closest to this moment in time is collected on the 21st of August. In the days between the 16th and the 21st an additional 41.5 mm rain is observed. This rain volume is not considered in the simulation of the 2018 event.

In 2019 the measured peak discharge at Kurudamannil occurred on the 9th of August. The available radar imagery is from the 10th of August. An important remark is that, in the week after the peak discharge still high rainfall intensities were observed. Form the 10th till the 14th an additional 137 mm rain occurred. These rain volumes are not included in the 2019 simulation or radar flood extent imagery, nevertheless they could have led to damages.

The radar flood extent maps show an inundation pattern with many local patches, especially in the midland region. This pattern indicates many local depressions in which rainwater accumulates. Interesting is the observation that there are limited inundated areas connected with the main Pamba river. This indicates dominantly the occurrence of pluvial flooding and limited fluvial flooding.

The GGE flood extent maps combined with the natural water occurrence to create binary water extent maps with a resolution of 30 meters, see figure 45 and 46 in appendix G. Subsequently, the 2018 and 2019 extreme rainfall events are simulated using the non-uniform 72h cumulative rainfall per grid cell. For the simulated flood extent, all flood depth values of more than 0.05 meter are considered.
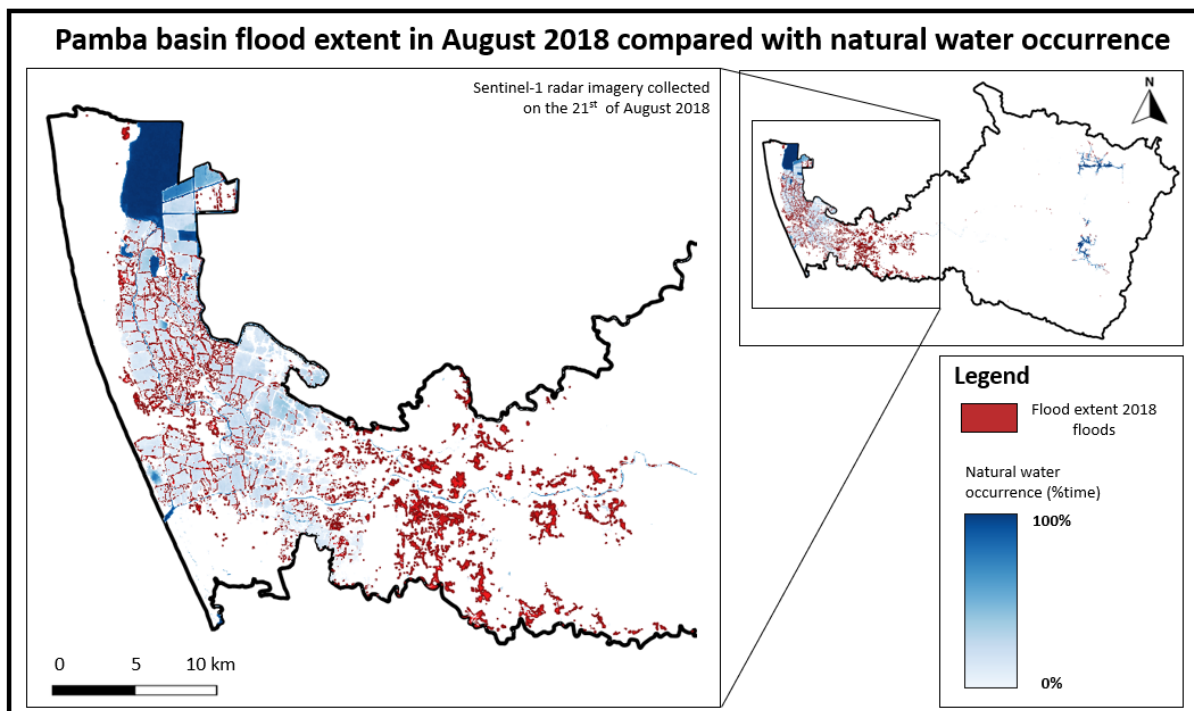
Figure 21 Pamba basin flood extent in August 2018 compared with natural water (Global Surface water, 2020)

Figure 22 shows the spatial comparison of flood extent between radar and FFS-model output for 2018. For 2019 the results can be found in figure 47 in appendix G. It is visible that the FFS-model represents the different side channels in much more detail than the radar and percentual water occurrence data. Therefor the false positive ratio is significant. Pamba Basin is densely vegetated, this likely has a large influence on the completeness of the radar data. When comparing the simulated flood extent patterns with aerial photographs it is visible that natural water patterns are often followed.

Due to limitations with the completeness of the radar flood extent data, the false negative ratio is a more important performance indicator. It is visible that the upstream located reservoirs are not well represented in the simulated data. This can logically be explained by the fact that no base reservoir boundary condition is applied in the FFS-model. The FFS-model functionalities are not fit for detailed reservoir extent analyses and therefor the focus is put on downstream flood behaviour. In the downstream region it is visible that

the FFS-model sometimes underestimates the flood extent in the river delta region. For 2019 a similar pattern can be detected.
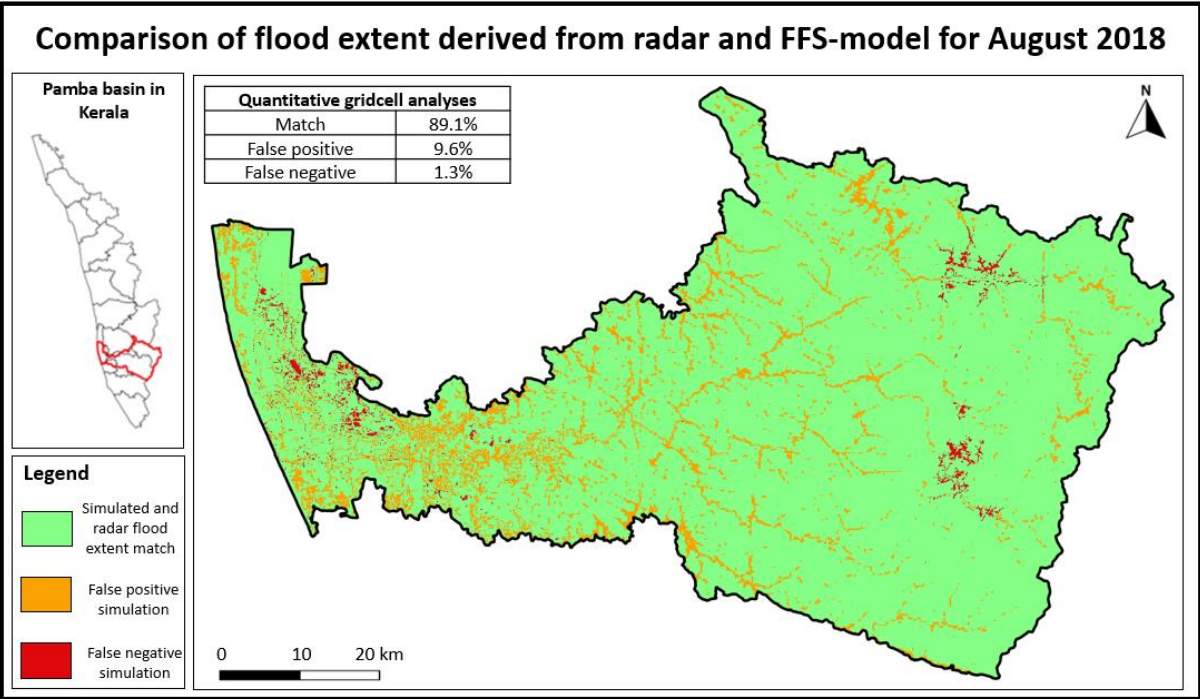
Figure 22 Comparison of flood extent derived from radar and FFS-model for August 2018

For the five selected validation test areas, as presented in figure 8, the calibration tool of the FFS model is used to derive the Cohens kappa and the % accuracy. Table 17 present the performance indicators per validation test area. Moreover, figure 50 and 51 in appendix G visualise, for two example areas, the difference between the simulated and the observed water extent. It is visible that the 2018 event scores higher on the performance indicators then 2019. Moreover, there is a significant difference in performance per validation region. It is important to note that the performance indicators are significantly influenced by the high false positive ratios. According to McHugh, (2012) and Rafieyan, (2016) Cohen kappa values between 0.23 and 0.56 are indicated as fair to moderate agreement.

Table 17 Validation performance indicators of flood extent analyses for 2018 and 2019 flood events

Validation performance indicators for flood extent analyses 2018 flood event					
Validation area	**1**	**2**	**3**	**4**	**5**
Cohens kappa	0.56	0.40	0.42	0.49	0.26
% accuracy	88.2%	69.7%	80.4%	78.5%	97.6%
Validation performance indicators for flood extent analyses 2019 flood event					
Validation area	**1**	**2**	**3**	**4**	**5**
Cohens kappa	0.42	0.34	0.26	0.41	0.23
% accuracy	86.2%	66.7%	77.9%	73.1%	96.5%

Additionally, a flood simulation and extent analyses for the three case-study LSGs is performed on a resolution of 30 meters. For Pandanad the results are presented in figure 23, similar results for Aranmula and Edathua are presented in figure 50 and 51 in appendix G. Additionally, in table 18 the performance indicators for the three LSGs are shown.

The different maps show clearly visible similarities in the water extent patterns between the radar and simulated data. However, it is visible that the radar water extent is less extensive than the simulated one. During the 2018 floods, a large number of damaged houses were registered at locations where the radar data does not show any inundation. This observation substantiates the assumption that the radar flood extent is uncomplete and underestimating the actual extent of the flood events. In conclusion, eventough

the Cohens Kappa performance indicators show only a moderate agreement, the similarities in water flow patterns are promising when reflecting on the validation of the FFS-model.
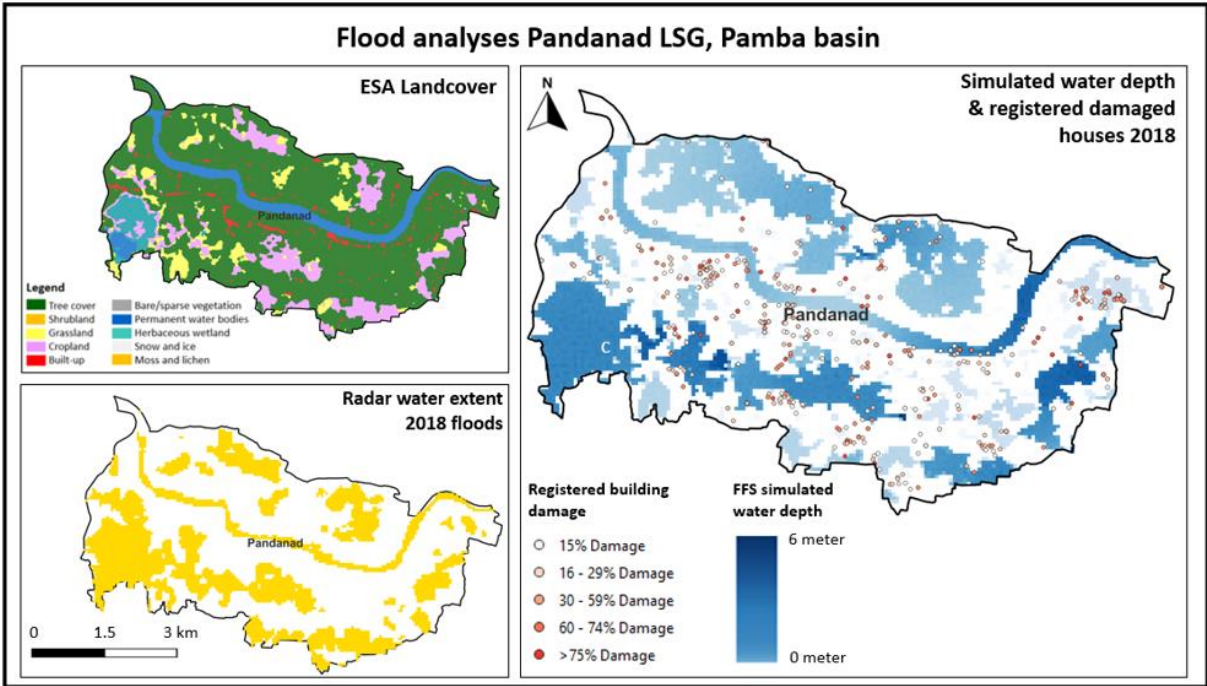
Figure 23 Flood extent analyses Pandanad 2018 floods

Table 18 Validation performance indicators of flood extent analyses for case-study LSGs

Validation performance indicators for flood extent analyses 2018 flood event			
Local-self government	Aranmula	Edathua	Pandanad
Cohens kappa	0.44	0.38	0.53
% accuracy	82.1%	74.9%	78.3%

5.3.3. Comparison with registered flood data

During the floods in August 2018, crowdsourced flood depth measurements are collected. Figure 24 shows the location and quantification of the flood depth measurements on top of the simulated flood depth results of the FFS-model. The graph in figure 25 shows for each crowdsourced measurement point the associated simulated flood depth. It is visible that the correlation is weak to non-existing. This raises question regarding the validity of the FFS-model.

Nevertheless, it is important to consider the accuracy of the crowdsourced flood data. As discussed in the internship report of Glas et al., (2022), this data layer comes with significant limitations. Firstly, there is no time component registered with the flood dept measurements. Therefore, it is uncertain if the measurements represent the peak water depth. Moreover, the measurements are taken by volunteers during a crisis situation with the usage of an app. During the crisis, the network service was limited in the region. Consequently, it is possible that measurement data is saved as soon as the network connection was re-established. This location can differ from the flood depth measurement location. Taken these major factors of uncertainties into account, it is concluded that the crowdsourced flood depth measurements do not contribute to the validation of the FFS-model, however they are also not undermining the potential accuracy of the model.
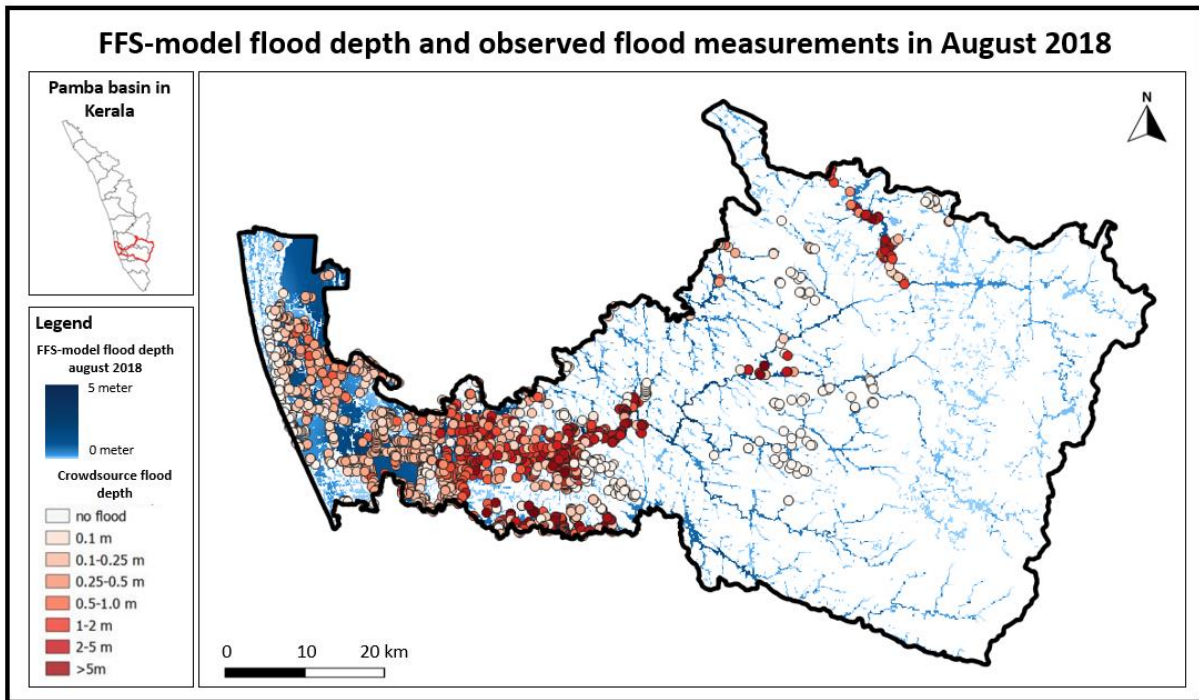
Figure 24 FFS-model flood depth and observed flood measurements in August 2018
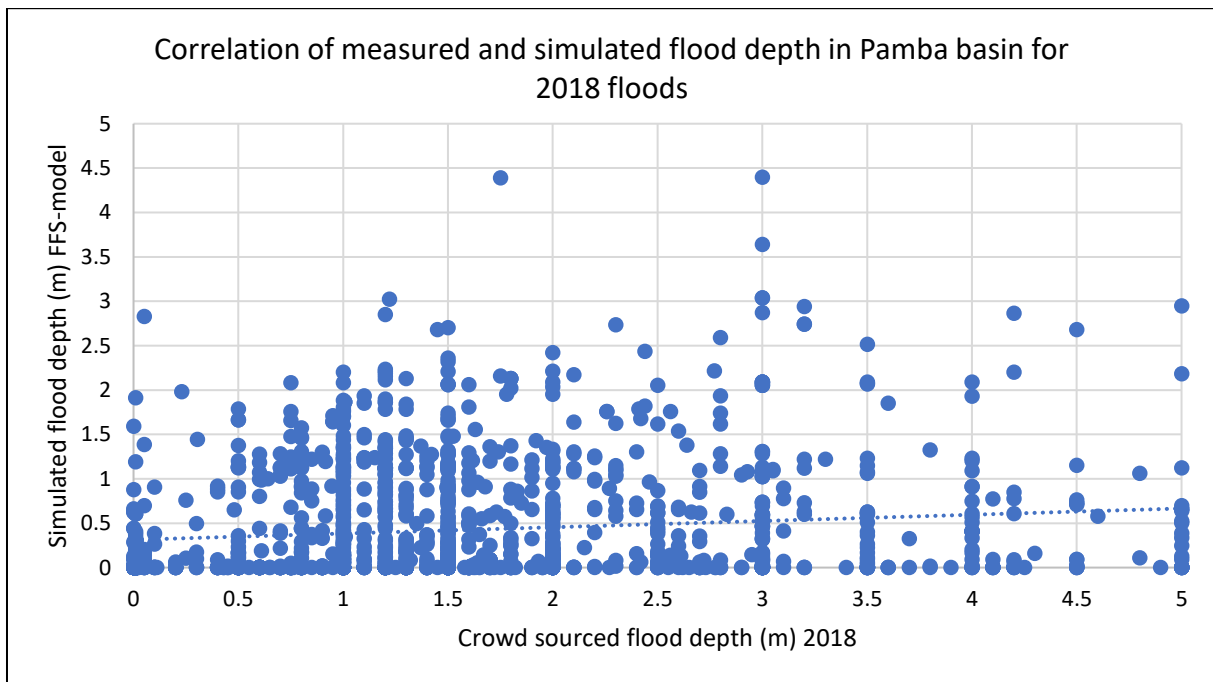
Figure 25 Correlation of measured and simulated flood depth in Pamba Basin for 2018 floods

An additional data set, that is available from the 2018 floods, are the house damages, see figure 52 in appendix H. The house damages are categorized in different damages classes. For each of the registered houses the simulated flood depth value, resulting from the 2018 FFS-model simulation, is determined. In the boxplot, as presented in figure 26, the flood depts per damage category are presented. It is visible that the spread in flood depths per damage category is enormous and that an increase in house damage percentage is not associated with an increased average in flood depth. Also, this observation raises questions about the validity of the FFS-model.

However, it is important to consider the limitations associated with the damaged houses dataset. As described in the internship report of Glas et al., (2022), house damages are also dependent on flow velocity and duration attributes. Moreover, the construction material of a house is of high importance when

assessing flood damages. These datasets are currently not available or accessible. Additionally, the house damage registration after the 2018 and 2019 floods is performed by a large group of government employees with likely some differentiation in interpretation of house damages. Local experts indicated that the large amount of money that came available to compensate for residential flood damages was also distributed to people that already had a low living standard and could use the money well to improve their housing situation. This made the money distribution partly independent from the question if a specific house was damaged by the floods.

Overall, this analysis shows the difficulty to link flood depth to building vulnerability. The results do not contribute to the validation of the FFS-model. Nevertheless, due to the limitations associated with the damage houses dataset the results can also not serve as prove of disfunction of the FFS-model.
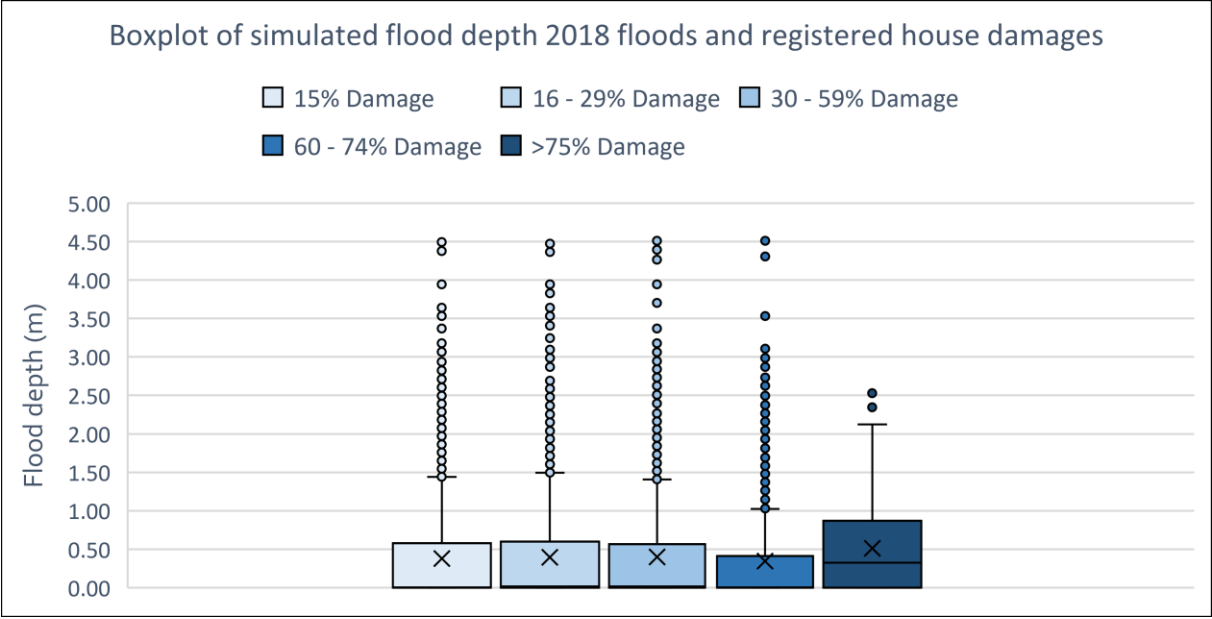
Figure 26 Boxplot of simulated flood depth 2018 floods and registered house damages

5.3.4. Comparison with CIMA flood hazard results

In 2020 the CIMA research foundation provided KSDMA with simulated flood depth data for 10-, 25-, 50-, 100-, 200- and 500-year return period flood events, on a resolution of 150 meters. These results are generated using Continuum model, which is a conventional dynamic flood model set-up. The resulting hazard maps are currently the most detailed flood hazard data that is locally available for flood exposure and hazard assessments. Unfortunately, a lot of information on how these flood hazard maps were developed is unknown. There is, for example, no access to data that indicates the rainfall quantification used for the return period hazard maps. It is known that discharge measurements are used for model calibration, however the associated performance indicators or validation approaches are uncertain. Despite the uncertainties related to the development of the CIMA flood hazard maps, it are currently the only flood hazard simulation data that is available to local decision makers. Therefor it is of value to compare the outcomes of the simulations the FFS-model results.

The flood extent of the CIMA and FFS-model flood maps are compared, see figure 27. It is visible that the main river pattern is similar. However, the FFS-model shows much more upstream side channels and local depressions then the CIMA hazard map. Additionally, the downstream CIMA inundation extent is more extensive then the FFS-model results.

It is difficult to access why and how the difference in flood extent occurs due to the limited knowledge about the CIMA flood model set-up. It could be possible that the CIMA foundation used a more course DEM what led to a less defined channel network. It is also possible that the CIMA research institute utilized discharge as main water input and purely focused on fluvial flooding. The FFS-model uses, besides a base discharge component, dominantly rainfall as water input. Therefore, flash flood and pluvial flood consequences in side-channels and local depressions become more apparent.

When comparing the damaged house dataset of 2018 with the CIMA hazard maps, it is visible that there are quite some damaged houses where, according to the CIMA simulations, no inundation finds place. The FFS-model does show inundation on locations further away from the main Pamba river. This leads to the reasoning that the FFS-model shows a more accurate representation of reality. In the internship report by Glas et al., (2022) the CIMA flood maps were correlated with the crowdsourced flood depth measurements and the house damage data using a similar method as shown in section 5.3.4. Similar as the FFS-model results, also the CIMA flood maps did not show any correlation.

The validation efforts using radar data, as discussed in section 5.3.2, reveal that certain downstream regions show radar inundation despite not being inundated in the FFS-model. In the CIMA results, these areas are inundated. This contributes to the statement that the FFS-model indeed underestimates the downstream flood extent.

The comparison of flood depth values shows no clear correlation between the FFS-flood and CIMA flood hazard maps. It is interesting to note that the CIMA results show extreme inundation depths up to 80 meters, whereas the FFS-model never shows inundation depths above the 6 meters. The extreme water depths in the CIMA results are likely due to elevation model errors which create small depressions who fill up during a simulation. Overall, the lacking correlation between the FFS-model and CIMA inundation depths lead to questions about both the models their validity.
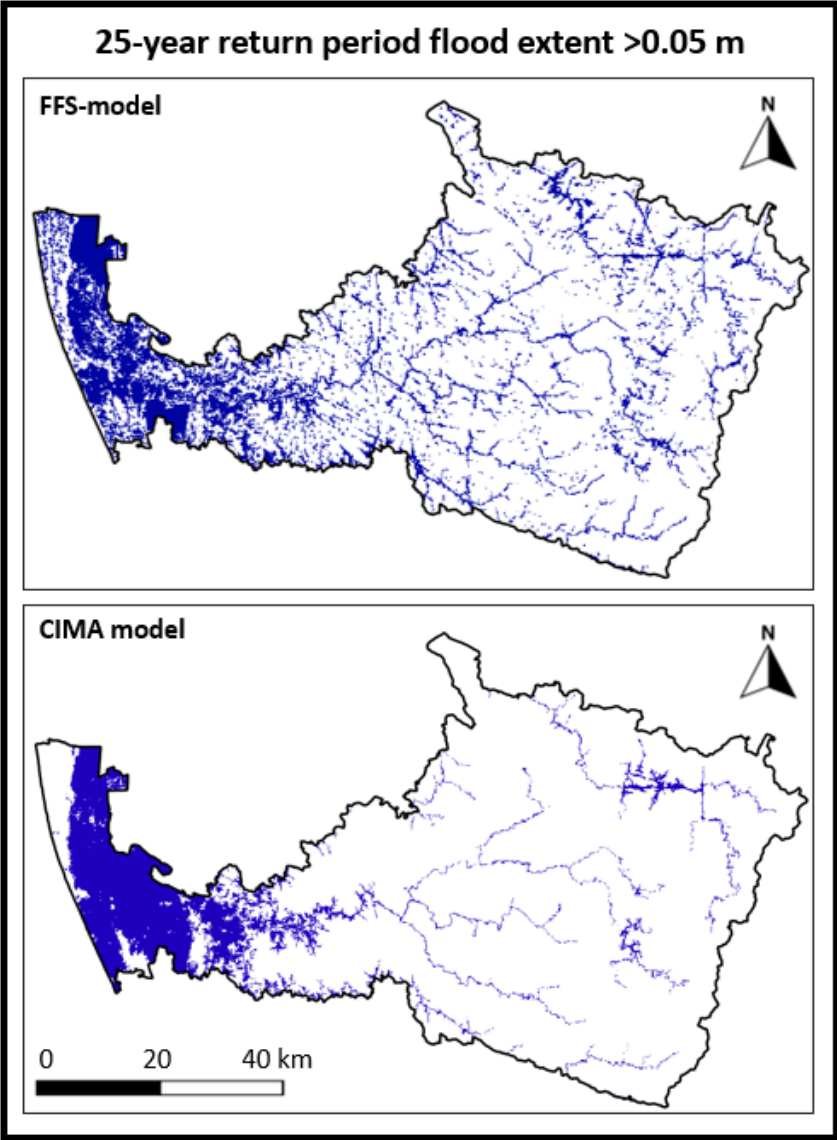
Figure 27 Flood extent comparison CIMA and FFS flood hazard maps with 25-year return period

5.4. Discussion sub-objective 2

The results in this chapter contribute to the research goal to investigate the applicability of the FFS-model for the Pamba Basin region. In the following sections a discussion related to the calibration and validation of the FFS-model is given.

5.4.1. FFS-model calibration

For the calibration process a selection of six historic peak events is used. A limitation of this selection is that five out of the six events have a 72-hour rainfall intensity lower than the 5-year return period threshold. As consequence the calibration process potentially lacks the representation of extreme peak events. During extreme peak events hydrological processes such as infiltration and flow velocities can change what leads to variations in rainfall-discharge relationships.

Utilizing a calibration set-up derived from six independent events mitigates the risks over overfitting the model. In the calibration test set-up, it is visible that a variation of calibration settings could lead to more accurate representations of one individual event. Nevertheless, the final concluded calibration set-up leads to overall good calibration performance indicators.

An important remark to make is that the complete calibration of the FFS-model for Pamba Basin is focussed on one river discharge gauging station. This creates a large dependency and is for catchment calibration processes undesirable. Preferably complete time series of river discharge data for a variation of regions (upstream & downstream) are considered. Especially in the downstream region of the Pamba Basin, the river network splits in numerous small natural and man-made side branches and canals. The height differences in this region are limited and potentially water from the Manimala and Achankovil river are also contributing to the downstream water volume. The complexity of this downstream river system is currently not well represented in the calibration set-up.

Additionally, a major difficulty in the calibration set-up is the estimation of base discharges. Input data representing the initial condition is an important attribute in hydraulic modelling (Bates & Anderson, 1996; Massaria et al., 2014). Also, the sensitivity analyses indicated that the base discharge input has a significant impact on the simulated discharges. Infiltration and runoff form the largest contributions in the water balance of a flood. Therefore, soil water conditions are required to model infiltration accurately (Paul et al., 2014). For a flood event it makes a significant difference if an extreme precipitation event is preceded by a long period of drought or by a period of rain that already filled much of the river and reservoir storages.

For the six calibration events, the three-day average discharge preceding the peak event is used. This choice is catchment specific and the spread in the correlation scatterplots clearly indicates the uncertainty related the base discharge thresholds. Additionally, the approach is not applicable when simulating potential future events, simply because the base discharge preceding future events is not known. The choice to use an uniform base discharge of 640 m^3/s for all hazard return period simulations is questionable. Unfortunately, the existing data and FFS-model set-up do not give the ability for an easily interpretable approach which considers a probability density related base discharge attribute.

5.4.2. FFS-model validation

To validate the concluded calibration set-up for Pamba Basin a variation of approaches is used. Firstly, the flow network patterns of the FFS-model are compared with high resolution satellite images. This analysis showed in the lower mid-lands and downstream regions quite some disparities. This is likely due to the limited elevation changes in the downstream region. By uploading a river network map in the FFS-model, the simulated river patterns increased in accuracy compared to the high resolution satellite images. Important to note is that the available river network map mainly focussed on the main river stream. Upstream river tributaries and downstream side branches are not included in the channel maps.

Additionally, a comparative flood extent analyses is performed using Sentinel-1 radar data. Flood extent maps resulting from radar come with a considerable list of sidenotes. Firstly, radar imagery is affected by terrain attributes such as vegetation. The Pamba Basin is a densely vegetated region, it is likely that the radar observed flood extent is underestimated due to the fact that inundated regions were covered by vegetation. Especially the many tributaries of the Pamba river, are not detachable on the radar water extent imagery.

A next origin of uncertainty is the course temporal resolution of Sentinel-1 data. For this reason, it is uncertain if the available 2018 and 2019 flood event radar imagery has captured the most extreme flood

extent of the hazard events. The 2018 the radar imagery is collected 6 days after the peak rainfall event. Infiltration and runoff processes during that period of time can have had significant effects on the flood extent in the region. Moreover, the event simulations focussed on rainfall volumes during the highest 72h rainfall peak. Rainfall preceding and after this peak, does have an important role in the hydrological behaviour of a flood. These effects are currently not well represented in the simulation.

Finally, technical radar settings such as the incidence angle, polarisation of a radar signal and image processing attributes come with variating levels of accuracy. For this research, the recommended practise for flood extent analyses by the United Nations for of outer space affairs is applied in GEE. For this research the different thresholds for SAR parameters and data (pre)processing are not adjusted or optimized for the Pamba Basin area. Tiwari et al., (2020) describes a study concerning flood inundation mapping for the 2018 Kerala floods also using GEE. This study applies an Otsu method and validates the results with sentinel-2 images for the 10th and 20th of August 2018. The overall accuracy was determined as respectively 94.3% and 94.1%. Potentially, the radar flood imagery, as used in this research, could be further improved using this Otsu method. Additionally, novel methods using machine learning, for example described by Tiampo et al., (2021), show promising results to improve the accuracy of radar-based flood extent mapping. These methods are not considered in the scope of this research.

Overall, the radar validation attempts do indicate similar inundation patterns as simulated by the FFS-model. However, the flood extents of the radar imagery are significantly smaller than the simulated flood extents. This is likely due to the described limitations associated with radar imagery flood extent. It is interesting to see that the radar imagery shows a spotted inundation pattern instead of large increases in river width. This inundation pattern indicates dominantly pluvial flooding more than extensive fluvial flooding. Concerning are the regions that show radar inundation and no flood extent for the FFS-model. This could lead to an underestimation of flood risk in the downstream located LSGs. A potential cause for this underestimation is a too low selected base discharge setting for the 2018 flood event. Due to the broken discharge measurement station no clear base discharge could be defined, therefor the extreme return period threshold of 640 m^3/s is applied. This is likely too small, especially because in the weeks before the flood events of 2018, already extreme precipitation volumes were experienced. Moreover, the choice was made to not incorporate dam discharge in the 2018 and 2019 flood simulations. Especially for the 2018 event, this could have led to an underestimation of river discharge and consequently a false negative representation of flood extent in the downstream area.

The next validation approach focussed on the collected flood depth and damage data of the 2018 floods. As already discussed in the result sections, the completeness and accuracy of the available datasets are highly uncertain. This is also confirmed by local experts. For this reason, it is determined that validation of the FFS-model using these data sets is not a reliable possibility.

The final analyses discussed in this chapter is the comparison of the FFS-model with the available CIMA hazard maps. It is unknown how the CIMA hazard simulations are validated, therefor it is questionable if this comparison can be seen as a validation method of the FFS-model. The comparison of flood depths did not show any clear correlation. This is a concerning observation and difficult to explain to local decision makers. The unknown CIMA simulation set-up makes it difficult to get grip on causes of disparities. It does seem that the CIMA results are generated from a discharge-based water input configuration whereas the FFS-model mainly considers rainfall. The radar imagery shows a more pluvial flooding inundation pattern then a fluvial inundation pattern. This observation argues for a flood modelling approach which incorporates spatial rainfall intensities and local depressions independent from the main river channel. From this perspective the FFS-model seems more applicable then the CIMA hazard maps.

A final remark is that in the current hazard analyses, coastal flooding is not considered. It is unknown if the CIMA research foundation included coastal dynamics in their model set-up.

Chapter 6: Results: Application of FFS-model

The last research sub-objective aims to analyse the applicability of the FFS-model in combination with the RiskChanges tool for flood risk assessments and provide insight in the effects of interventions. In the first sections, the flood hazard maps for different return periods and climate scenarios are discussed. Next, the flood exposure for schools and hospitals in the Pamba Basin is presented. Subsequently, a flood exposure, loss and risk assessment for built-up areas in the three case-study LSGs is described. Additionally, an analysis is made regarding the effects of different flood mitigation measures on the flood hazards and exposure at a Local Self-Government (LSG) level. This chapter finalizes with a discussion reflecting on the presented results.

6.1. Analyses of flood hazard maps

In figure 17 of section 5.1 the flood hazard maps for different return periods in the Pamba Basin are presented. Visually the differences between the return period maps are hard to detect. In figure 28 the flood extent of the different return periods is visualised. Additionally, figure 53 in appendix I shows the water depth difference between a 5- and 50-year return period rainfall event. The difference in flood volume for the flood events with different return periods is presented in table 19. It is important to note that the FFS-model flood maps are not a snapshot in time. They represent the most extreme water depth for each grid cell over the period of a hazard occurrence. Consequently, the same "drop of water" can contribute to the maximum flood depth in multiple grid cells.

Table 19 Flood volume comparison for flood events with different return periods

Return period (RP) of flood event	72h rainfall intensity (mm/h)	% increase in rainfall intensity compared to 5-year RP	Volume of water in flood hazard map (m³)	% volume difference compared to 5-year RP
5 years	2.36		19169.4	
10 years	2.68	13.6%	20877.0	8.91%
25 years	3.07	30.1%	22857.9	19.24%
50 years	3.40	44.1%	24467.3	27.64%

In figure 28 it can be observed that, at a 150-meter resolution, the flood extent varies very minimally. From the volume analyses, it can be concluded that an increase in rain does significantly affect the flood volume, however rainfall intensity and flood volume are not linearly correlated. Meaning that 10% of additional rain does not automatically lead to 10% additional hazardous water volume. The additional water volume mostly effects the observed water depths. The difference in water depth between a 5- and 50-year return period flood event fluctuates on most places between 20 and 50 cm.

Overall, the differences in flood extent and depth for different return periods seem smaller than would be expected. This could be caused by the fact that the difference in return period is purely driven by changes in rainfall intensity. The base-discharge condition remains equal. Moreover, the course DEM and related course modelling resolution could affect the limited spread of water to neighbouring grid cells. In a course DEM the height difference between cells is relatively larger as compared to a higher resolution DEM. Therefor the spatial spread is less visible. Moreover, the 72-hour cumulative rainfall is uniformly spread over time and space for the hazard maps. This leads to relative lower rain intensities per hour and less extreme rainfall accumulations at specific locations.
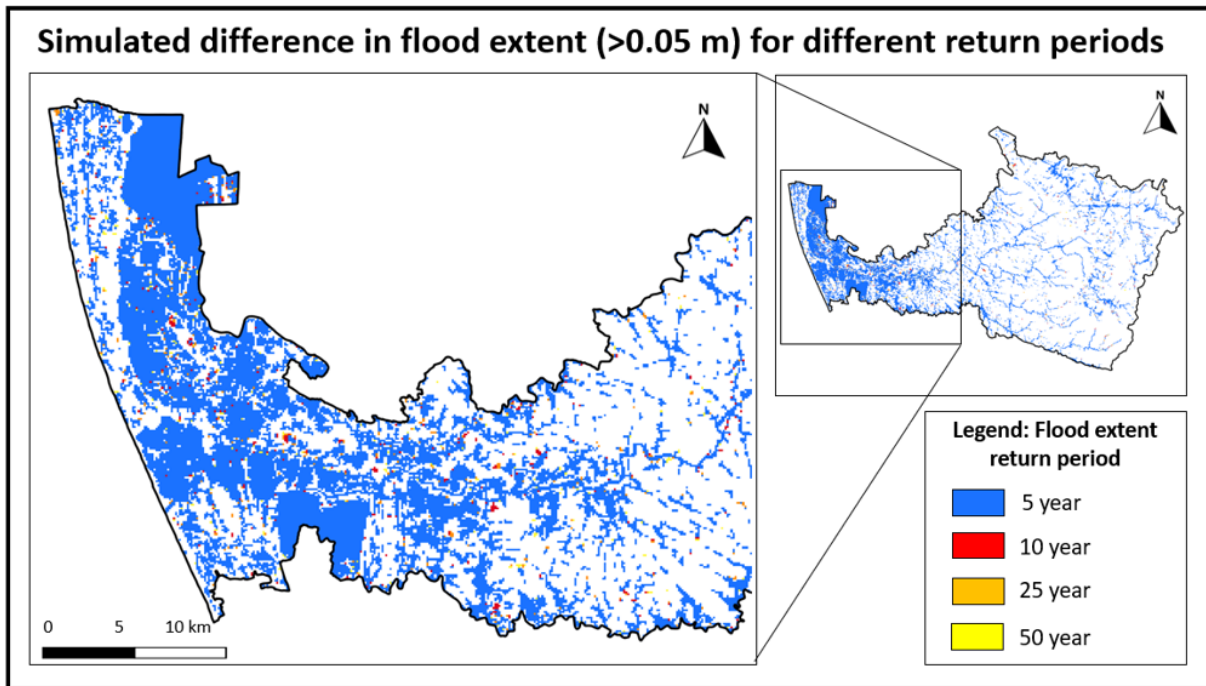
Figure 28 Simulated difference in flood extent (>0.05 m) for different return periods

6.2. Flood hazard under a changing climate

Flood hazard maps for the different climate scenarios are composed using the calibrated model set-up and climate scenario rainfall thresholds. In figure 29 the difference in flood depth between a 10-year return period hazard map derived from a historic inventory is compared with the RCP 4.5 and RCP 8.5 scenarios. It is clearly visible that a higher rainfall multiplier leads to larger increases in flood depth. Figure 54 in appendix I shows the flood extent difference between the 10-year historic inventory hazard map and the most extreme climate scenario of 2075 RCP 8.5. In this figure it is visible that the flood extent expands, however this expansion is limited. This is in line with the observations regarding flood extents for different return periods in section 6.1.
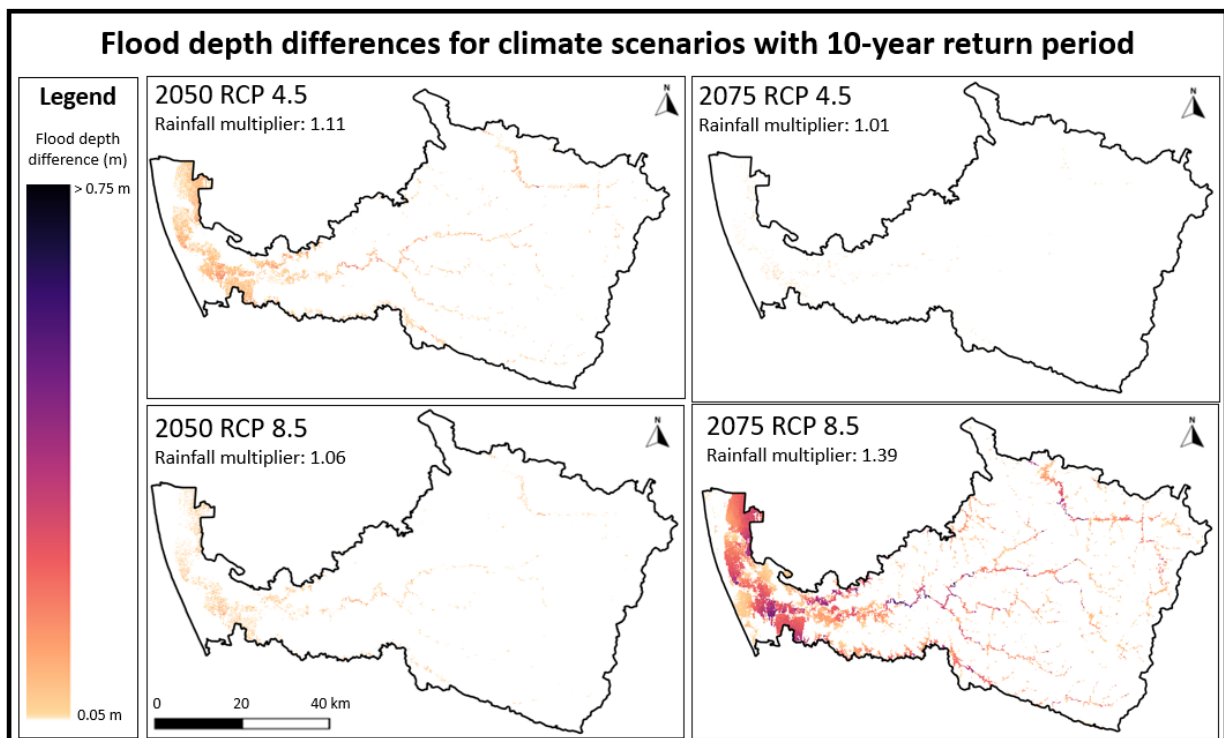
Figure 29 Flood depth differences for climate scenarios with 10-year return period as compared to a 10-year flood event based on recent historical information

Furthermore, the flood volume of the different climate scenarios is compared, similarly as presented in section 6.1. The results of this analyses are shown in table 20. The results indicate again that a percentual increase in rain intensity is not linearly linked to an increase in hazardous water volume.

Table 20 Changes in rainfall and flood hazard volume for different climate scenarios

	10-year RP 72h rain (mm/h)	% difference in rain volume	Volume of water in flood hazard map (m³)	% difference in water volume
Historic	2.68		20877.0	
2025 RCP 4.5	2.60	-3.0%	20508.8	-1.8%
2050 RCP 4.5	2.98	11.0%	22412.8	7.4%
2075 RCP 4.5	2.71	1.0%	21033.9	0.8%
2025 RCP 8.5	2.81	5.0%	21548.4	3.2%
2050 RCP 8.5	2.84	6.0%	21702.7	4.0%
2075 RCP 8.5	3.73	39.0%	25962.7	24.4%

6.3. Flood exposure of schools and hospitals

Using the RiskChanges software, the exposure of schools and hospitals in Pamba Basin is derived and presented in table 21. Additionally, figure 55 and figure 56 in appendix J show the exposure of these elements-at-risk on a map. School and hospitals are chosen as elements of interest because hospitals are of high importance in any crisis situation and schools are often used as temporary shelter location during crisis. Overall, the results show a concerningly high percentage of schools and hospitals that are exposed to floods. This emphasises the need for flood risk mitigation measures in the region. Moreover, a limited difference in exposure between the return periods is observed. This is caused by the limited differences in flood hazard as discussed in the previous section. An additional point of interest is that most flood-exposed schools and hospitals face flood heights of 5 to 55 cm. These water depths can be considered as flood nuisance and mitigation measures could focus on increasing the foundation height and local drainage and storage applications.

To validate the exposure results, a comparison is made with schools affected during the 2018 floods. It is unknow which exact schools were damaged during these events. However it is known that in the districts that are partly covered by the Pamba basin (Kottayam, Alappuzha, Idukki and Pathanamthitta) 206 out of the 3410 schools were damaged (State Relief Commissioner, 2018). In the Pamba basin catchment 1085 schools are located, when assuming a linear relationship an approximate of 65 damaged schools would be located in the Pamba catchment. The results of the FFS exposure analyses are significantly higher. This can be caused by the fact that in particular the Pamba basin area was more exposed then other regions in the districts. Another possibility is that local elevation deviations, for example caused by foundation height, mitigated flood damages.

Table 21 Flood exposure of schools and hospitals in Pamba Basin

	Schools				Hospitals			
Water depth (m)	5-year	10-year	25-year	50-year	5-year	10-year	25-year	50-year
Not exposed	806	797	786	774	42	40	39	39
0.05-0.55 m	197	199	206	210	10	11	12	12
0.55-1.05 m	51	52	49	49	4	5	5	5
1.05-1.55 m	18	18	24	30	2	1	1	0
1.55-2.55 m	13	19	19	19	1	2	2	3
> 2.55 m	0	0	1	3	0	0	0	0
% exposed >0.05 m	25.7%	26.5%	27.6%	28.7%	28.8%	32.2%	33.9%	33.9%

6.4. Flood exposure, loss and risk assessment built-up area

Using the RiskChanges software the built-up area exposure for the three case-study LSGs is derived, see figure 30. The map in figure 31 shows the spatial distribution of exposed built-up areas in Aranmula. In the presented results it can be observed that approximately half of the buildings in LSGs are exposed to floods.

This is quite concerning and emphasizes the need for flood risk mitigation measures. Similarly, as the school and hospital exposure, most built-up area is exposed to flood depths up to 55 cm.

Flood exposure of build-up area in LSGs of Pamba basin

	5 year RP	10 year RP	25 year RP	50 year RP	5 year RP	10 year RP	25 year RP	50 year RP	5 year RP	10 year RP	25 year RP	50 year RP
		Aran	mula			Edu	thua			Pan	danad	
> 4.05 m	0.0	0.0	0.0	0.0	0.0	0.0	0.0	0.0	0.0	0.0	0.0	0.0
2.55-4.05 m	0.3	0.2	0.1	0.2	0.0	0.0	0.0	0.0	0.3	0.4	0.6	0.8
1.55-2.55 m	4.5	1.8	2.6	2.5	0.0	0.0	0.0	0.0	1.7	2.4	3.2	3.3
1.05-1.55 m	2.3	2.2	2.2	2.6	0.3	0.4	0.5	0.5	2.6	2.1	1.6	1.8
0.55-1.05 m	9.2	9.2	11.8	11.4	0.8	0.7	1.1	1.2	4.8	4.8	4.1	3.8
0.05-0.55 m	26.7	29.9	27.4	27.3	39.3	39.9	39.3	39.9	20.8	21.5	22.3	22.2
No exposure	52.4	52.1	51.4	51.3	47.1	46.5	46.7	46.0	25.5	24.5	23.8	23.7

Flood depth exposure class (m)

Figure 30 Flood exposure of built-up area in LSGs of Pamba Basin
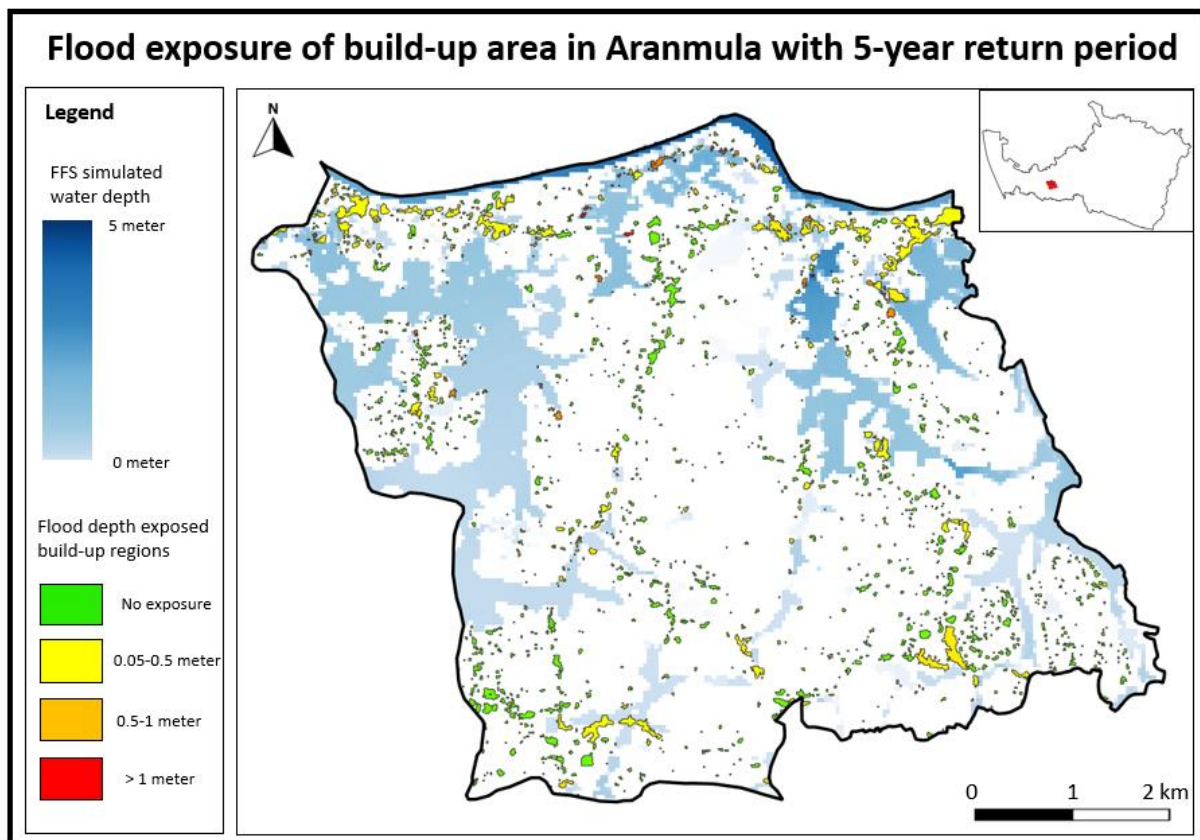
Figure 31 Flood exposure of built-up area in Aranmula with 5-year return period

To analyse the amount of people exposed to floods, the KSDMA population statistics from 2011 are compared with WorldPop data of 2020, see table 22. It is visible that the population counts of KSDMA are

significantly larger than the WorldPop data. Local experts did not observe a drastic population decrease over the past years. To avoid underestimation of the flood exposure analyses, the KSDMA 2011 population data is used in this research. To determine the amount of people exposed to floods, the population count per LSG is uniformly divided over all built-up area grid cells, the built-up area cells have an area of 85 m². In table 22 the total population per LSG, the amount of built-up area grid cells and consequently the population count per building grid cell is presented. Figure 57 in appendix J presents the population exposure for the different LSGs. In Aranmula an approximate count of 13.000 people is exposed to floods, in Edathua and Pandanad respectively 9.000 and 6.000.

Table 22 Population statistics for built-up area at LSG level

Population exposure	Population according to WorldPop data (2020)	Total population of LSG (KSDMA, 2011)	Amount built-up grid cells (85 m²)	Population counts per building grid cell
Aranmula	18430	28695	11219	2.56
Edathua	10736	11489	6554	1.75
Pandanad	6565	19094	10299	1.85

The next step in a flood risk assessment is the vulnerability analyses using a vulnerability curve. Vulnerability curves express a correlation between a flood metric (e.g., flood height) and damage ratio for a specific type of element-at-risk (Yum et al., 2021). Local experts indicated that the JRC vulnerability curve for residential buildings in Asia is not suitable for the Pamba Basin. In their opinion a flood depth of 50 cm should not lead to an average building loss of 33%. Therefore an adjusted vulnerability curve is composed which integrates local expert insights. In figure 32 the JRC vulnerability cure for residential buildings in Asia and the adjusted vulnerability curve for the Pamba Basin are presented in relation to an estimated average setup of a building in Pamba Basin. In general, more valuable objects are positioned on the first floor, such as kitchen appliances or the goods in a shop. For this reason, flood vulnerability up to 2.5 meter shows a larger increase in vulnerability then for the second floor.
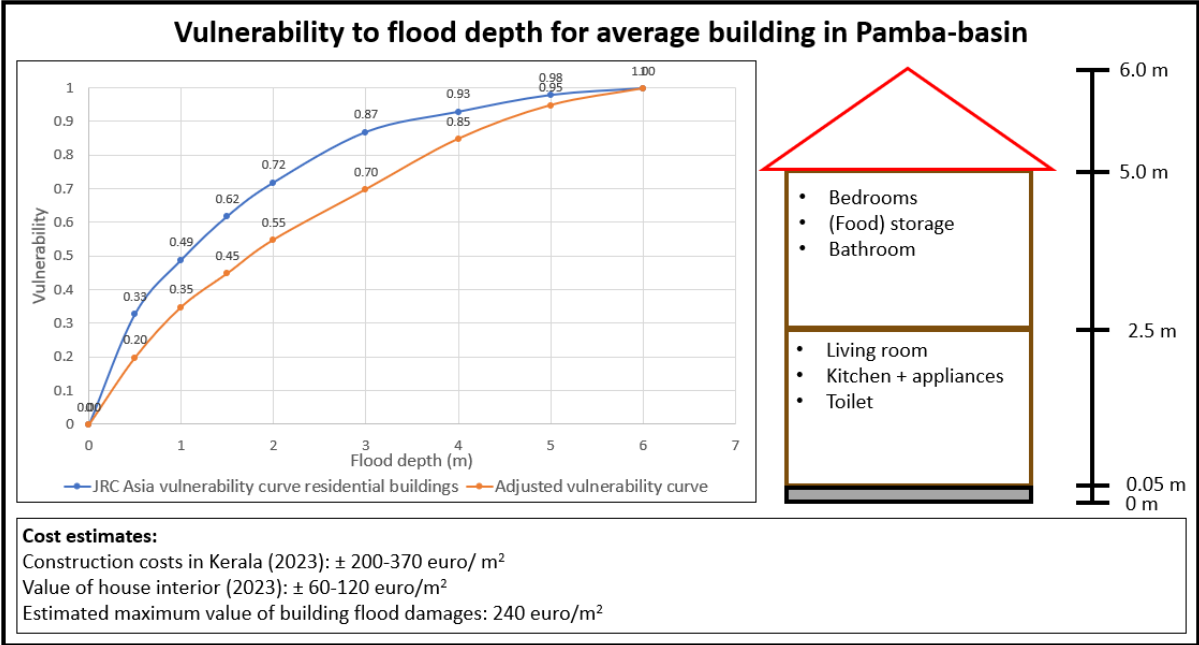
Figure 32 Vulnerability to flood depth for average building in Pamba Basin

The final input that is needed for a flood risk assessment is a cost estimation. For a cost estimate the replacement costs of building contents as well as construction damages needs to be considered. Contracting calculation tools indicate a construction cost between 200 and 370 euro per m² for newly build constructions in Kerala (Property.todaypricerates, 2023; Kishore, 2023). This includes labour and material costs. For flood damaged houses, it is likely that some of the construction elements, for example the foundation, can be reused. For interior house design, including appliances and furniture, value estimates

vary between 60 and 120 euro per m² (NoBroker, 2022). Besides, it is possible that people move valuable items to the second flood of their house when floods are approaching.

The large variation in construction types and interior design luxuries make it complicated to define one average value estimate for all buildings in Pamba basin. In consultation with local experts a value of 240 euro per m² of built-up area is selected as average maximum flood damage. This value includes the repair costs of damaged constructions as well as the replacement costs of interior items. Overall, the threshold is an educated estimation and has no validated research basis.

Using the adjusted vulnerability curve and loss estimate, the flood losses per return period and the risk assessment for built-up area are presented in table 23. It can be concluded that the annual flood risk for LSGs is extensive and dominantly influenced by the 5- and 10-year return period hazard events. Based on these results it is likely that investments in flood mitigation measures are cost-effective. In the discussion section 6.7, an extensive elaboration addressing the uncertainties related to this (quantified) risk assessment is given.

To put the derived loss and risk results in perspective, table 24 shows the distributed damage compensation for household that suffered from the 2018 floods. It is visible that the distributed financial aid is significantly lower than the derived annual flood risks. This is something that would not be expected and indicates a large overestimation in the derived loss and risk results. This could be caused by a too highly estimated building value or a too steep vulnerability curve. Nevertheless, it is good to remember the limitations of the damaged building data set as described in section 6.4. Moreover, the distributed financial aid likely did not cover the all flood damages of households.

Table 23 Loss and risk estimations for three LSGs in Pamba Basin

Return Period (year)	Annual probability	Loss Aranmula (10^6 euro)	Annual Risk Aranmula	Loss Edathua (10^6 euro)	Annual Risk Edathua	Loss Pandanad (10^6 euro)	Annual Risk Pandanad
5	0.2	16.57		6.33		12.02	
10	0.1	17.59		6.48		12.74	
25	0.04	18.40		6.62		13.16	
50	0.02	19.35		6.94		13.71	
Annual risk (10^6 euro)			3.55		1.31		2.56

Tabel 24 Financial aid to households after 2018 floods Kerala

Building damage percentages	Received financial aid in Indian Rupee from the State Disaster Response Fund (SDRF)	Amount of damaged houses in 2018 floods		
		Aranmula	Pandanad	Edathua
15% Damage	10000	292	248	760
16 - 29% Damage	60000	324	186	624
30 - 59% Damage	125000	240	174	287
60 - 74% Damage	250000	93	73	89
>75% Damage	400000	27	0	10
Complete loss of Buildings	400000	39	6	18
Total distributed compensation (Indian Rupee)		1.02×10^8	5.60×10^7	1.14×10^8
Total distributed compensation (10^6 euro, 2023 exchange rate)		1.12	0.62	1.26

6.5. Simulation of flood mitigation measures

This section evaluates on the simulation of different mitigation interventions on flood hazard in Pandanad LSG. For the flood risk assessment of built-up area, as described in section 6.4, the scale-up function of the FFS-model is used to create the flood hazard maps on LSG level. As described in the section 3.6, this method

is not applicable for mitigation design testing on LSG level. Consequently, an FFS-model on LSG scale with a discharge boundary condition is applied. For a rainfall event with a return period of 50-years, the discharge boundary condition of Pandanad LSG is 1721 m³/s. When comparing the hazard map that applied the scale-up function with the hazard map using the discharge boundary condition, significant differences are visible. In figure 33 these differences are visualised for Pandanad, research attempts for other LSG showed similar results. In the discharge boundary condition hazard map, the flood depth of the main river is significantly deeper compared to the scaled-up version. Consequently, the scale-up map has much smaller water depths in the river and higher water depts in the surrounding areas. Logically, the water depth of a river should not differ between the two model set-ups. After discussing these observations with dr. B. van den Bout, the conclusion was made that there currently is a high sensitivity to grid cell size in the FFS-model that should not occur. This is a model flaw, and the exact origin of this problem is currently not yet known. Dr. B van den Bout will look further into the cause of the problem.
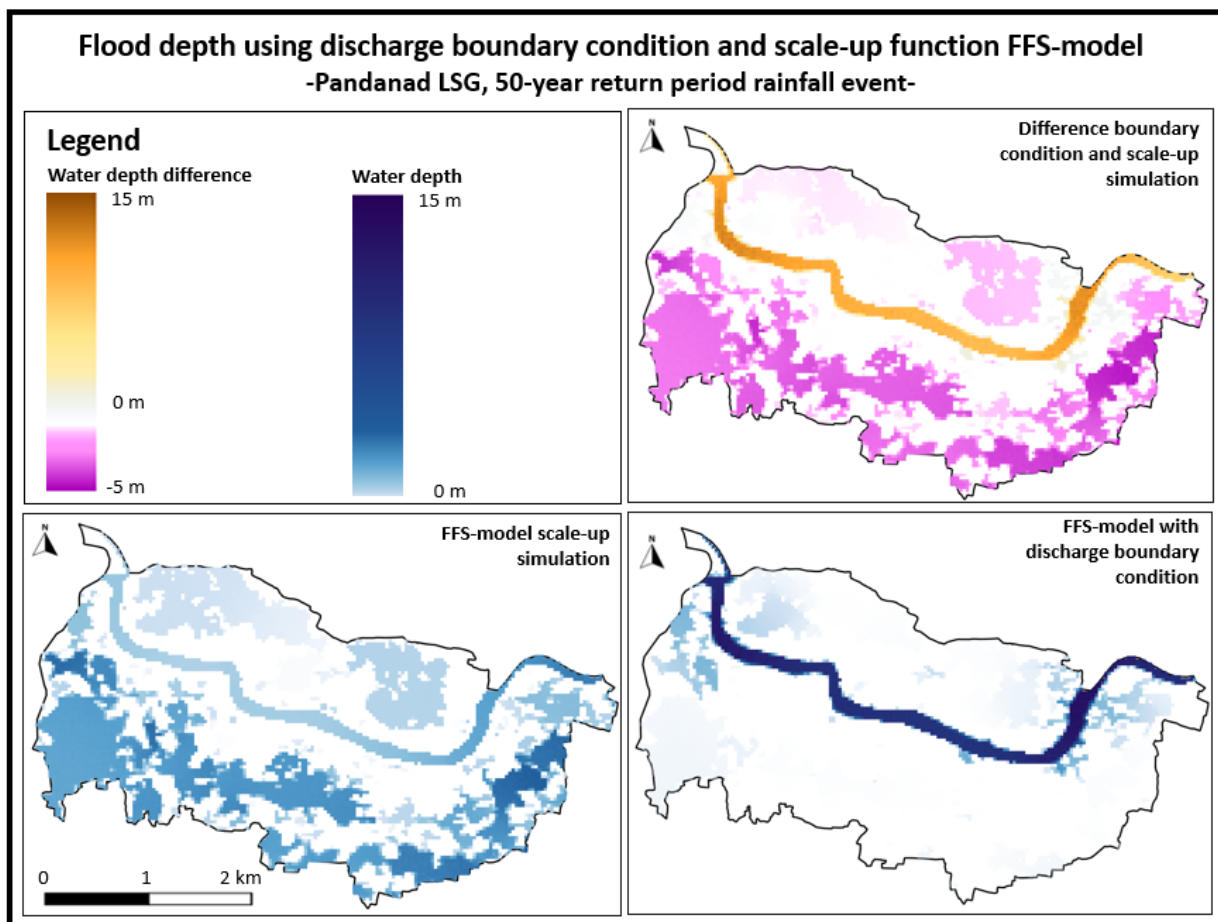
Figure 33 Flood depth using discharge boundary condition and scale-up function FFS-model

Due to the observed model defect, it is concluded that flood mitigation options cannot be verified with the current version of the FFS-model. Nevertheless, the choice is made to still analyse the effects of different mitigation measures on flood hazard. These results cannot be evaluated in a quantitative manner, but with a comparative approach. By comparing the discharge boundary condition flood hazard maps for different mitigation designs, the effects of interventions can be analysed.

In figure 34 the effects of a dike on the flood hazard along the Pamba river in Pandanad LSG is visualised. For the same study area also the effects of river dredging, and floodplain construction is derived, these results are visible in figure 58 and 59 in appendix K. In the original flood hazard map, it is visible that there are many built-up regions exposed to flood. For all three the interventions, the flood extent reduces in size and many of the inundated areas are not exposed anymore. Remarkable is that the flood exposure is reduced quite significantly with measures in the order of magnitude of 50 cm. Due to the scaling problems it is not possible to conclude if this resembles the actual situation. However, when measures such as a 50

cm dike height construction would significantly reduce flood exposure and the related risks, it is quite likely cost-efficient to apply such measures.
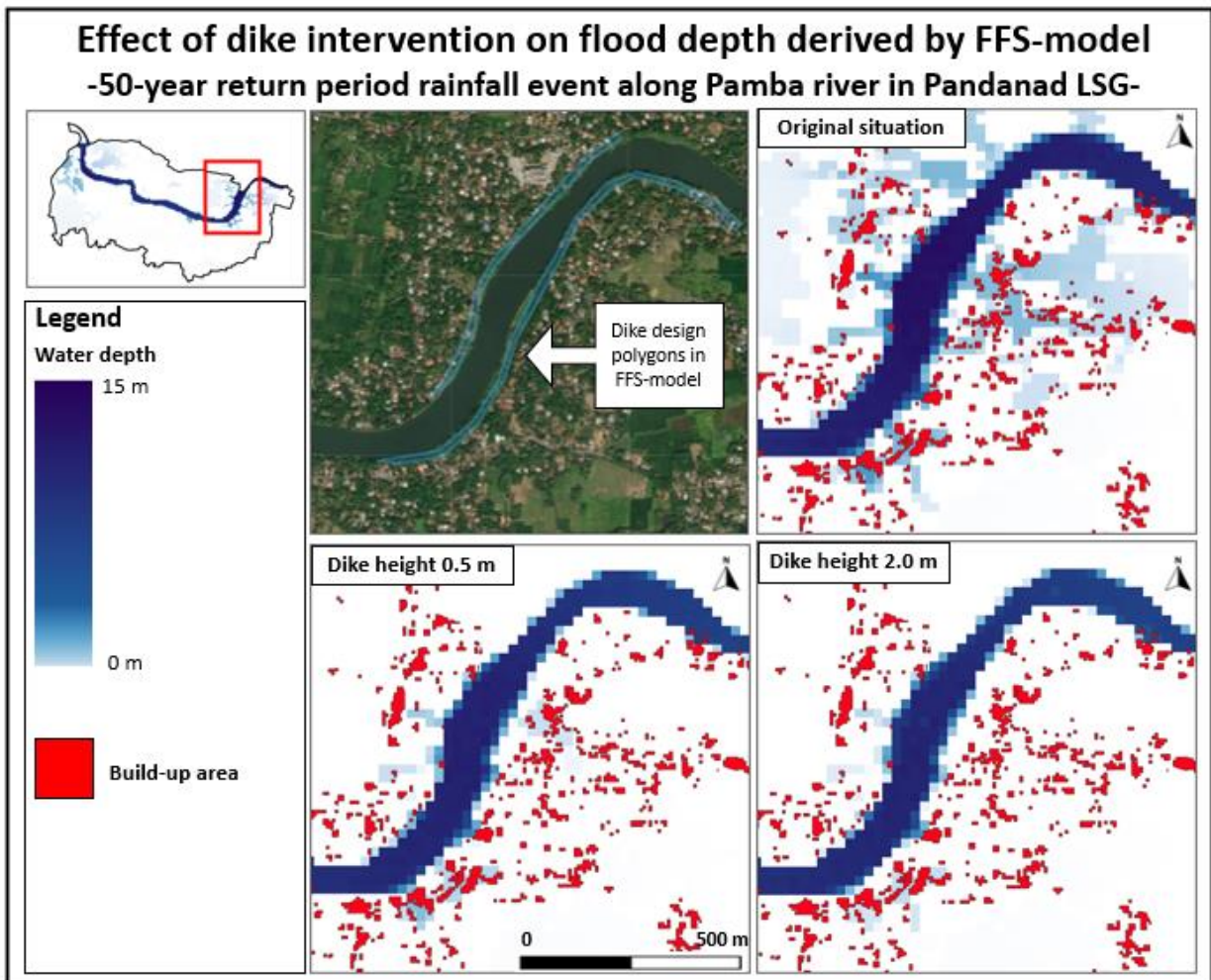
Figure 34 Effect of dike intervention of flood depth derived by FFS-model

6.6. Effects of mitigation measures on flood exposure

To analyse the effects of mitigation measures on flood exposure, the same RiskChanges based approach as in section 6.4 is used. The results of the exposure analyses are presented in figure 35. Moreover, figure 36 shows a visual representation of the flood exposure per building polygon for a dike intervention scenario. It is visible that the intervention designs certainly reduce the built-up flood exposure in the area. In the original situation 7.8 ha of the total 13 ha built-up area is exposed to flood height >0.05m. With the 2-meter dike intervention, this exposed area is reduced to 3.3 ha of built-up area. To reach similar results with a relocation intervention, 4.5 ha of built-up area, with an approximate value of 10.8 million euro, and 1000 inhabitants need to be permanently relocated. These estimates are based on the same building value and population statistics as used in section 6.4. Eventough the quantitative quality of the presented results is subject to strong limitations, the applied method and potential for visual presentation can be insightful for local policy makers in the face of risk-based decision-making.

Build-up area exposure under various intervention design options -50 year retrun period rainfall event along Pamba River in Pandanad LSG-

	Original	Dike intervention		River dredging		Flood plain intervention	
	no intervention	0.5 m height	2.0 m height	0.5 m deepening	2.0 m deepening	0.5 m floodplains	2.0 m floodplains
> 6.05 m	0.6	0.1	0.1	0.0	0.1	0.1	0.2
4.05 - 6.05 m	0.0	0.1	0.2	0.2	0.3	0.0	0.0
2.55-4.05 m	0.0	0.0	0.0	0.1	0.1	0.0	0.0
1.55-2.55 m	0.2	0.0	0.2	0.0	0.0	0.0	0.0
1.05-1.55 m	1.1	0.6	0.2	0.8	0.1	0.8	0.0
0.55-1.05 m	2.3	0.3	0.1	0.1	0.6	0.1	0.8
0.05-0.55 m	3.6	3.1	2.5	2.0	1.9	2.3	2.1
No exposure	5.1	8.8	9.7	9.9	9.9	9.7	9.9

Figure 35 Built-up area exposure under various intervention design option
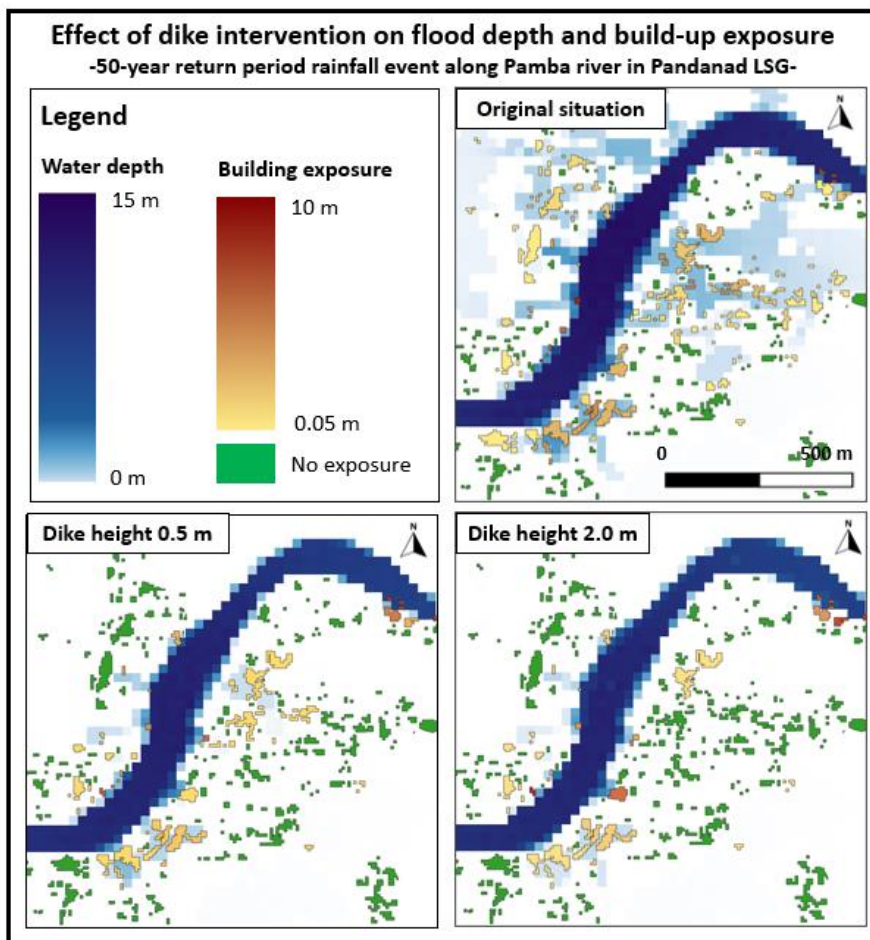
Figure 36 Effect of dike intervention of flood depth and built-up exposure

6.7. Discussion sub-objective 3

The research goal of sub-objective three is to evaluate on the applicability of the FFS-model in combination with the RiskChanges to create insight in flood exposure, loss and risk on LSG level. Additionally, the effects of climate change and mitigation measures on flood hazard is analysed. In this discussion section the presented results are discussed and elaborations concerning associated uncertainties are given.

6.7.1. Flood hazard results

With respect to the flood hazard results, a first important remark relates to the DEM uncertainties. Oksanen (2003) defines three main types of errors in DEM's. Firstly, the gross errors due to topographical misinterpretations during the mapping process. Additionally, systematic DEM errors as biases or artifacts due to applied procedures or systems. Finally, a DEM can be subject to random errors which are the results of mistakes such as inaccurate surveying or improper recording of data (Oksanen, 2003; Wechsler, n.d.).

The vertical accuracy of the Copernicus DEM is evaluated in different research papers such as H. Li et al., (2022) and Ghannadi et al., (2023). Per study area the accuracy slightly differs. Overall, a vertical accuracy around 6 meters is estimated. In the presented flood hazard maps, flood depths in the order of magnitude of decimetres is discussed. In relation to each other, these flood hazard maps are valuable to analyse. However, it is important to consider that the quantitative values of flood depths come with a large range of uncertainty.

Moreover, the flood hazard maps are all derived using 72h uniformly spread cumulative rainfall. This set-up is chosen as it showed the highest correlation in the rainfall-discharge analyses used in the calibration of the FFS-model. Nevertheless, it is very likely that flood hazards behave differently when evaluating hourly or daily peak rainfall. These scenarios are currently not included in the flood hazard maps and this can give a distorted image of flood hazard. Nevertheless, in the rainfall analyses the daily, 72h and weakly return period cumulative rainfall quantifications all differ around the 44% when comparing the 5-year with the 50-year return periods. Therefore, you can argue that differences in flood extent and flood depth hazard are in comparable orders of magnitude. Still, it is important to consider that the calibration set-up, as used in this research, is fully focussed on 72h cumulative rainfall. The accuracy of the FFS-model for different cumulative rainfall event durations is currently unknown and likely deviates due to differences related to flow velocities and infiltration rates.

Concerning the climate scenario flood hazard results, besides the uncertainties associated with the rainfall multipliers, the base discharge setting is the largest source of uncertainty. For the current analyses this base discharge setting is not adjusted and a constant parameter setting of 640 m^3/s is used. Logically, the base discharge setting would change as consequence of climatic developments. Unfortunately, too many uncertainties are currently associated with the base discharge estimation to give a quantified estimation of its climatic developments. An additional source of uncertainty is the future land-use and associated Manning's N parameter used in the FFS-model. For the climate scenario flood hazard maps, the assumption is made that no land-use changes occur. In reality this is, over a time span up to 2075 quite unlikely.

A final remark regarding the flood hazard analyses, is fact that flow velocities and flood duration are not considered in this research. Currently, the FFS-model does not have the features to derive these hazard attributes as output. Nevertheless, it is important to be aware of the fact that flow velocity and duration can have a big impact on the hazardous occurrence of a flood and the related loss and risk calculations.

6.7.2. Flood exposure, loss and risk assessment

The flood exposure, loss and risk assessments are affected by the discussed uncertainties and limitations associated with the flood hazard maps. Additionally, the exposure analyses highly depend on the completeness and accuracy of the element-at-risk (EAR) data (Koivumaki et al., 2010). For school and hospitals, the available data from KSDMA is used. The quality of these data layers is not validated within the scope of this research.

As discussed in section 3.5, the completeness of the available opensource built-up area data is lacking. Molch (2009) describes that buildings, that are constructed in densely vegetated regions such as the Pamba basin, are often hard to detect on radar imagery. Initiatives concerning Volunteered Geographic Information (VGI) have significantly increased the global availability of EAR data over the last decade (Goodchild & Li, 2012). OpenStreetMap (OSM) is an example of these extensive VGI efforts. A variety of

studies are available who reflect on the completes of OSM data for specific countries (Yuan Jian tian & Zhou, 2019; Hecht et al., 2013). Unfortunately, there is currently no research available that reflects on the completeness of OSM data for Kerala. Additionally, there are recent developments using Artificial Intelligence (AI) for the creation of building footprints. In example Google Open Buildings has a coverage in Kerala. Lakshmipriya, an ITC student in Geo information science analyses the quality of this novel building data in her thesis. Opensource AI initiatives show promising results for further improvements in accuracy and completeness of Element-At-Risk data.

For this research, the completeness of the built-up area map is improved by merging the World Settlement Footprint data of 2019 with the ESA built-up WordCover classification from 2021. Still, when comparing the results with satellite images there are built-up areas missing in the constructed dataset. Additionally, no data is available assessing building function, height, or construction material. The value of an agricultural shed is currently equal to the value of a residential building or a commercial centre.

It is important to consider that processes such as migration, urbanization, deforestation and the construction of critical infrastructure have a large impact on EAR datasets (Tollan, 2002). In this study, the outdated population data from 2011 is equally divided over the built-up area cells to approximate population exposure. Logically, these assumptions effect the degree of certainty in which the exposure and loss analyses approximate reality.

In the flood exposure results, it is visible that a large number of buildings is exposed to flood with shallow depths from 5 to 55 cm. With these shallow flood depths, individual building characteristics such as foundation height have a significant impact on the actual exposure of a building. As discussed, the used DEM comes with a vertical accuracy up to 6 meters. With this knowledge, it is difficult to give certainty on flood exposure results with an order of magnitude in decimetres. A final made assumption in the flood exposure analyses, is that only exposures depths higher than 5 cm are included in the analyses. In the flood hazard maps there were extensive regions with flood depths up to 5 cm. Considering uncertainties in local terrain and construction heights, the choice is made to only include flood exposure with flood depths higher than 5 cm.

The next step, in the establishment of a risk assessment, is the loss estimation, which comes with major uncertainties. Membele et al., (2022) provides a literary review addressing flood vulnerability in developing countries. The paper concludes that there is large need for flood vulnerability studies and emphasizes the need for community participation in the establishment of such vulnerability assessments. For the case-study region of Pamba Basin there is currently no validated vulnerability curve available. As stated by Praveen et al., (2012) building damages are not just depended on inundation depth but also effected by building height, construction materials, construction maintenance state, flow velocity and flood duration. Information on all these attributes is not available for Pamba Basin. This leads to an oversimplify of the complexity related to vulnerability.

Furthermore, the building value of 240 euro per m^2 is a simplified threshold. In reality, built-up areas have varying building values per m^2 depending on building height, function and construction. In addition, the household effects can highly differ per building. The different described assumptions and simplifications result to very uncertain quantitative loss results.

The final risk assessment depends on the quality of the loss assessment in combination with the temporal accuracy of the flood hazard results. It is difficult to validate the quantitative flood risk results. Nevertheless, the values are of interest when comparing flood risks between different LSGs and defining priorities in policy making. Moreover, the flood risk result can contribute to awareness raising concerning the monetary risks associated with floods. This is valuable when evaluating on the effectiveness and need for different flood risk mitigation measures.

Due to the multifaceted character of uncertainty related to flood risk assessment, it is challenging to quantify and communicate the overall range of uncertainty for the final results. To give a compact insight in the involved uncertainty factors, an overview is created and presented in table 25. In this table the main causes of uncertainty are summarised, and an attempt is made to quantify its magnitude. It is important to consider that this quantification does not have a validated research basis.

Tabel 25 Overview of combined uncertainties involved in flood risk assessment

Factors of uncertainty related to the performed flood risk assessment	Main causes of uncertainty	Approximate quantification of uncertainty
Flood frequency	-Uncertain effects of climate change -Limited certainty on accuracy of used rainfall dataset -Limited calibration and validation data	15-50%
Flood intensity	-Limited DEM quality -Simplified consideration of base discharge condition -Dam discharges are not considered	15-50%
Built-up area data	-High vegetation density complicates radar based built-up area mapping -No consideration of building function or construction type	<15%
School & hospital data	-Uncertain if and how available data is validated or updated	<15%
Population spread	-Usage of outdated population data (2011) -Assumption that population is uniformly spread over built-up area	15%-50%
Building vulnerability	-No consideration of building height or used construction materials and techniques -No consideration of flood duration and flow velocities	50%-100%
Loss estimation	-Highly simplified average building value	50%-100%

6.7.3. Intervention design testing

As discussed in section 6.5, the current function of the FFS-model to test interventions is not working as intended. Consequently, it is uncertain if the presented results are quantitatively representing reality. Taken this into consideration, it is still interesting to critically evaluate on the executed intervention testing approach and results. These discussion points will remain of relevance when the model flaw related to the grid cell sensitivity is solved in the future.

Firstly, the design detailing of interventions in the FFS-model is limited. The functionality to manually adjust the DEM has the same resolution as the applied DEM resolution. Therefore, all measures tested in this research have a size of at least 30 x 30 meters. This is quite course and limits the possibilities for testing smaller scale interventions such as urban streams or wadies. Additionally, the FFS-model does not include any form of morphodynamics analyses. When creating physical river interventions, the sediment balance of a river can significantly change. This can influence the river depth, flow velocity and discharge capacity in the short and long run. Before implementing river interventions, a morphodynamics analyses is needed to ensure that the designed intervention will have the intended result.

Moreover, the effect of interventions on the occurrence of, for example back water curves, is not considered in the FFS-model. When designing river interventions, it is crucial to analyse the influence of these interventions on the upstream and downstream region. The set-up of the FFS-model is currently not capable to evaluate on these effects. A final major uncertainty in the intervention design testing, is the lack of DEM data for the riverbed. In the used Copernicus DEM, the riverbed values are all 0. When testing, for example the effect of river dredging, it is relevant to know the original height of the riverbed.

Chapter 7: Conclusions

In this research, the practical applicability of the Fast Flood Simulation (FFS) model for flood hazard and risk assessments was thoroughly tested for a specific case-study area. The set-up of the FFS-model allows for flood simulations covering the complete Pamba Basin with a run time around 5 seconds. Compared to traditional food models, this is an enormous reduction in computational time.

In the calibration of the FFS-model, different challenges were identified. Firstly, for large catchment areas with a dynamic landscape, the model shows a high sensitivity to the solver accuracy setting. Subsequently, the definition of a base discharge condition is challenging and is preferably substantiated by a complete and accurate rainfall-discharge timeseries. Additionally, it is observed that, especially in areas with limited elevation differences, the FFS-model has difficulties detecting the channel network. This challenge was tackled with the newly designed functionality to upload a channel map in the FFS-model.

The final calibration set-up resulted in a Nash-Sutcliffe Efficiency (NSE) of 0.79 and a PBIAS of 2.4%, this indicates good model performances. The validity of the FFS-model was tested using different approaches. Overall, it is challenging to reflect on the validity of the FFS-model due to large limitations and uncertainties associated with the different validation datasets. The radar extent validation approach led to Cohen's kappa performance values with moderate agreements. This highlights the importance of investment in high-quality validation data for local water authorities.

Overall, the FFS-model, in combination with the RiskChanges tool, offers the possibility to create insightful information regarding flood hazard, exposure and risk. The uncertainties related to the used element-at-risk data, vulnerability curve and loss estimate effect the quantitative quality of the final risk assessment results. Nevertheless, the methodology set-up, as descried in this research, showed a proof of concept on how the FFS-model can practically be used as tool in flood risk assessments.

Additionally, the objective of this research was to assess the suitability of the FFS-model for analysing flood hazard in the face of climatic changes and mitigation measures. The limited computational time offers the possibility to run a large variation of climate scenarios. At this moment in time, there is too limited knowledge about the effects of climatic changes on rainfall variability and base discharge conditions to present well substantiated flood hazard or risk results for the Pamba Basin. Nevertheless, the general set-up of the FFS-model shows the potential to be applied in flood hazard studies reflecting on climatic developments.

During the analysis of the FFS-model suitability in assessing physical mitigation measures, a model flaw was identified. Currently, the model has an unintentional high sensitivity to grid cell resolution. This resulted in large water depth deviations when comparing flood hazard simulations derived with the upscaling functionality and a discharge boundary condition. Consequently, the current model set-up is considered as unsuitable to analyse the quantitative effects of mitigation measures on water height. Nevertheless, the model does offer the ability to create insight in the rough changes in flood hazard after intervention implementation.

In conclusion, the applicability of FFS-model surely creates increased understanding of flood hazard in Pamba Basin under varying conditions. However, a critical view is needed to reflect on the results and consider the remaining limitations and uncertainties when using the FFS-model as tool for risk-informed decision-making.

Chapter 8: Recommendations

In this chapter recommendation concerning future steps in the development and implementation of the Fast Flood Simulation (FFS) model are given. The first section focuses on recommendations specified on the FFS-model application in the Pamba Basin study area. Subsequently, the second section addresses recommendations regarding the FFS-model from a larger perspective and independent of the case-study area.

In the three discussion sections, extensive elaborations regarding the large variety of uncertainties and limitations related to the presented results are given. Many of these uncertainties are related to the accuracy and completeness of data. Obviously, more and higher quality data will result in an increased reliability of research results. However, data associated with natural hazards and risks are in its core subject to many limitations. One of the assets of the FFS-model is its applicability in data-scare regions for which hydraulic modelling tools are currently only limited available. For this reason, the recommendations in this chapter focus on suggestions for the development and implementation of the FFS-model, taken into considerations the limitation of data quality and access.

8.1. FFS-model implementation in Pamba Basin

This section starts with recommendations concerning the flood hazard simulations. Subsequently, suggestion regarding the applicability of the FFS-model for flood risk assessments and risk-informed decision-making in Pamba Basin are given.

8.1.1. Development of flood hazard maps

The first recommendation is to compare the FFS-flood hazard maps with flood hazard maps generated using a conventional (dynamic) flood model. The state-of-the-art setup of the FFS-model, that causes the reduction in computational time, also comes with uncertainties. Dynamic and physically-based flood modelling, using the Saint Venant equations for shallow water flow, have been tested and validated for many areas in the world. It is unknown what exact methodology is used to derive CIMA flood hazard simulations. However, the CIMA results showed large differences with the FFS-model output. This raises questions on the validity of the FFS-model for Pamba Basin.

A local modelling team on state level is, in collaboration with KSDMA, developing a flood model using the HEC-HMS and HEC-RAS software. Unfortunately, insufficient access was provided to these models to compare flood hazard results with the FFS-model. Moreover, a local expert indicated that their flood modelling efforts focus on simulating historic rainfall-discharge relationships. Flood hazard maps for different return periods, as required for flood risk assessments, are currently not composed. It is recommended to compare the results of the FFS-model with the HEC-RAS model when available. If comparison with the HEC-RAS model is not possible, it is recommended to create a conventional flood model in another software, for example openLISEM, and compare the flood hazard results with the FFS-model. Besides openLISEM, also a 1D-2D coupled flood model structure, as used in the paper of Anju at al., (2020) for Pamba basin, could be applied.

Subsequently, the presented flood hazard maps, for different return periods, highly depend on return period rainfall occurrence. The base discharge condition for extreme events is set at a uniform value. This simplification, in combination with the assumption that excessive dam discharges are not considered, is questionable. For future research it is recommended apply a more probabilistic approach towards the composition of return period flood hazard maps. This can be done by combining probability density functions of base discharge, dam discharge and rainfall return periods. Subsequently, it is interesting to analyse the effects of coastal water dynamics on river flood scenarios. These effects are currently completely neglected in the flood hazard maps.

Moreover, the flood hazard simulations in this research are focussed on a 72h cumulative rainfall occurrence. To get a complete view on flood hazard, it is recommended to also apply the presented calibration methodology on other event durations and compare the resulting flood hazard maps.

A final recommendation concerning the flood hazard simulations is to construct a more detailed channel map and upload this in the FFS-model. In the smaller tributaries and side branches of the FFS-model it is

visible that the simulated flow patterns do not always represent the river flow as visible on aerial photographs.

8.1.2. Flood risk assessments and risk-informed decision-making

Currently, local authorities in Pamba Basin do not have access to flood simulation tools. This research showed in which manner the FFS-model in combination with the RiskChanges tool can be applied to derive flood exposure and risk results. However, the many applied simplifications and assumptions create uncertainty regarding the quality of the risk assessments results. A recommended next step is to select several case-study LSGs in Pamba Basin and derive a flood risk assessment in close collaboration with local experts and decision makers. Possibly, Mapathon initiatives and AI developments can contribute to the quality and completeness of local element-at-risk data. Moreover, local experts have a much better understanding of building vulnerabilities and value. Additionally, it could be of interest to obtain higher resolution DEM data for flood prone LSGs and analyse the effect of improved DEM quality on the flood hazard simulations. During this collaboration process, a better understanding of the needs and priorities of local authorities can be created. Furthermore, the interpretability of the FFS-model and the RiskChanges tool by local decision makers can be tested.

Depending on the experiences in the pilot LSGs a well substantiated answer can be created on the question if and how the FFS-model, in combination with the RiskChanges tool, should be applied by local authorities in Kerala. This question mainly depends on the validity of the model output and the interpretability of remaining uncertainties by local decision makers. As described in the wicked problem statement in section 1.1.1, the FFS-model shows large potential for the empowerment of local authorities in decision-making concerning flood risk reduction. However, there is a risk of dangerously removing the required experience for interpreting flood modelling results.

After integrating the collected feedback, the FFS-model application by local authorities could be expanded. It is recommended to collaborate with the Kerala Institute of Local Administration (KILA) in the organization of this initiative. The KILA organization organizes trainings, workshops and seminars with as main objective to facilitate capacity building of LSGs. Perhaps, a training addressing the applicability of the FFS-model in combination with the RiskChanges tool can be organized. To streamline the implementation of the FFS-model by local authorities, it is advisable to minimize the need for local statistical analyses related to rainfall return periods, base flow quantification, and calibration processes. To facilitate this, a manual containing LSG specific calibration settings and recommended ranges of input thresholds could be compiled and distributed to local authorities. This manual should be regularly updated with data addressing, for example, climate change developments.

8.2. Overarching FFS-model development

This section firstly presents recommendation that are applicable on the current usage and setup of the FFS-model and the associated fastflood.org website. Subsequently, different features are suggested for further development of the FFS-model.

8.2.1. Current FFS-model

The FFS-model is rapidly developing. Even over the course of this research, numerous features are added to the model. These developments are impressive, exciting and contribute to the overarching goal to create a globally applicable opensource fast flood modelling tool. Due the novel set-up of the modelling approach, it can be difficult to get grip on the physical relations between model input and output. Consequently, it is as model user challenging to understand the origin of unexpected flood simulation results. A background knowledge in hydrology helps to detect anomalous simulation results. A risk is that FFS-model users without a hydrological modelling background are unable to recognise questionable modelling results and misinterpret the associated flood hazard. To mitigate the risk of misinterpretation, it is recommended to add a technical explanation of the FFS-modelling principles to the website. Moreover, it is advised to compile a tutorial on how to calibrate and validate the FFS-model.

During this research a model flaw related to the sensitivity of grid cell sizes was detected. Besides solving this issue, it is recommended to research the sensitivity of the FFS-model on grid cell size. This research should examine whether and what adjustments in calibration set-up are necessary when applying the FFS-model on varying resolutions for the same case study area.

In a novel and rapidly developing model it is logical that developing issues occur. To detect and solve these issues it is important to keep validating the accuracy of the FFS-model results for different functionalities and landscapes. It is in particular recommended to perform additional tests reflecting on the FFS-model accuracy in areas with limited elevation changes and a course DEM (30 meter). For these tests it is suggested to use a case-study area with complete and accurate discharge measurements on multiple points in a river catchment.

A final recommendation, with respect to the current set-up of the FFS-model, is to perform an accuracy study for the integration of physical mitigation measures. It is currently unknown to what extent the effects of interventions are accurately represented in the flood hazard maps. Especially the up- and downstream effects of interventions are of interest. For this proposed study, it is recommended to select a case-study area for which observed discharge and flood extent data is available representing an situation before and after an intervention implementation. Moreover, it is recommended to compare the flood hazard output of intervention design using the FFS-model with similar simulations using a conventional flood model.

8.2.2. Additional features for the FFS-model

The first recommended feature for the FFS-model is the possibility to compose and download maximum flow velocity and inundation duration maps. These hazard features are of large relevance when evaluating on flood hazard, damage and risk. Obviously, the accuracy of these results should be validated with observation data.

Additionally, the ability to include unsteady rainfall data would be of value. Currently, only uniform hourly rainfall can be included. In reality, rainfall is not steady over time. By composing the possibility to include unsteady rainfall waves over a specific time period the FFS-model can also be linked to real time rain forecast data. Subsequently, it is recommended to create the possibility to run a batch process for indicated differences in input variables. Currently, all model input variations need to be manually adjusted and exported one-by-one. This is a time-consuming process.

The current FFS-model setup compiles deterministic flood hazard maps. As discussed, flood hazard return period analyses come with a variety of uncertainties. A deterministic hazard map is not able to capture these uncertainties. It would be interesting to create a possibility in the FFS-model to generate probabilistic flood hazard maps. In this feature a range and probability density function for rainfall, base discharge, infiltration rate and manning's N can be given as input for a specific return period or climate scenario. Subsequently, the FFS-model runs a batch process with varying input values, similar as a Monte Carlo analyses. The quantitative results for each grid cell are sorted in order of magnitude. Finally, flood hazard maps representing the median and, for example, the lowest and highest 10% flood depth can be exported. Also, the hydrographs can represent the range of derived discharges using a probabilistic approach. Using this method more insight can be created in the effects of unavoidable variations and uncertainties related to flood simulation input parameters. Obviously, the computational time for such an analysis is larger than running a single simulation. Nevertheless, the remarkable fast computational times of the FFS-model, makes this model particularly interesting for probabilistic flood modelling studies.

Finally, some recommendations concerning the intervention design abilities of the FFS-model. Firstly, it would be valuable to create a feature in which the drawing and polygon function can also be used to locally adjust the Manning's N and infiltration rate of an area. With this functionally, effects of land-use changes and nature-based solutions can be analysed. Additionally, it would be convenient to have the ability to easily enable or disable different intervention designs within the interface setup. In this manner the comparison between different interventions is easier. Moreover, this feature enables the possibility to analyse different combinations of interventions.

References

Akbari, G., & Firoozi, B. (2010). *Implicit and Explicit Numerical Solution of Saint-Venent Equations for Simulating Flood Wave in Natural Rivers*.

Ali, S., & George, A. (2021). Social Inclusivity: A Case Studyon Community Resilience on KeralaFlood-2018. *Sustainable Urban Architecture*.

Anju, Drissia, D., & Nowshaja, D. (2020). Flood modelling of pamba river using MIKE FLOOD. *SSRN Electronic Journal*. https://doi.org/10.2139/ssrn.3793880

Apel, H., Thieken, A. H., Merz, B., & Blöschl, G. (2004). Flood risk assessment and associated uncertainty. *Natural Hazards and Earth System Sciences*, *4*(2), 295–308. https://doi.org/10.5194/nhess-4-295-2004

Bates, P. D., & Anderson, M. G. (1996). A preliminary investigation into the impact of initial conditions on flood inundation predictions using a time/space distributed sensitivity analysis. *Catena*, *26*(1–2), 115–134. https://doi.org/10.1016/0341-8162(95)00041-0

Bout, B., & Jetten, V. G. (2018). The validity of flow approximations when simulating catchment-integrated flash floods. *Journal of Hydrology*, *556*, 674–688. https://doi.org/10.1016/j.jhydrol.2017.11.033

Bulti, D. T., & Abebe, B. G. (2020). A review of flood modeling methods for urban pluvial flood application. *Modeling Earth Systems and Environment*, *6*(3), 1293–1302. https://doi.org/10.1007/s40808-020-00803-z

Cardoso de Salis, H. H., Monteiro da Costa, A., Moreira Vianna, J. H., Azeneth Schuler, M., Künne, A., Sanches Fernandes, L. F., & Leal Pacheco, F. A. (2019). Hydrologic modeling for sustainable water resources management in urbanized Karst areas. *International Journal of Environmental Research and Public Health*, *16*(14), 2542. https://doi.org/10.3390/ijerph16142542

Construction cost in Kerala. (n.d.). Todaypricerates.com. Retrieved August 1, 2023, from

https://property.todaypricerates.com/construction-cost-calculator-in-Kerala

Digital elevation model (DEM) uncertainty: Evaluation and effect on topographic parameters. (n.d.). Esri.com. Retrieved July 12, 2023, from https://proceedings.esri.com/library/userconf/proc99/proceed/papers/pap262/p262.htm

Dixit, A., Sahany, S., Rajagopalan, B., & Choubey, S. (2022). Role of changing land use and land cover (LULC) on the 2018 megafloods over Kerala, India. *Climate Research*, *89*, 1–14. https://doi.org/10.3354/cr01701

Du, W., FitzGerald, G. J., Clark, M., & Hou, X.-Y. (2010). Health impacts of floods. *Prehospital and Disaster Medicine*, *25*(3), 265–272. https://doi.org/10.1017/s1049023x00008141

El Adlouni, S., & Ouarda, T. B. M. J. (2010). Frequency analysis of extreme rainfall events. In *Geophysical Monograph Series* (pp. 171–188). American Geophysical Union.

EM-DAT. (n.d.). Emdat.Be. Retrieved July 12, 2023, from https://public.emdat.be/

Exposure. (2009, January 23). Undrr.org. https://www.undrr.org/terminology/exposure

Fewtrell, T. J., Bates, P. D., Horritt, M., & Hunter, N. M. (2008). Evaluating the effect of scale in flood inundation modelling in urban environments. *Hydrological Processes*, *22*(26), 5107–5118. https://doi.org/10.1002/hyp.7148

George, A. (2020). *Kerala flood mitigation: Chengannur canal case study*.

Ghannadi, M. A., Alebooye, S., Izadi, M., & Ghanadi, A. (2023). Vertical accuracy assessment of Copernicus Dem (case study: Tehran and Jam cities). *ISPRS Annals of Photogrammetry Remote Sensing and Spatial Information Sciences*, *X-4/W1-2022*, 209–214. https://doi.org/10.5194/isprs-annals-x-4-w1-2022-209-2023

Glas, V.G.E., Dr. Sekhar Lukose Kuriakose, Dr. Shinu Sheela Wilson, Professor Cees van Westen. 2022. Internship report "*Assessing changing flood risk under climate change for local risk reduction planning in Kerala, India.*"

Goodchild, M. F., & Li, L. (2012). Assuring the quality of volunteered geographic information. *Spatial Statistics*, *1*, 110–120. https://doi.org/10.1016/j.spasta.2012.03.002

Guidolin, M., Chen, A. S., Ghimire, B., Keedwell, E. C., Djordjević, S., & Savić, D. A. (2016). A weighted cellular automata 2D inundation model for rapid flood analysis. *Environmental Modelling & Software: With Environment Data News*, *84*, 378–394. https://doi.org/10.1016/j.envsoft.2016.07.008

Hamidifar, H., & Nones, M. (2021). *Global to regional overview of floods fatality: the 1951–2020 period*. https://doi.org/10.5194/nhess-2021-357

Hecht, R., Kunze, C., & Hahmann, S. (2013). Measuring completeness of building footprints in OpenStreetMap over space and time. *ISPRS International Journal of Geo-Information*, *2*(4), 1066–1091. https://doi.org/10.3390/ijgi2041066

Henonin, J., Russo, B., Mark, O., & Gourbesville, P. (2013). Real-time urban flood forecasting and modelling – a state of the art. *Journal of Hydroinformatics*, *15*(3), 717–736. https://doi.org/10.2166/hydro.2013.132

Home: ENVIS Center of Kerala State Council for Science, Technology & environment. (n.d.). Nic.In. Retrieved July 12, 2023, from https://kerenvis.nic.in/

Horritt, M. S., & Bates, P. D. (2002). Evaluation of 1D and 2D numerical models for predicting river flood inundation. *Journal of Hydrology*, *268*(1–4), 87–99. https://doi.org/10.1016/s0022-1694(02)00121-x

Hunt, K. M. R., & Menon, A. (2020). The 2018 Kerala floods: a climate change perspective. *Climate Dynamics*, *54*(3–4), 2433–2446. https://doi.org/10.1007/s00382-020-05123-7

Hunt, K., & Menon, A. (2022). *Understanding the role of climate change in the 2018 Kerala flood*.

Jamali, B., Bach, P. M., Cunningham, L., & Deletic, A. (2019). A cellular automata fast flood evaluation (CA-ffé) model. *Water Resources Research*, *55*(6), 4936–4953. https://doi.org/10.1029/2018wr023679

Katzenberger, A., Levermann, A., Schewe, J., & Pongratz, J. (2022). Intensification of very wet monsoon seasons in India under global warming. *Geophysical Research Letters*, *49*(15). https://doi.org/10.1029/2022gl098856

Kerala state disaster management authority. (n.d.). Gov.In. Retrieved July 12, 2023, from https://sdma.kerala.gov.in/

Khac-Tien Nguyen, P., & Hock-Chye Chua, L. (2012). The data-driven approach as an operational real-time flood forecasting model: DATA-DRIVEN APPROACH FOR REAL-TIME FLOOD FORECASTING. *Hydrological Processes*, *26*(19), 2878–2893. https://doi.org/10.1002/hyp.8347

Kieran, M. R., & Hunt, A. (2020). The 2018 Kerala floods: a climate change perspective. *Climate Dynamics*, 2433–2446.

Kishore, P. (2023, April 20). *Planning to build a house in Kerala? Rs 50 lakh likely to cost for a 1,500 sqft structure*. Onmanorama. https://www.onmanorama.com/news/kerala/2023/04/20/house-construction-expense-kerala-hike-in-application-fees.html

Koivumäki, L., Alho, P., Lotsari, E., Käyhkö, J., Saari, A., & Hyyppä, H. (2010). Uncertainties in flood risk mapping: a case study on estimating building damages for a river flood in Finland: Uncertainties in flood risk mapping. *Journal of Flood Risk Management*, *3*(2), 166–183. https://doi.org/10.1111/j.1753-318x.2010.01064.x

Krishnakumar, K. N., Prasada Rao, G. S. L. H. V., & Gopakumar, C. S. (2009). Rainfall trends in twentieth century over Kerala, India. *Atmospheric Environment (Oxford, England: 1994)*, *43*(11), 1940–1944. https://doi.org/10.1016/j.atmosenv.2008.12.053

Liang, Q., Du, G., Hall, J. W., & Borthwick, A. G. (2008). Flood inundation modeling with an adaptive quadtree grid Shallow Water equation solver. *Journal of Hydraulic Engineering*, *134*(11), 1603–1610. https://doi.org/10.1061/(asce)0733-9429(2008)134:11(1603)

Li, C., Zwiers, F., Zhang, X., Li, G., Sun, Y., & Wehner, M. (2021). Changes in annual extremes of daily temperature and precipitation in CMIP6 models. *Journal of Climate*, *34*(9), 3441–3460. https://doi.org/10.1175/jcli-d-19-1013.1

Li, H., Zhao, J., Yan, B., Yue, L., & Wang, L. (2022). Global DEMs vary from one to another: an evaluation of newly released Copernicus, NASA and AW3D30 DEM on selected terrains of China using ICESat-2 altimetry data. *International Journal of Digital Earth*, *15*(1), 1149–1168. https://doi.org/10.1080/17538947.2022.2094002

Li, Z., Chen, M., Gao, S., Hong, Z., Tang, G., Wen, Y., Gourley, J. J., & Hong, Y. (2020). Cross-examination of similarity, difference and deficiency of gauge, radar and satellite precipitation measuring uncertainties for extreme events using conventional metrics and multiplicative triple collocation. *Remote Sensing*, *12*(8), 1258. https://doi.org/10.3390/rs12081258

Liu, X. C., Gao, T. C., & Liu, L. (2013). A comparison of rainfall measurements from multiple instruments. *Atmospheric Measurement Techniques*, *6*(7), 1585–1595. https://doi.org/10.5194/amt-6-1585-2013

Local self government department. (n.d.). Gov.In. Retrieved July 18, 2023, from http://lsgkerala.gov.in/en/lsgd

Loyola-Gonzalez, O. (2019). Black-box vs. White-box: Understanding their advantages and weaknesses from a practical Point of View. *IEEE Access: Practical Innovations, Open Solutions*, *7*, 154096–154113. https://doi.org/10.1109/access.2019.2949286

Luo, Z., & Shao, Q. (2022). A modified hydrologic model for examining the capability of global gridded PET products in improving hydrological simulation accuracy of surface runoff, streamflow and baseflow. *Journal of Hydrology*, *610*(127960), 127960. https://doi.org/10.1016/j.jhydrol.2022.127960

Massaria, C., Brocca, L., Moramarco, T., Tramblay, Y., & Lescot, J.-F. D. (2014). Potential of soil moisture observations in flood modelling: Estimating initial conditions and correcting rainfall. In *Advances in water resources* (pp. 44–53).

Mayaja, N. A. (2016). Flood hazard zoning using analytic hierarchy process: A case study for Pampa river basin, Kerala, India. *Journal of Geomatics*.

Mayaja, N. A., & Srinivasa, C. V. (2016). Land use and land cover changes and their impacts on floods in Pampa river basin in Kerala: A remote sensing based analysis. In *Geostatistical and Geospatial Approaches for the Characterization of Natural Resources in the Environment* (pp. 779–783). Springer International Publishing.

Mayaja, N. A., & Srinivasa, C. V. (2021). GIS-based impact analysis of revitalisation of dried rivulets in Pampa River Basin, Kerala, India. *International Journal of Hydrology Science and Technology*, *11*(1), 38. https://doi.org/10.1504/ijhst.2021.112655

McHugh, M. L. (2012). Interrater reliability: the kappa statistic. *Biochemia Medica*, *22*(3), 276–282. https://doi.org/10.11613/bm.2012.031

Membele, G. M., Naidu, M., & Mutanga, O. (2022). Examining flood vulnerability mapping approaches in developing countries: A scoping review. *International Journal of Disaster Risk Reduction: IJDRR*, *69*(102766), 102766. https://doi.org/10.1016/j.ijdrr.2021.102766

Michael, J., Dragan, A., Savic, S., Djordjevic, A. S., Chen, S., & Fraser, T. (2016). Accuracy and Computational Efficiency of 2D Urban Surface Flood Modelling Based on Cellular Automata. *Procedia Engineering*, 801–810.

Mishra, V., Aaadhar, S., Shah, H., Kumar, R., Pattanaik, D. R., & Tiwari, A. D. (2018). The Kerala flood of 2018: combined impact of extreme rainfall and reservoir storage. *Hydrology and Earth System Sciences Discussions*, 1–13. https://doi.org/10.5194/hess-2018-480

Mishra, V., & Shah, H. L. (2018). Hydroclimatological perspective of the Kerala flood of 2018. *Journal of the Geological Society of India*, *92*(5), 645–650. https://doi.org/10.1007/s12594-018-1079-3

Molch, K. (2009). Radar Earth Observation Imagery for Urban Area Characterisation. *JRC Scientific and Technical Reports*.

Morales-Hernández, M., Sharif, M. B., Kalyanapu, A., Ghafoor, S. K., Dullo, T. T., Gangrade, S., Kao, S.-C., Norman, M. R., & Evans, K. J. (2021). TRITON: A Multi-GPU open source 2D hydrodynamic flood model. *Environmental Modelling & Software: With Environment Data News*, *141*(105034), 105034. https://doi.org/10.1016/j.envsoft.2021.105034

Mosavi, A., Ozturk, P., & Chau, K.-W. (2018). Flood prediction using machine learning models: Literature review. *Water*, *10*(11), 1536. https://doi.org/10.3390/w10111536

Moussa, R., & Bocquillon, C. (2000). Approximation zones of the Saint-Venant equations f flood routing with overbank flow. *Hydrology and Earth System Sciences*, *4*(2), 251–260. https://doi.org/10.5194/hess-4-251-2000

Municipal Corporation of Thiruvananthapuram, Kerala. (2016). *Early Warning System Plan*.

Nandakumar, N., & Mein, R. G. (1997). Uncertainty in rainfall—runoff model simulations and the implications for predicting the hydrologic effects of land-use change. *Journal of Hydrology*, *192*(1–4), 211–232. https://doi.org/10.1016/s0022-1694(96)03106-x

Oksanen, J. (2003). Tracing the Gross Errors of DEM-Visualisation Techniques for Preliminary Quality Analysis. In *Proc. of the 21st International Cartographic Conference*.

Pai, D. S., Rajeevan, M., Sreejith, O. P., Mukhopadhyay, B., & Satbha, N. S. (2014). Development of a new high spatial resolution (0.25° × 0.25°) long period (1901-2010) daily gridded rainfall data set over India and its comparison with existing data sets over the region. *Mausam*, *65*(1), 1–18. https://doi.org/10.54302/mausam.v65i1.851

Pamba - INDIA WRIS WIKI. (n.d.). Gov.In. Retrieved July 12, 2023, from https://indiawris.gov.in/wiki/doku.php?id=pamba

Paul, D., Bates, F., & Pappenberger, R. J. (2014). *Applied Uncertainty Analysis for Flood Risk Management*.

Pelletier, P. M. (1989). Reply: Uncertainties in the single determination of river discharge: a literature review. *Canadian Journal of Civil Engineering*, *16*(5), 780–781. https://doi.org/10.1139/l89-116

Peter, A., François, P., & De Troch, W. (1993). Effective water table depth to describe initial conditions prior to storm rainfall in humid regions. *Water Resources Reseach*.

Petty, T. R., & Dhingra, P. (2018). Streamflow hydrology estimate using machine learning (SHEM). *Journal of the American Water Resources Association*, *54*(1), 55–68. https://doi.org/10.1111/1752-1688.12555

Prasad Basnayaka, A., & Sarukkalige, P. R. (2011). Comparing Hydrology and Hydraulics Surface Routing Approaches in Modeling an Urban Catchment. In *2nd International Conference on Environmental Engineering and Applications*.

Praveen, K., Thakur, S., Maiti, N. C., Kingma, V., Prasad, S. P., & Aggarwal, A. (2012). Estimation of structural vulnerability for flooding using geospatial tools in the rural area of Orissa, India. *Naturl Hazards*, 501–520.

Rafieyan, V. (2016). Effect of cultural distance on translation of culture-bound texts. *International Journal of Education and Literacy Studies*, *4*(2). https://doi.org/10.7575/aiac.ijels.v.4n.2p.67

Ramasamy, S. M., Gunasekaran, S., Rajagopal, N., Saravanavel, J., & Kumanan, C. J. (2019). Flood 2018 and the status of reservoir-induced seismicity in Kerala, India. *Natural Hazards (Dordrecht, Netherlands)*, *99*(1), 307–319. https://doi.org/10.1007/s11069-019-03741-x

Ramírez, J. A. (2000). Prediction and modeling of flood hydrology and hydraulics. In E. E. Wohl (Ed.), *Inland Flood Hazards* (pp. 293–333). Cambridge University Press.

Risk-informed planning. (n.d.). Inee.org. Retrieved July 19, 2023, from https://inee.org/eie-glossary/risk-informed-planning

Rudari, R., Campo, L., Gabellani, S., & Matano, A. (2020). Small-Scale Funding Agreement (SSFA) between United Nations Environment Programme and CIMA Foundation for "Flood model in Kerala." *CIMA Research Foundation*.

Saleh, F., Ducharne, A., Flipo, N., Oudin, L., & Ledoux, E. (2013). Impact of river bed morphology on discharge and water levels simulated by a 1D Saint–Venant hydraulic model at regional scale. *Journal of Hydrology*, *476*, 169–177. https://doi.org/10.1016/j.jhydrol.2012.10.027

Samuel, J., & George, A. (2019). *TOWARDS DISASTER RISK REDUCTION IN KERALA*.

Sharif Ahmadian, A. (2016). Mathematical modeling and algorithm development. In *Numerical Models for Submerged Breakwaters* (pp. 77–92). Elsevier.

State Relief Commissioner, Disaster Management (Additional Chief Secretary), Government of Kerala. (2018). *ADDITIONAL MEMORANDUM Kerala Floods – 2018 1 st August to 30th August 2018*.

Straatsma, M., & Huthoff, F. (2011). Uncertainty in 2D hydrodynamic models from errors in roughness parameterization based on aerial images. *Physics and Chemistry of the Earth (2002)*, *36*(7–8), 324–334. https://doi.org/10.1016/j.pce.2011.02.009

Sudheer, K. P., Murty Bhallamudi, S., Narasimhan, B., Thomas, J., Bindhu, V. M., Vema, V., & Kurian, C. (2019). Role of dams on the floods of august 2018 in periyar river basin, Kerala. *Current Science*, *116*(5), 780. https://doi.org/10.18520/cs/v116/i5/780-794

Technical Stakeholder Consultation as part of 'Nammal Namukkayi' Programme, RKI. (29-30 January 2020).

Tiampo, K., Woods, C., Huang, L., Sharma, P., Chen, Z., Kar, B., Bausch, D., Simmons, C., Estrada, R., Willis, M., & Glasscoe, M. (2021). A machine learning approach to flood depth and extent detection using sentinel 1A/B synthetic aperture radar. *2021 IEEE International Geoscience and Remote Sensing Symposium IGARSS*.

Tiwari, V., Kumar, V., Matin, M. A., Thapa, A., Ellenburg, W. L., Gupta, N., & Thapa, S. (2020). Flood inundation mapping- Kerala 2018; Harnessing the power of SAR, automatic threshold detection method and Google Earth Engine. *PloS One*, *15*(8), e0237324. https://doi.org/10.1371/journal.pone.0237324

Tollan, A. (2002). Land-use change and floods: what do we need most, research or management? *Water Science and Technology: A Journal of the International Association on Water Pollution Research*, *45*(8), 183–190. https://doi.org/10.2166/wst.2002.0176

Tsakiris, G. (2014). Flood risk assessment: concepts, modelling, applications. *Natural Hazards and Earth System Sciences*, *14*(5), 1361–1369. https://doi.org/10.5194/nhess-14-1361-2014

Uddin, K., & Matin, M. A. (2021). Potential flood hazard zonation and flood shelter suitability mapping for disaster risk mitigation in Bangladesh using geospatial technology. *Progress in Disaster Science*, *11*(100185), 100185. https://doi.org/10.1016/j.pdisas.2021.100185

Umar, A. J. (2019). Kerala spent Rs 1,8oo crore on restoration of houses. *The Times of India*, *12*.

UNDRR - homepage. (2023, March 3). Undrr.org. https://www.undrr.org/

Valeriy, Y., Ivanov, D., Xu, M. C., Dwelle, K., Sargsyan, D. B., Wright, N., Katopodes, J., Vinh, N., Tran, A., Warnock, S., Fatichi, P., Burlando, E., Caporali, P., Restrepo, B. F., & Sanders, M. M. (2021). Breaking Down the Computational Barriers to Real-Time Urban Flood Forecasting. *Geophysical Research Letters*.

Van den Bout, B., Jetten, V., van Westen, C., & Lombardo, L. (2022). A breakthrough in fast flood simulation. In *EarthArXiv*. https://doi.org/10.31223/x5mm2z

Varghese, N. E. (2020). *Capacities and gaps in early warning systems: Kerala floods*.

Walski, T. (2017). Procedure for hydraulic model calibration. *Journal - American Water Works Association*, *109*, 55–61. https://doi.org/10.5942/jawwa.2017.109.0075

What is risk-informed development? (2022, January 21). GNDR. https://www.gndr.org/resource/risk-informed-development/what-is-risk-informed-development/

What is the Average Cost to Furnish a House. (2022, August 5). Real Estate Forum by Nobroker.com; NoBroker.com. https://www.nobroker.in/forum/how-much-does-it-cost-to-furnish-a-house/

Yuan Jian Tian, Q., & Zhou, X. (2019). An Analysis of the Evolution, Completeness and Spatial Patterns of OpenStreetMap Building Data in China. *Geo-Inf*.

Yum, S.-G., Kim, J.-M., & Wei, H.-H. (2021). Development of vulnerability curves of buildings to windstorms using insurance data: An empirical study in South Korea. *Journal of Building Engineering*, *34*(101932), 101932. https://doi.org/10.1016/j.jobe.2020.101932

Zheng, X. (2021). The uncertainties of population research: Challenges and opportunities. *China CDC Weekly*, *3*(28), 591–592. https://doi.org/10.46234/ccdcw2021.156

Appendices

Appendix A: Historic flood records Kerala

Table 26 Historic flood records Kerala (EM-DAT, 2023)

Year	Affected area (km2)	Total Deaths	Total Affected	Total Damages (US$)
1980		1600	30000023	320000
1985	254240	95	25000	
1991	491400	72	300000	100000
1991		99		118000
1992		51	500	182100
1992		179	500	69000
1994		2001	12060050	175000
1996	177500	388	100000	90400
1996		500	100000	17600
1997	21840	1442	29259000	
1998	67610	1811	29227200	
1999		325	5500000	
2000	300000	867	22000000	43000
2000	300000	867	22000000	43000
2001	4470	86	40000	116924
2001		28	4	
2002	276600	549	42000000	30772
2002	9750	11		
2004	9000	45	1000	
2006	42690	32	10800	
2007	449300	127	200000	
2007	21120	44	35000	101151
2008			50000	
2009		992	1886000	220000
2010	147437	53	400000	447000
2013	131743	6054	504473	1100000
2018		504	23220000	2852480
2019		1900	3000000	10000000
2019		12	27500	
2019		32	17500	
2020		1922	1300000	7500000
2021		59	1000	100000
2021		39	3950	

Appendix B: Flood hazard maps CIMA research foundation
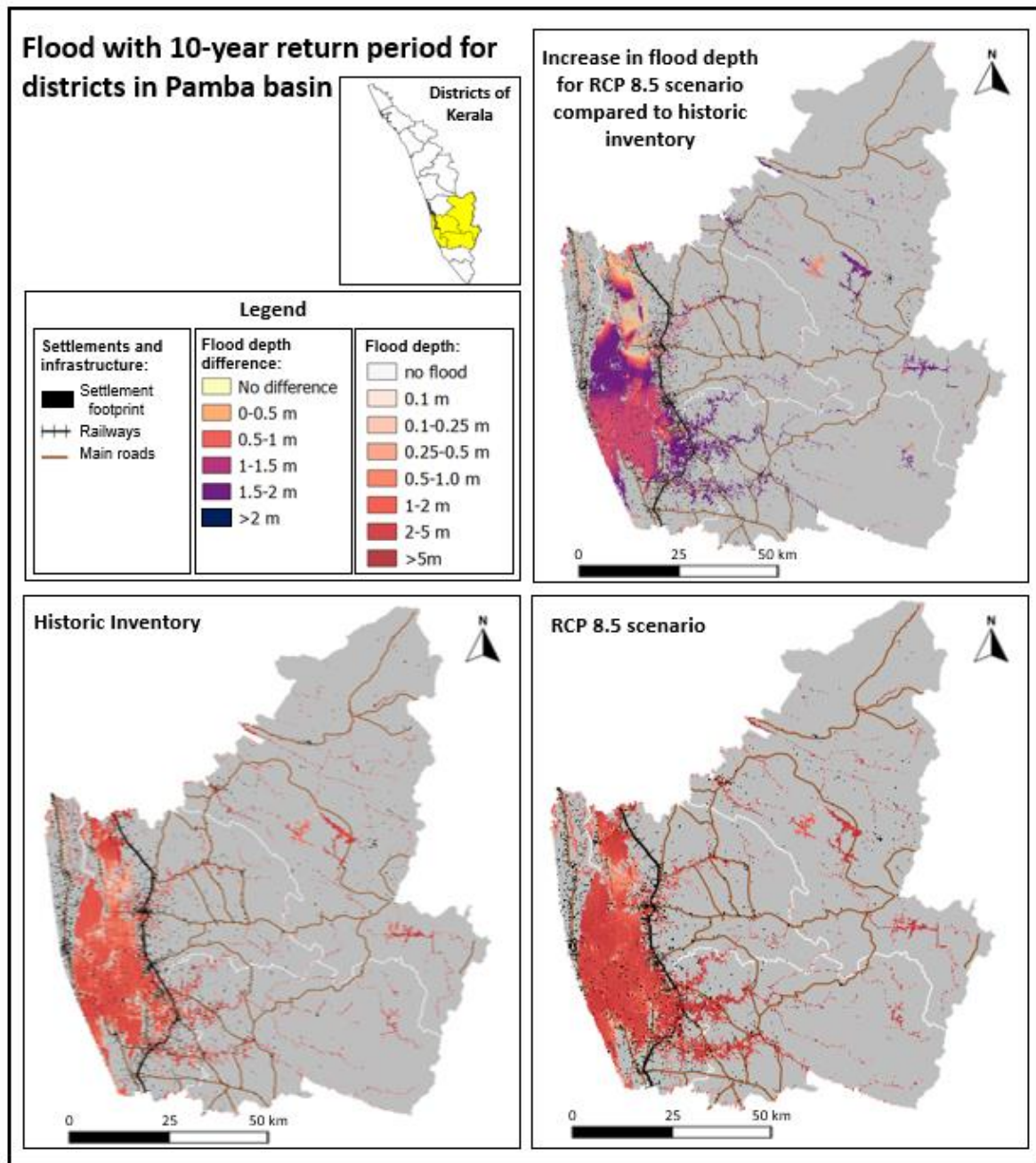
Figure 37 Flood with 10-year return period for districts in Pamba Basin
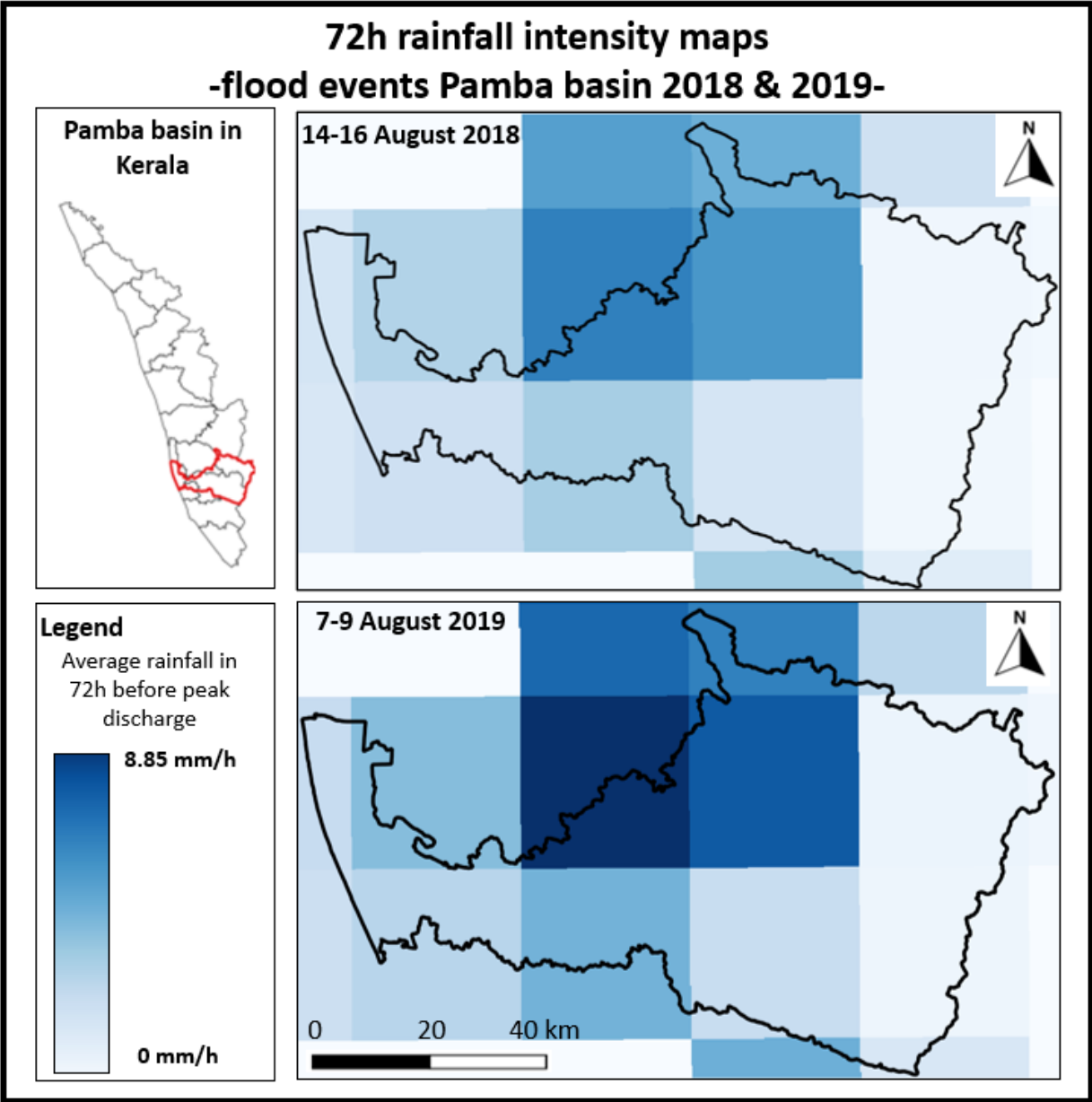
Figure 38 72h Rainfall intensity maps flood events Pamba Basin 2018 & 2019

Appendix D: Gumbel analyses of daily and weekly rainfall
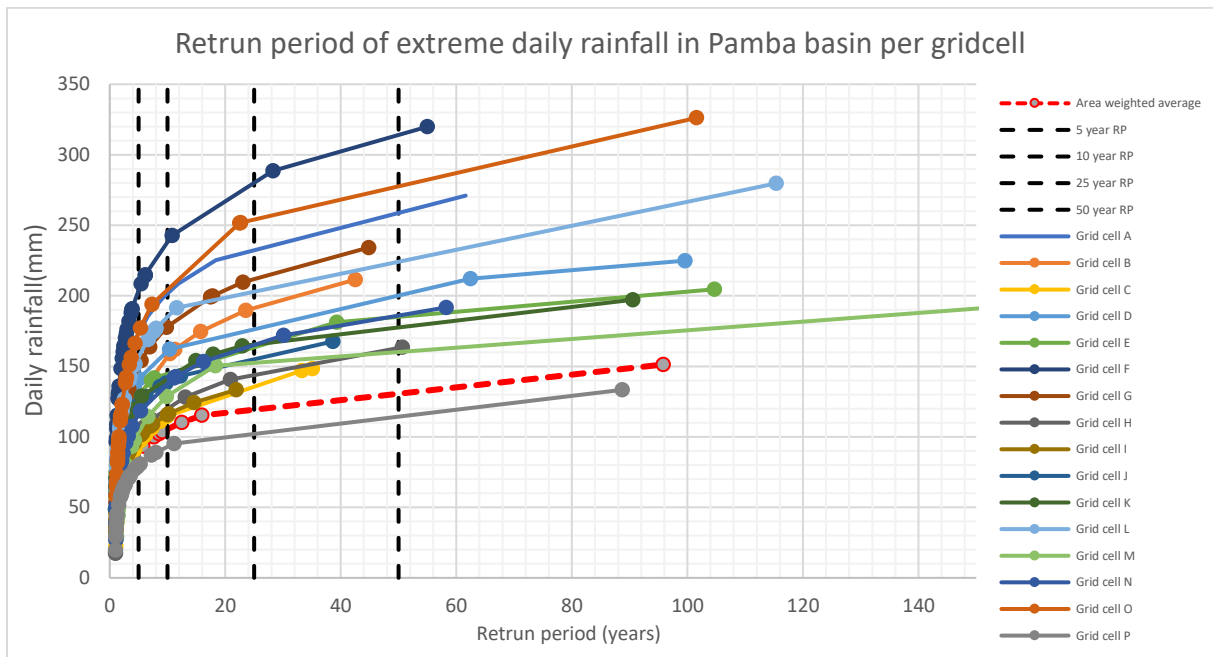
Figure 39 Return period of extreme daily rainfall in Pamba Basin per grid cell
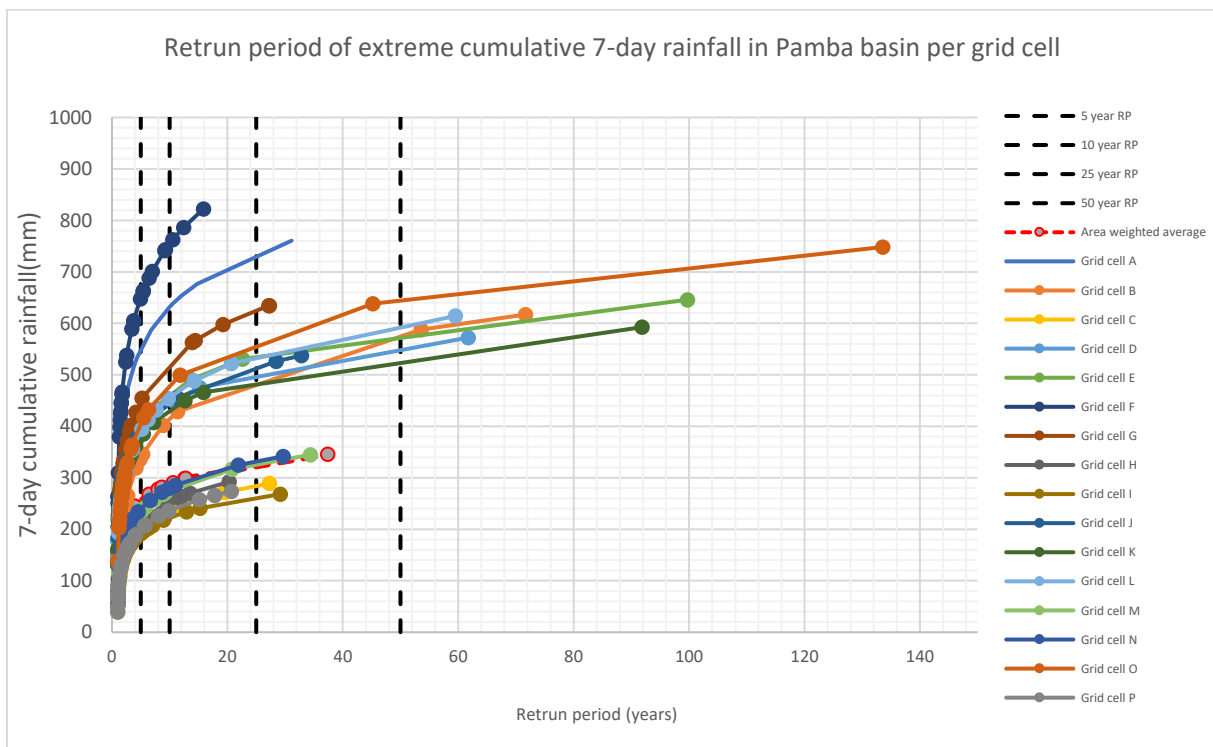
Figure 40 Return period of extreme daily rainfall in Pamba Basin per grid cell

Appendix E: Examples of rainfall-discharge timeseries
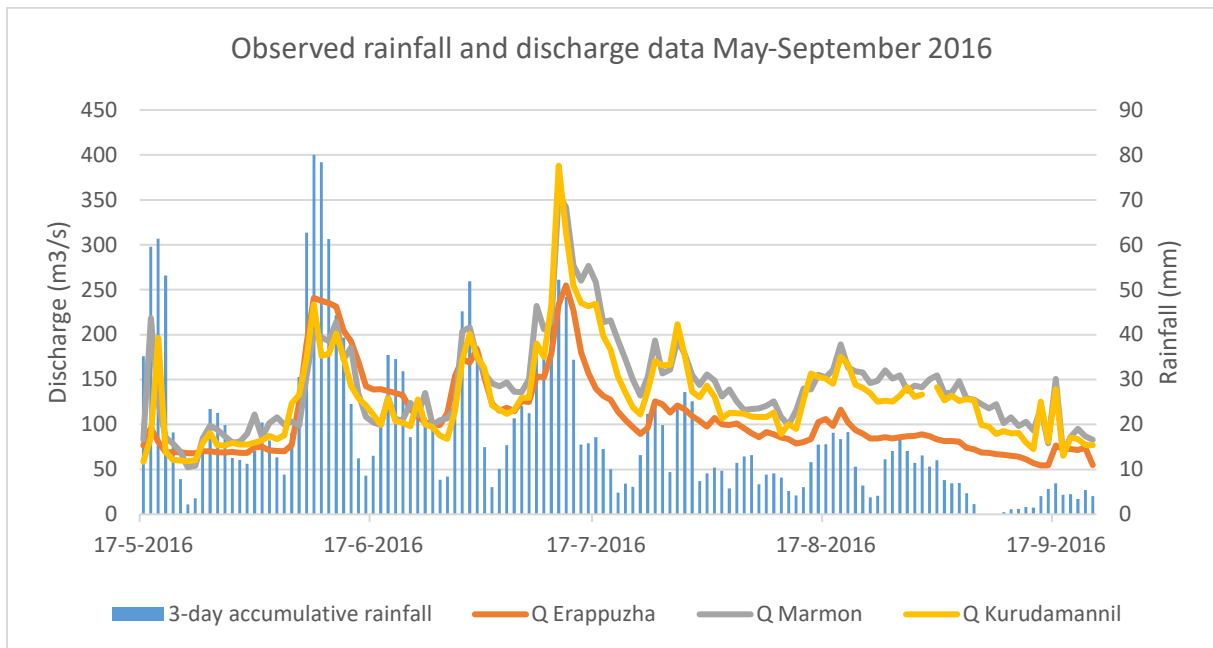
Figure 41 Observed rainfall and discharge data May-September 2016
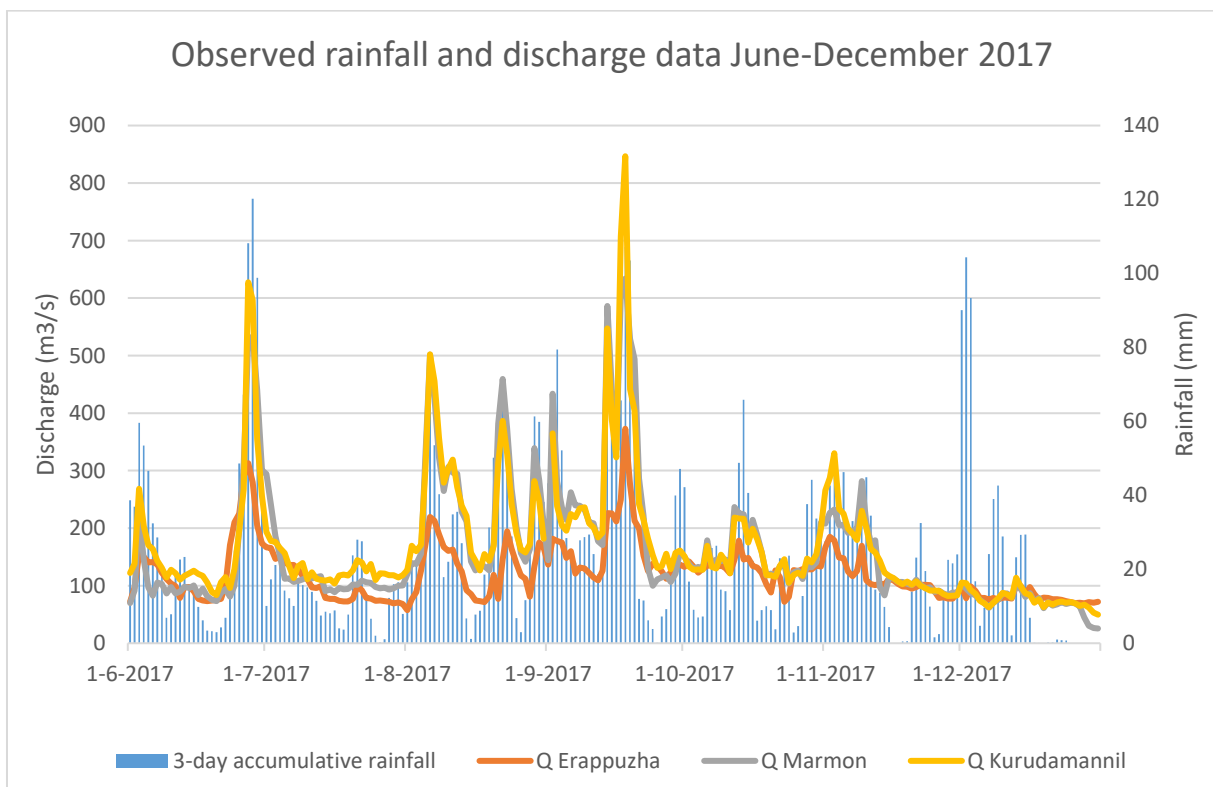
Figure 42 Observed rainfall and discharge data June-December 2017
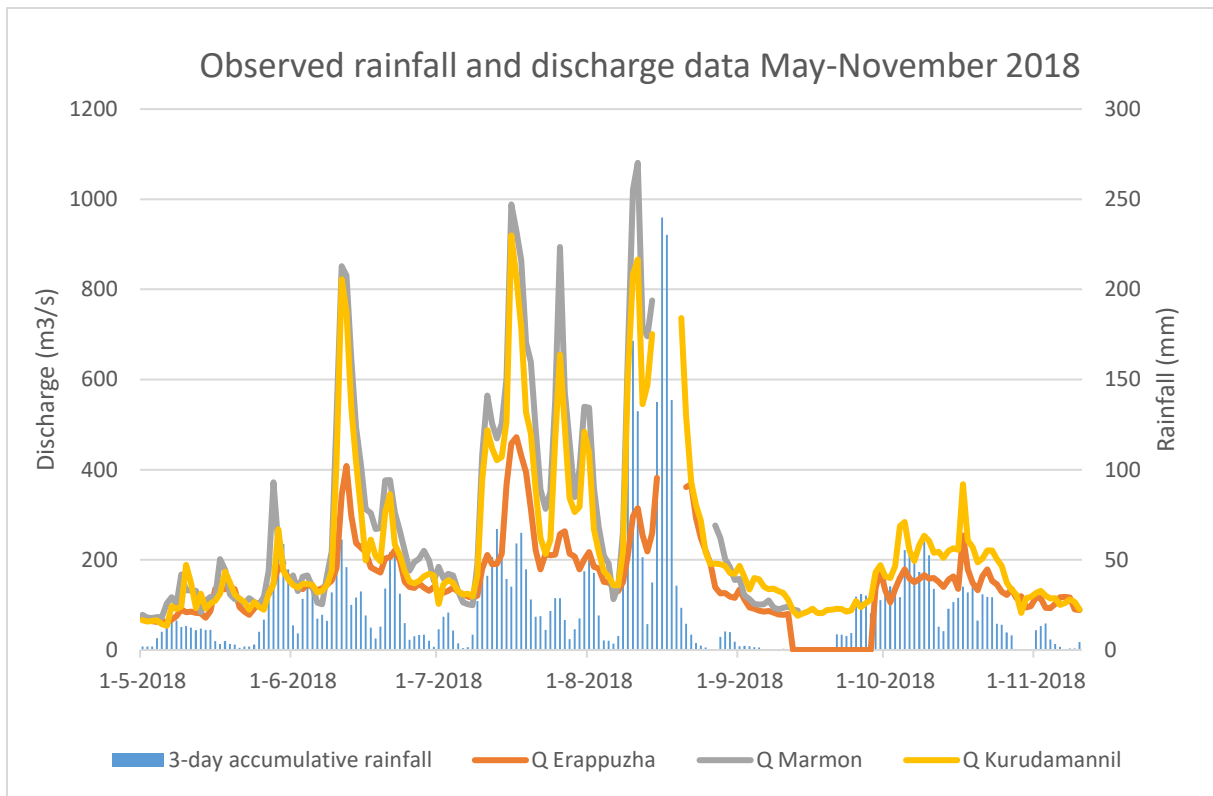
Figure 43 Observed rainfall and discharge data May-November 2018

Appendix F: Calibration of FFS-model

Table 27 Simulated discharge at Kurudamannil and associated values of calibration performance indicators

Calibration scenario	6-2017	9-2017	8-2018	8-2019	8-2020	9-2020	NSE
Simulated discharge at Kurudamannil (m³/s)							
Calibration setting 1	192.6	468.6	543.1	384.8	506.2	355.8	-3.42
Calibration setting 2	**563.9**	**835.1**	**1055.0**	**1201.8**	**1154.8**	**642.1**	**0.79**
Calibration setting 3	431.8	718.2	912.7	1000.6	988.0	535.7	0.50
Calibration setting 4	692.1	963.4	1183.4	1330.0	1083.1	772.0	0.62
Calibration setting 5	674.8	956.7	1183.4	1345.6	1298.1	752.6	0.47
Calibration setting 6	589.8	877.7	1099.3	1231.7	1193.8	680.2	0.73
Calibration setting 7	606.3	896.1	1116.0	1253.2	1212.6	693.8	0.70
Calibration setting 8	403.0	694.1	880.0	943.9	945.7	513.4	0.32
Calibration setting 9	536.2	825.0	1056.8	1215.7	1166.0	615.2	0.78
Percentual difference observed and simulated discharge							PBIAS
Calibration setting 1	-69.3%	-44.6%	-37.3%	-71.7%	-50.8%	-41.7%	-61.1%
Calibration setting 2	**-10.2%**	**-1.4%**	**21.8%**	**-11.7%**	**12.3%**	**5.3%**	2.4%
Calibration setting 3	-31.2%	-15.2%	5.4%	-26.4%	-3.9%	-12.2%	-15.9%
Calibration setting 4	10.3%	13.8%	36.6%	-2.2%	5.3%	26.6%	14.5%
Calibration setting 5	7.5%	13.0%	36.6%	-1.1%	26.2%	23.4%	18.4%
Calibration setting 6	-6.0%	3.7%	26.9%	-9.5%	16.1%	11.5%	7.0%
Calibration setting 7	-3.4%	5.8%	28.8%	-7.9%	17.9%	13.7%	9.3%
Calibration setting 8	-35.8%	-18.0%	1.6%	-30.6%	-8.0%	-15.8%	-20.3%
Calibration setting 9	-14.6%	-2.6%	22.0%	-10.6%	13.4%	0.9%	1.6%

Appendix G: Validation using flood extent maps
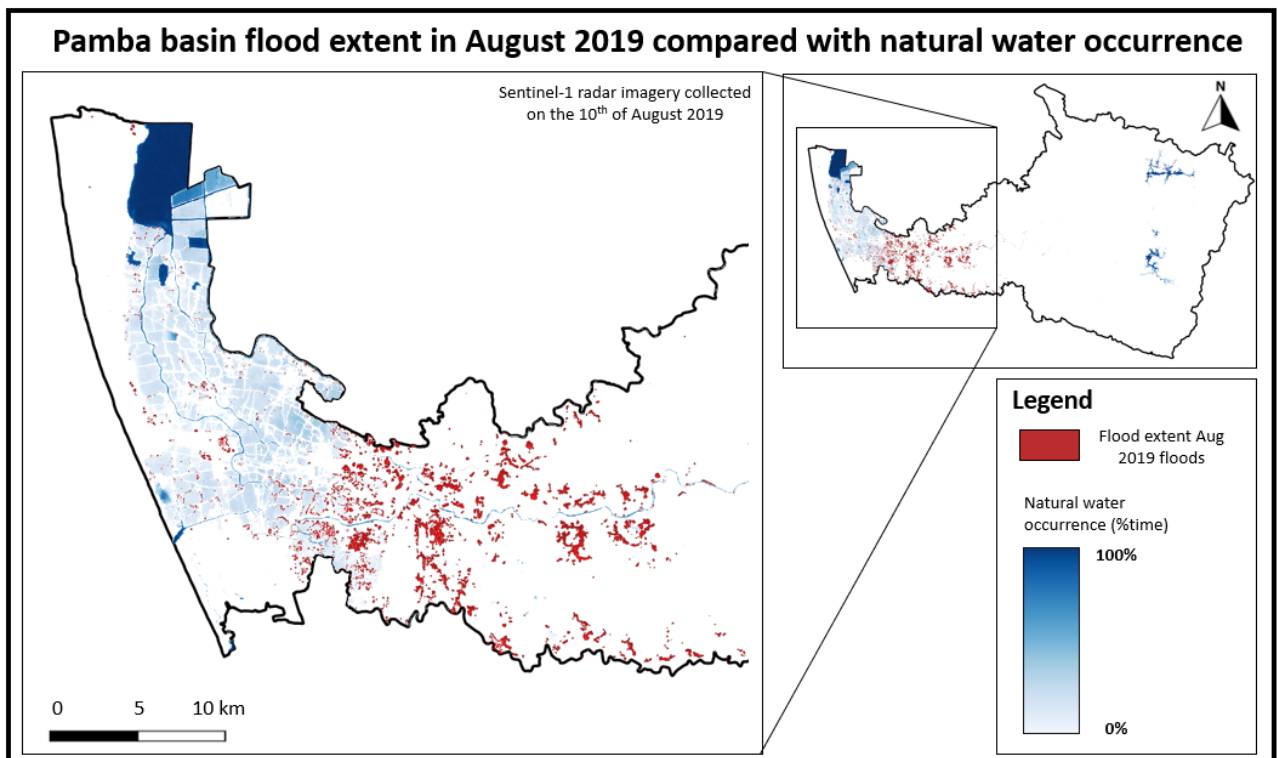
Figure 44 Pamba Basin flood extent in August 2019 compared with natural water occurrence
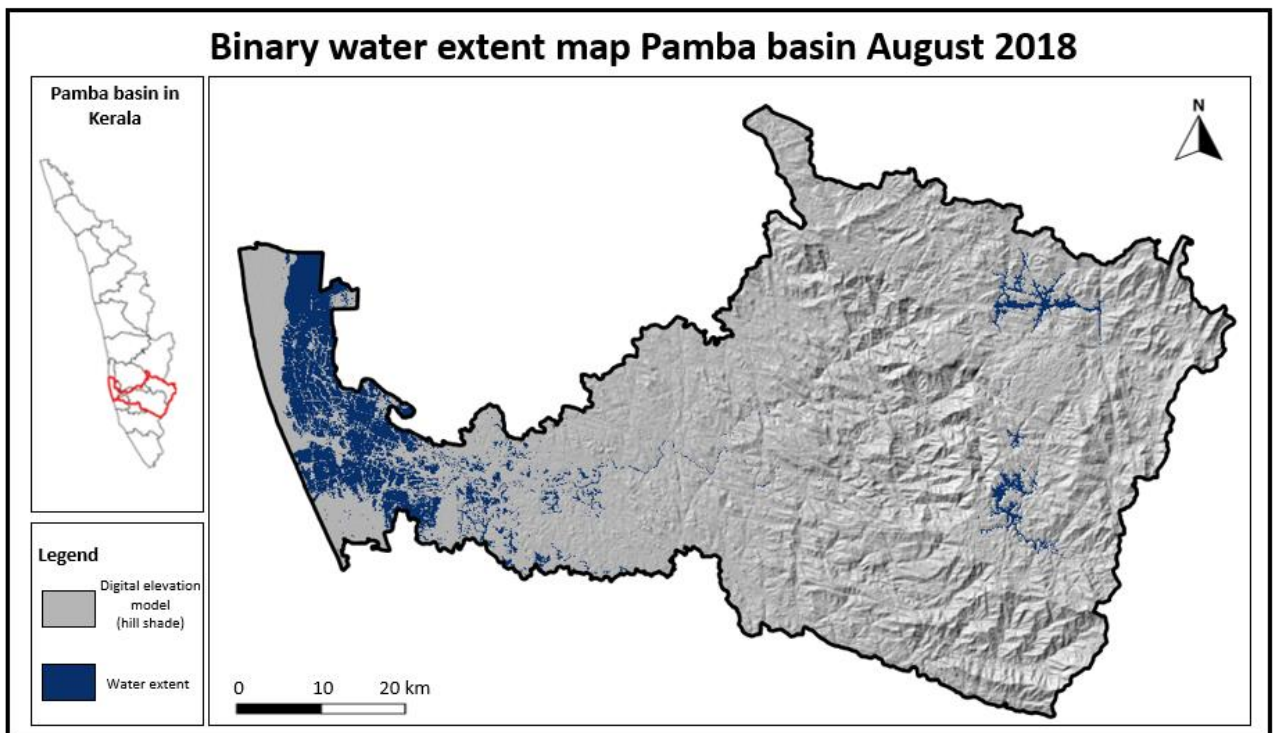
Figure 45 Binary water extent map Pamba Basin August 2018
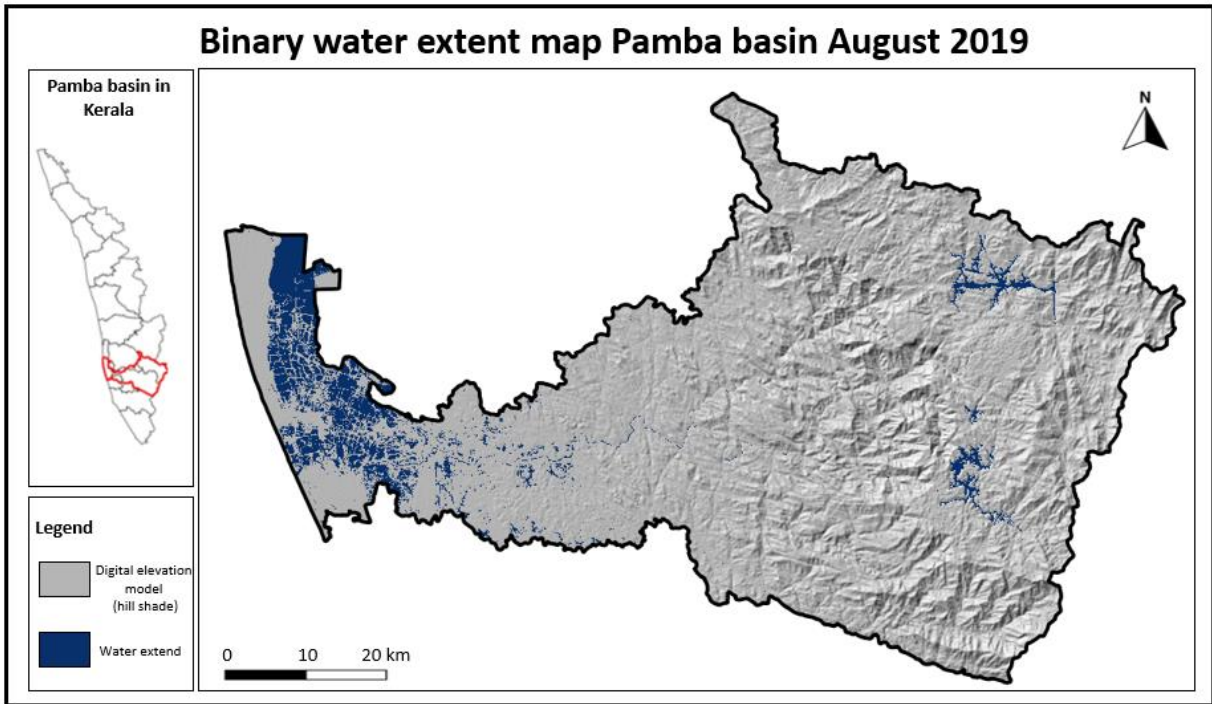
Figure 46 Binary water extent map Pamba Basin August 2019
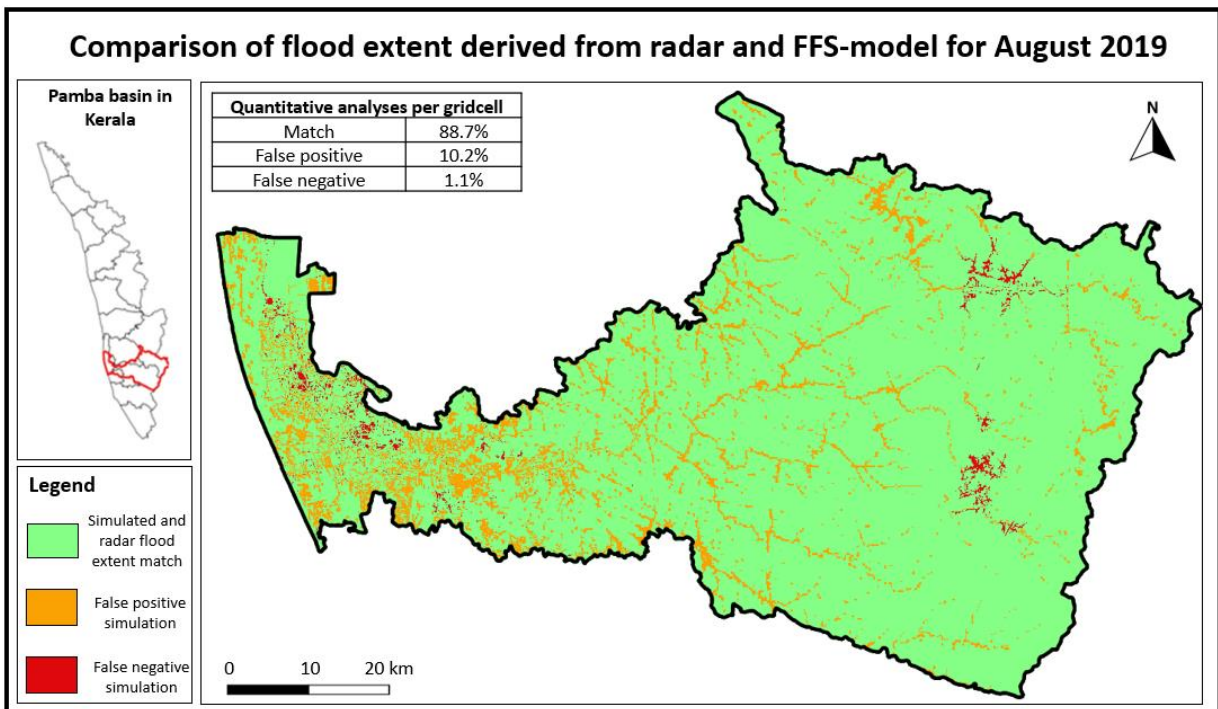
Figure 47 Comparison of flood extent derived from radar and FFS-model for August 2019
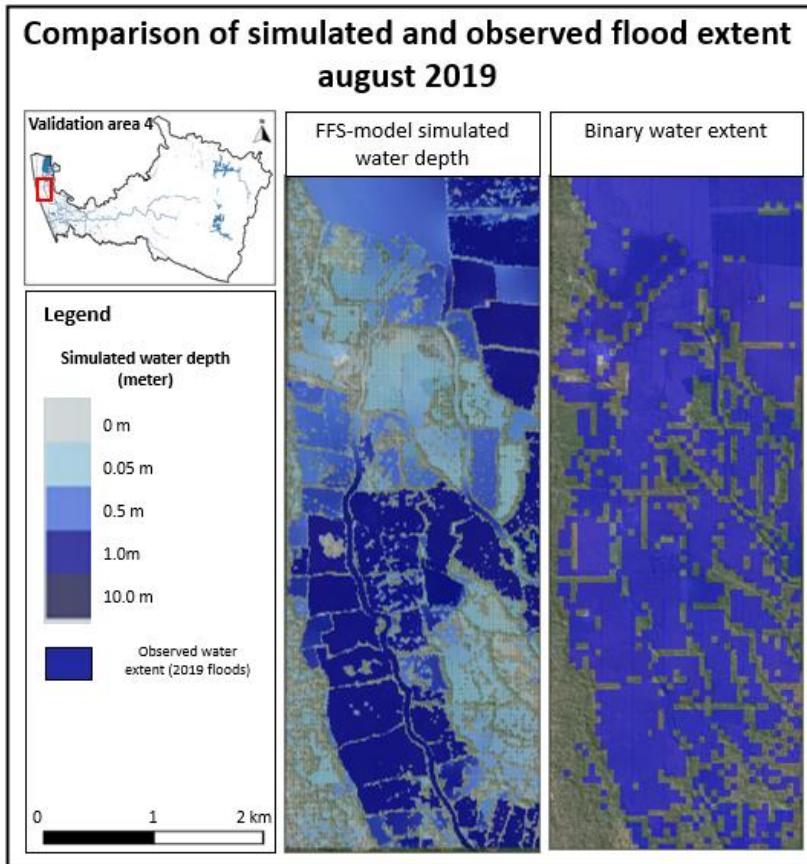
Figure 48 Comparison of simulated and observed flood extent August 2019
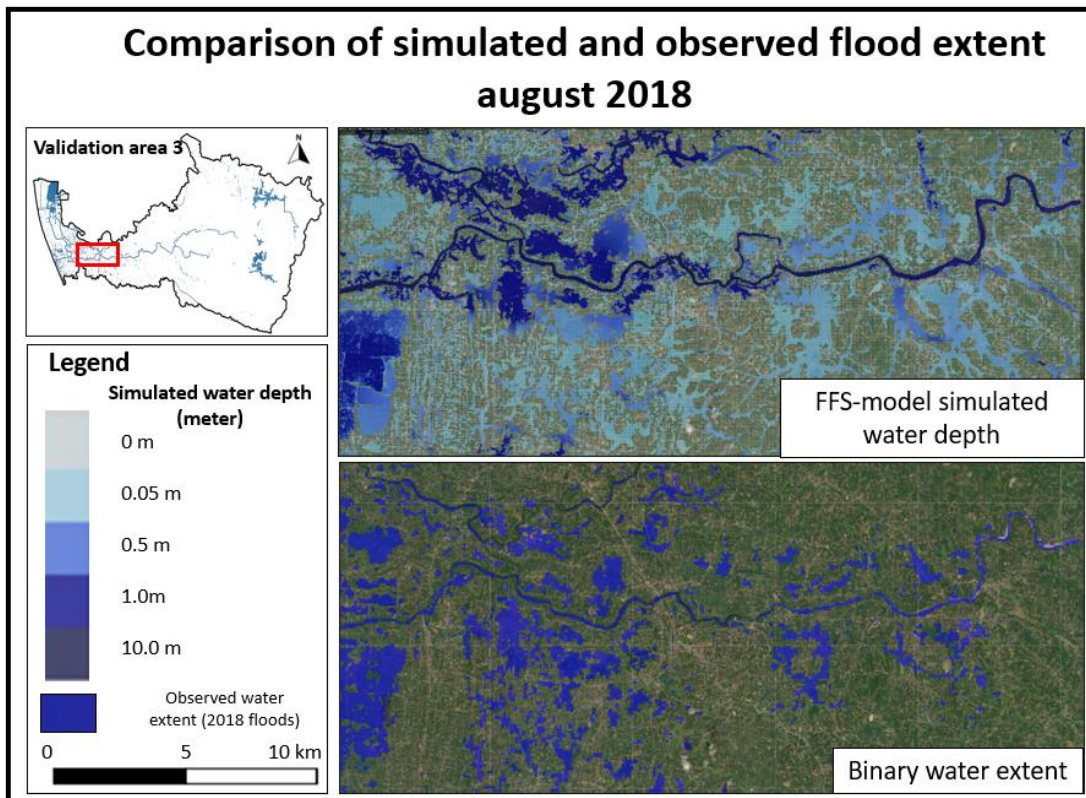
Figure 49 Comparison of simulated and observed flood extent August 2018
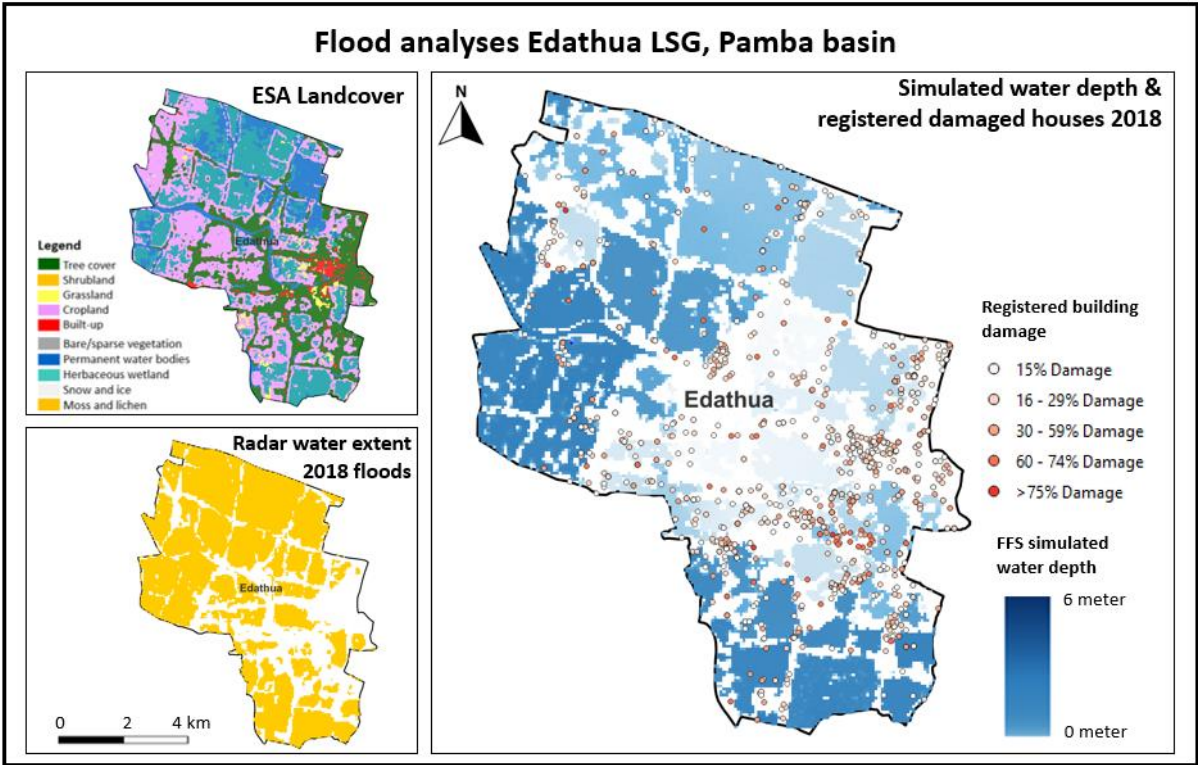
Figure 50 Flood analyses Edathua LSG, Pamba Basin
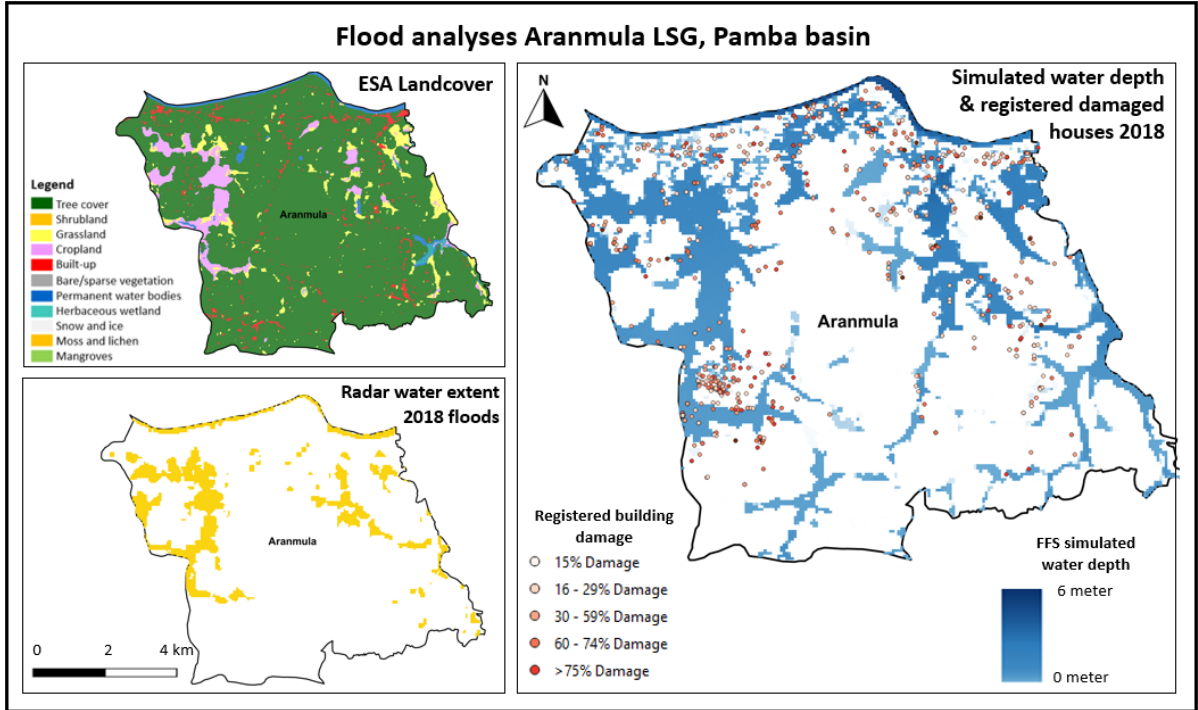
Figure 51 Flood analyses Aranmula LSG, Pamba Basin
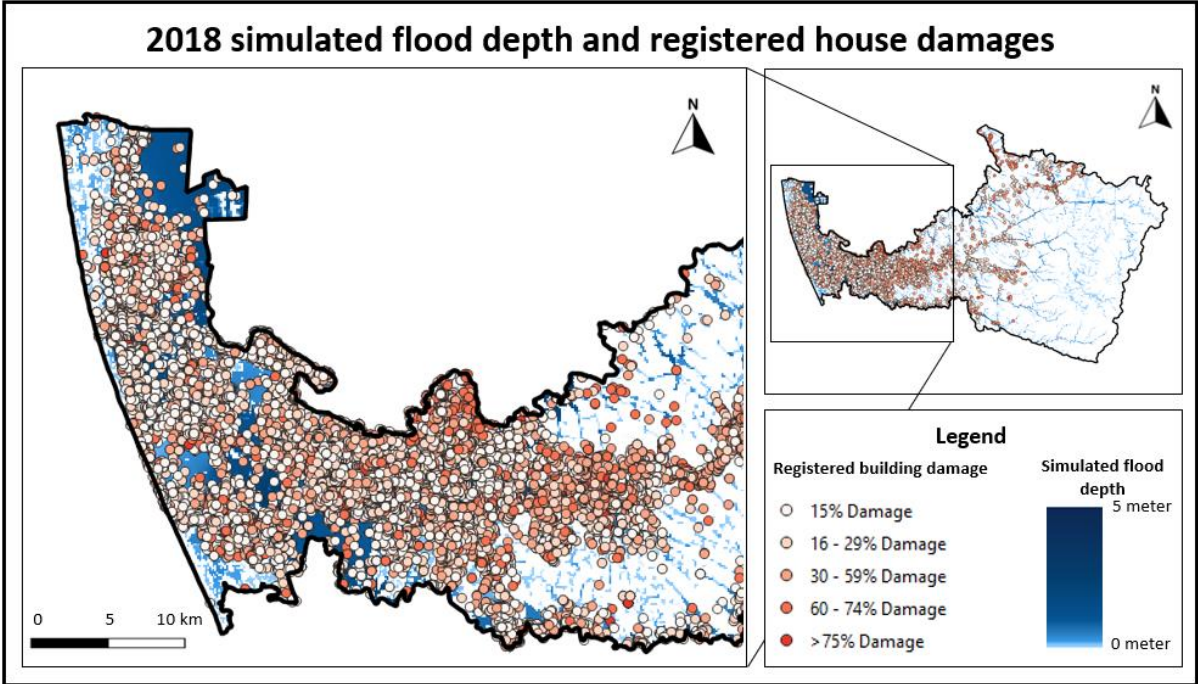
Figure 52 2018 simulated flood depth and registered house damages

Appendix I: Flood hazard analyses
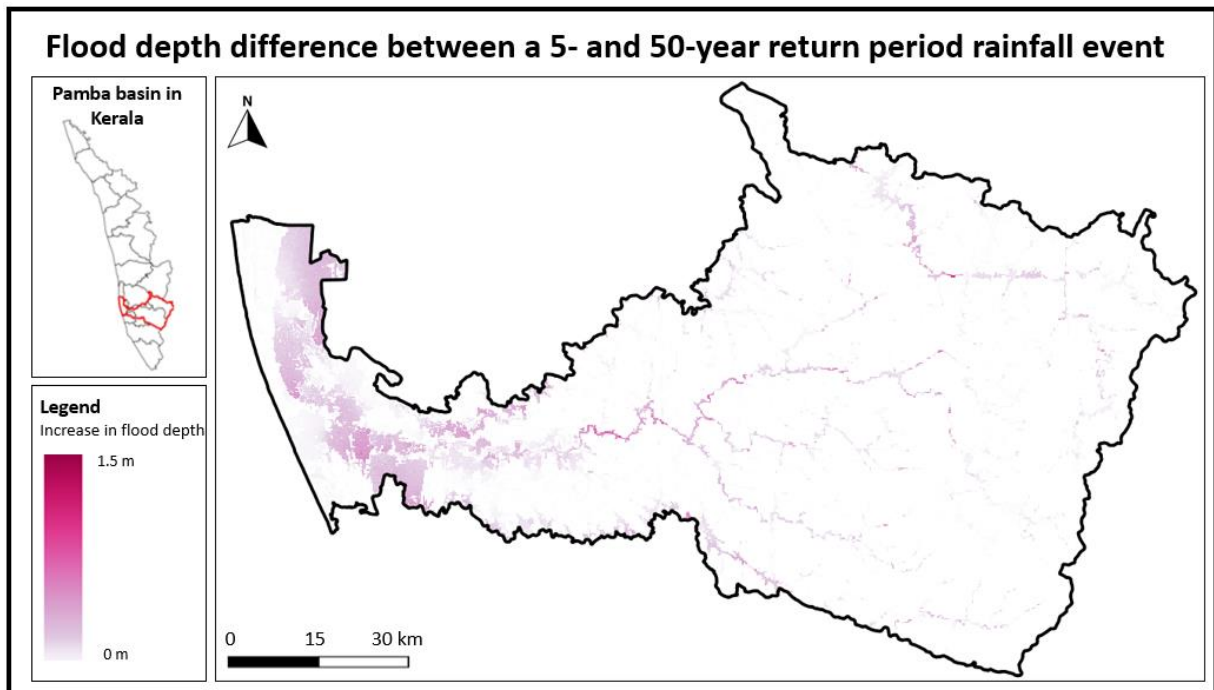
Figure 53 Flood depth difference between a 5- and 50-year return period rainfall event
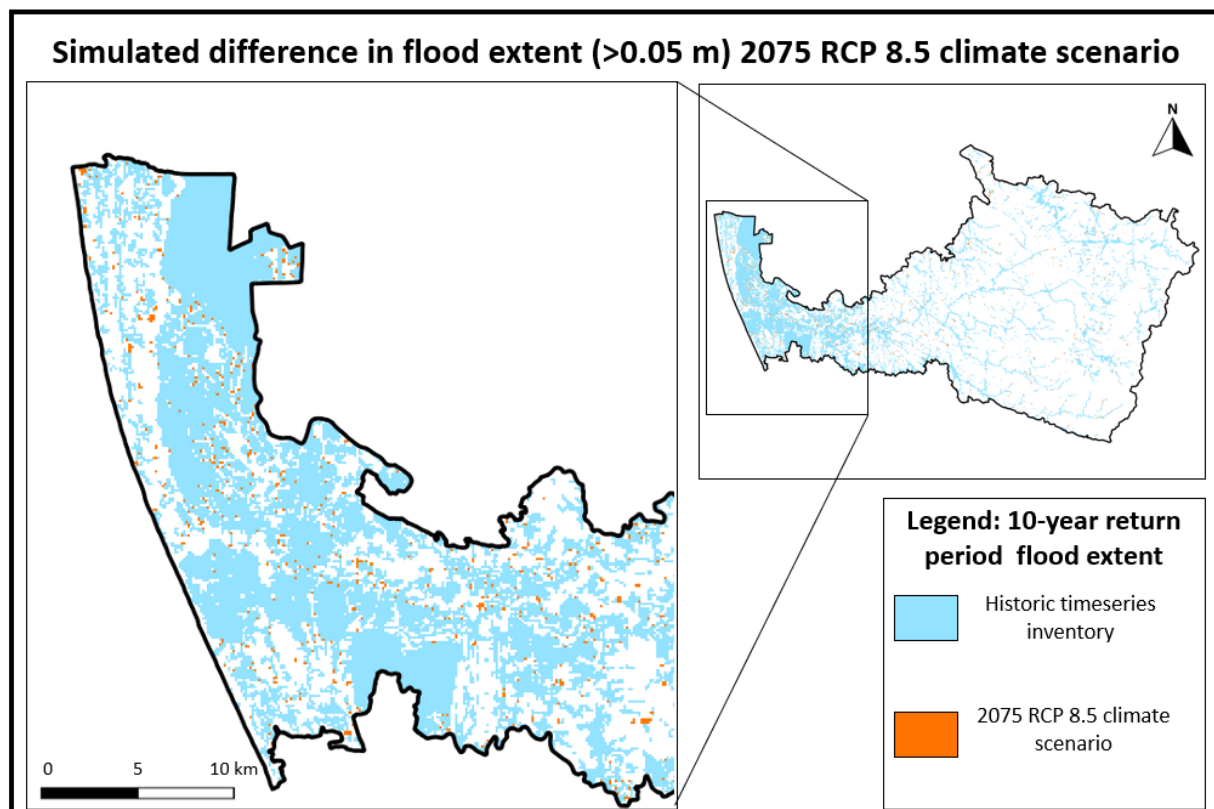
Figure 54 simulated difference in flood extent (>0.05m) 2075 RCP 8.5 climate scenario

Appendix J: Flood exposure analyses

Schools in Pamba basin exposed to 5-year return period flood event

Pamba basin in Kerala

Count school flood exposure	
Not exposed	806
Waterdepth > 0.05 m	279

Legend
- Not exposed school
- 0.05-0.3 m
- 0.3 - 0.55 m
- 0.55 - 0.8 m
- 0.8 - 1.05 m
- 1.05 -1.3 m
- 1.3 -1.55 m
- 1.55 -1.8 m
- 1.8 -2.05 m
- 2.05 - 2.3 m
- 2.3- 2.55 m

0   10   20 km
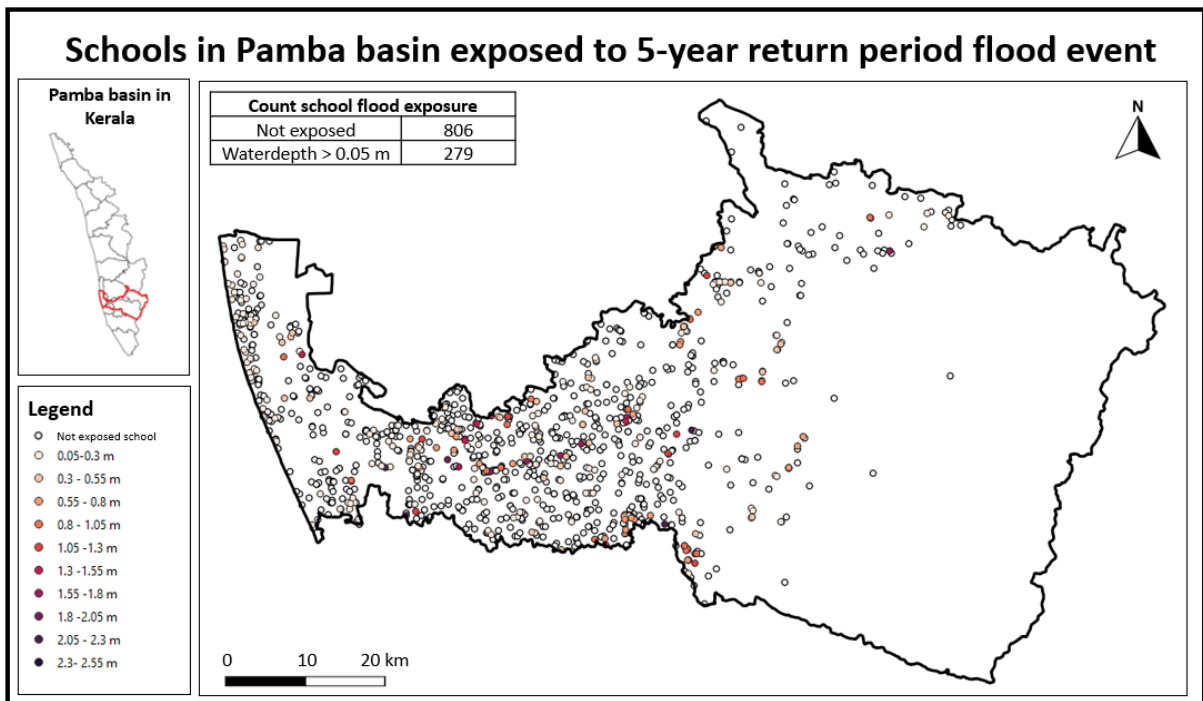
Figure 55 Schools in Pamba Basin exposed to 5-year return period flood event

Hospitals in Pamba basin exposed to 5-year return period flood event

Pamba basin in Kerala

Count school flood exposure	
Not exposed	42
Waterdepth > 0.05 m	17

Legend
- Not exposed hospital
- 0.05-0.3 m
- 0.3 - 0.55 m
- 0.55 - 0.8 m
- 0.8 - 1.05 m
- 1.05 -1.3 m
- 1.3 -1.55 m
- 1.55 -1.8 m
- 1.8 -2.05 m
- 2.05 - 2.3 m
- 2.3- 2.55 m

0   10   20 km
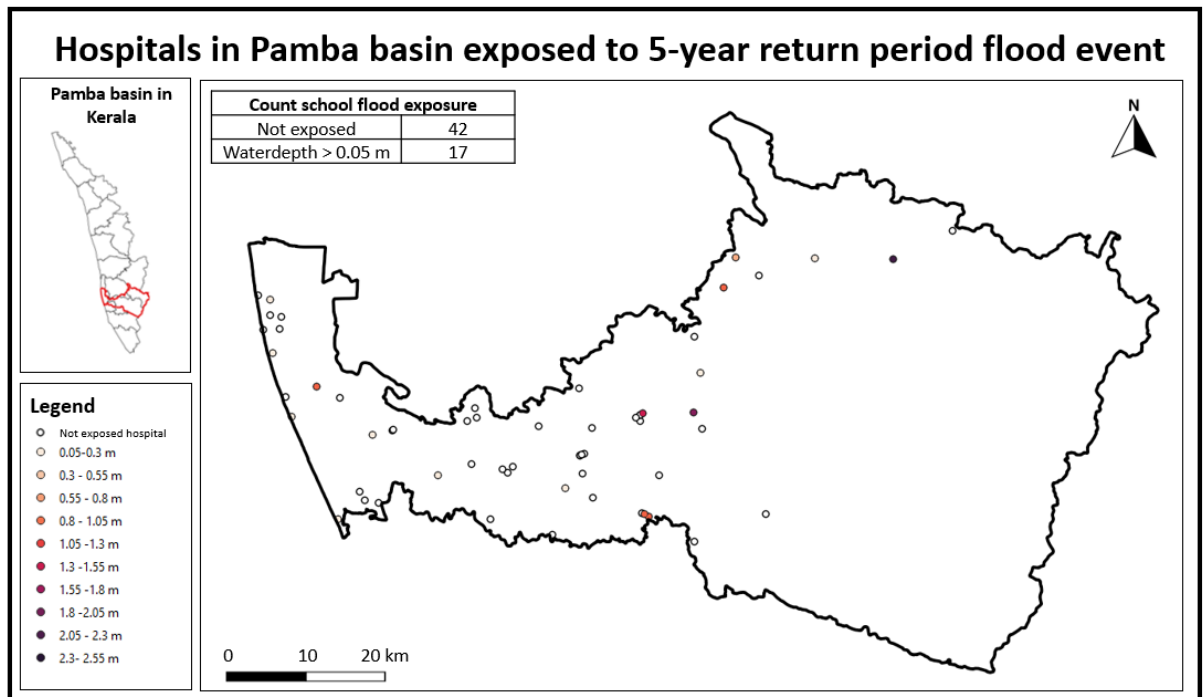
Figure 56 Hospitals in Pamba Basin exposed to 5-year return period flood event
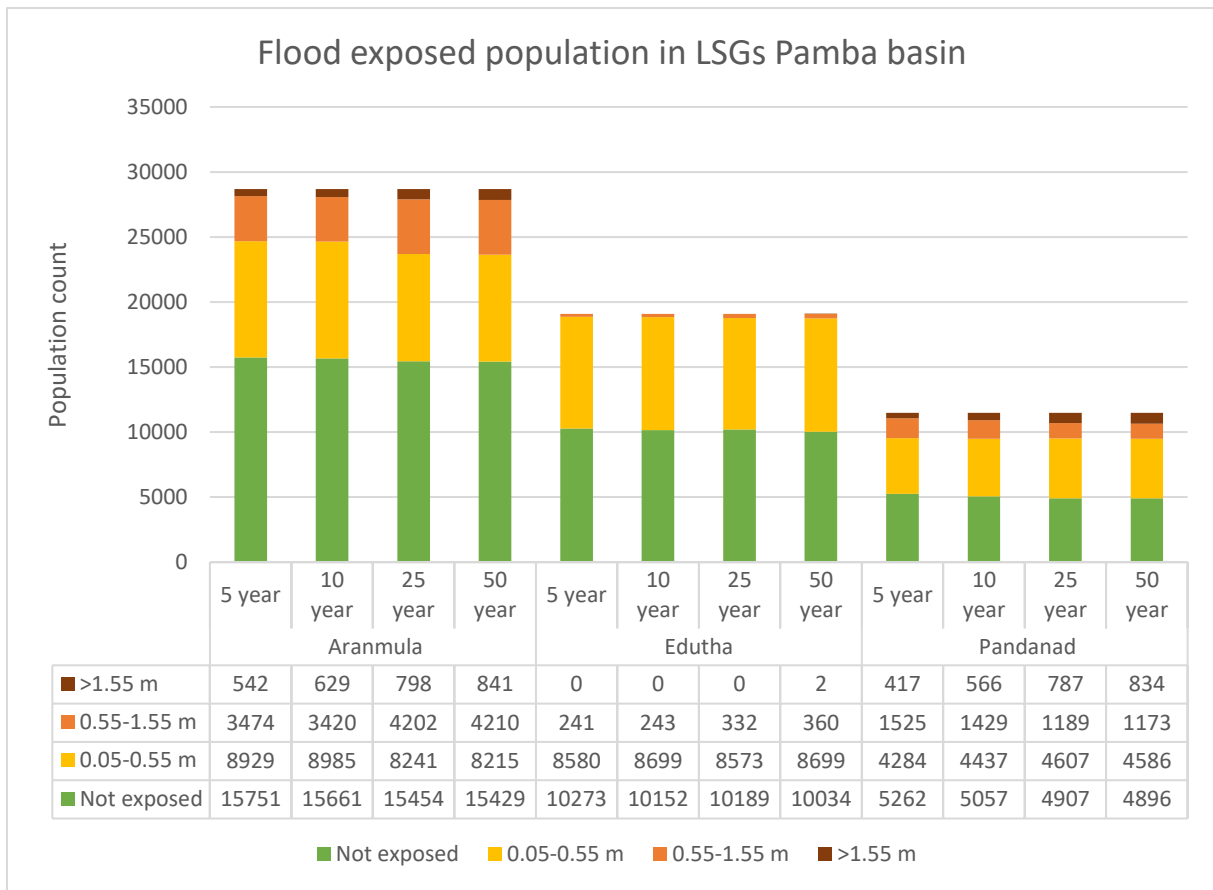
Figure 57 Flood exposed population in LSGs Pamba Basin

	5 year	10 year	25 year	50 year	5 year	10 year	25 year	50 year	5 year	10 year	25 year	50 year
		Aranmula				Edutha				Pandanad		
>1.55 m	542	629	798	841	0	0	0	2	417	566	787	834
0.55-1.55 m	3474	3420	4202	4210	241	243	332	360	1525	1429	1189	1173
0.05-0.55 m	8929	8985	8241	8215	8580	8699	8573	8699	4284	4437	4607	4586
Not exposed	15751	15661	15454	15429	10273	10152	10189	10034	5262	5057	4907	4896
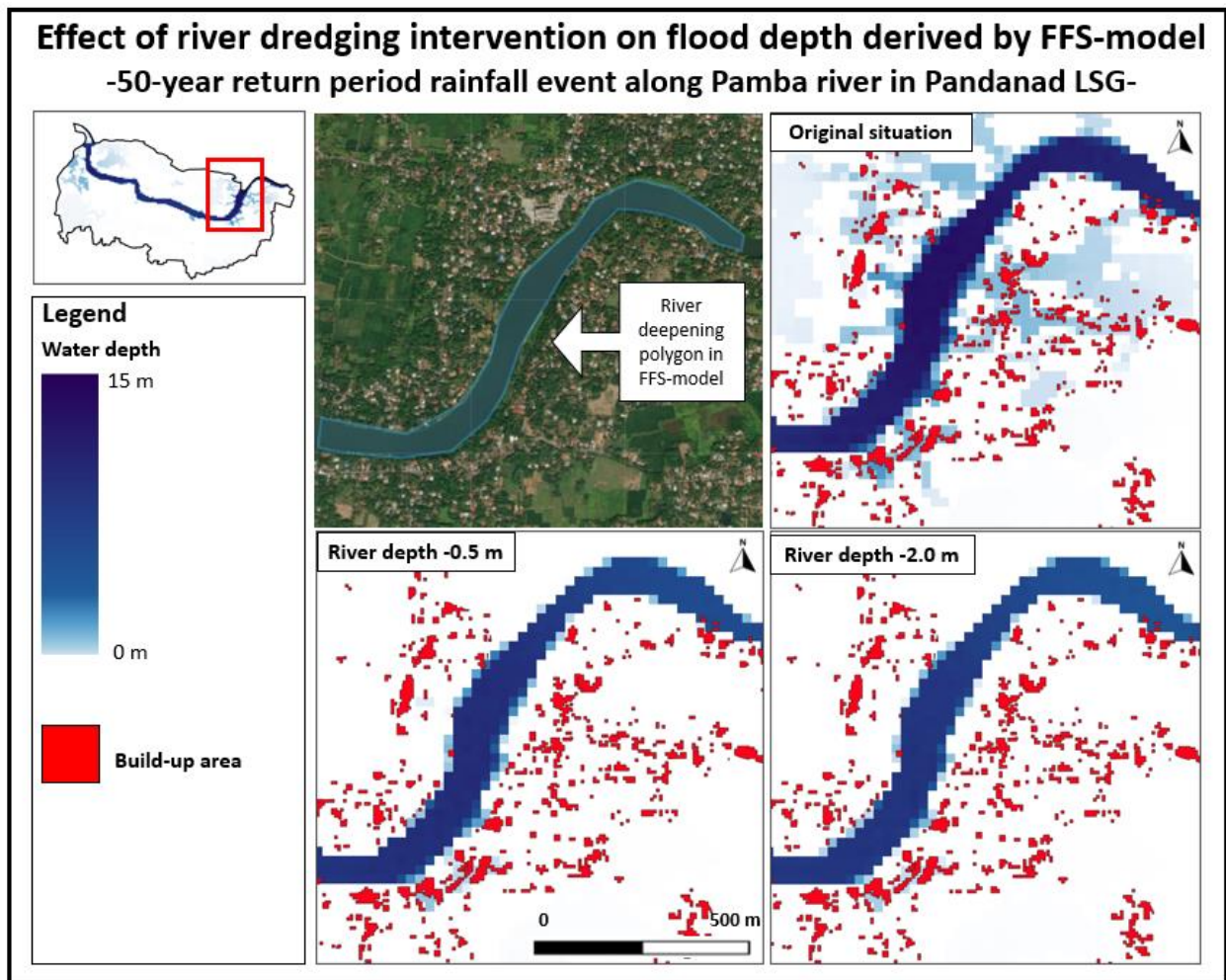
Figure 58 Effect of river dredging intervention on flood depth derived by FFS-model
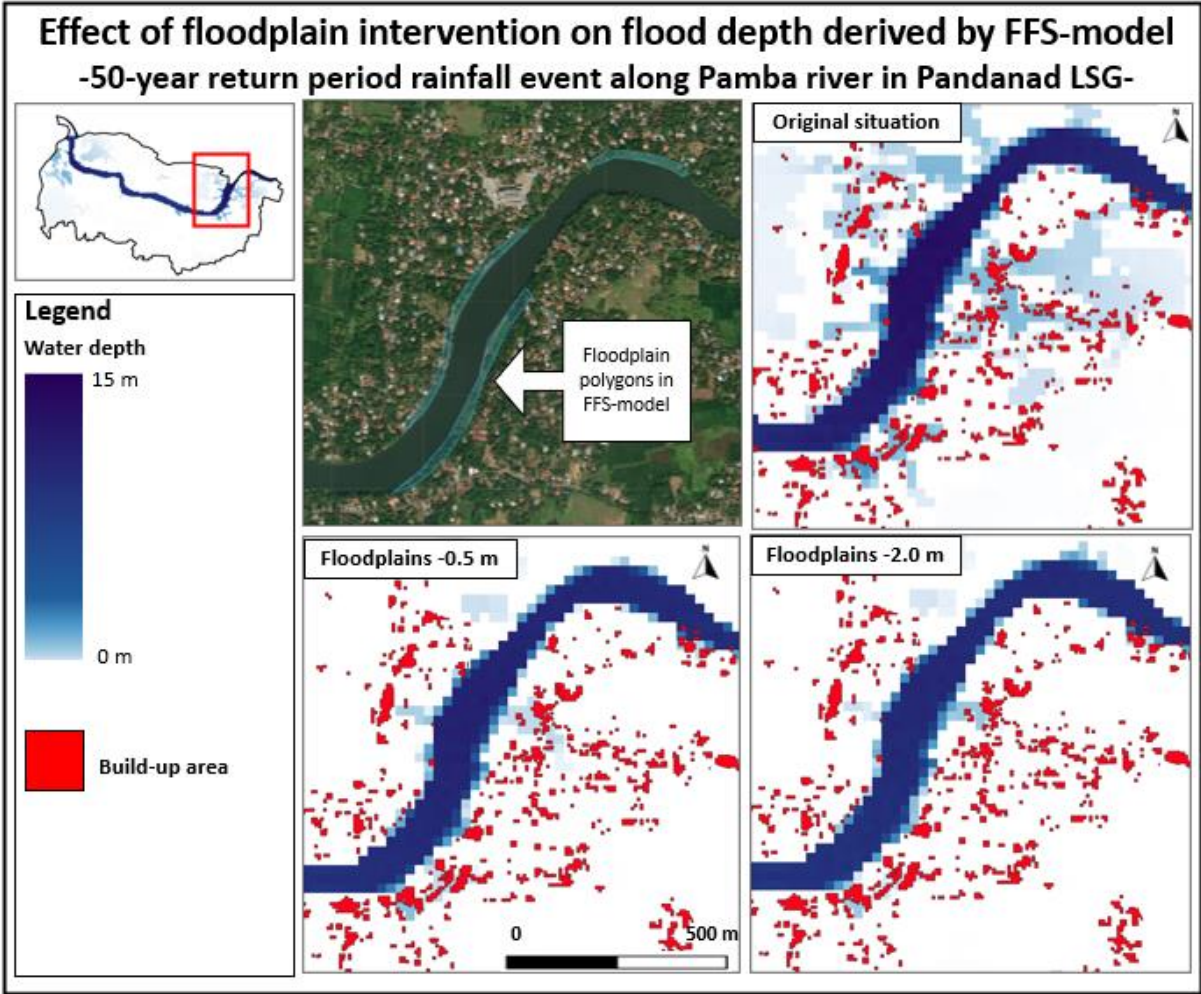
Figure 59 Effect of flood plain intervention on flood depth derived by FFS-model